

**PHOTO-TRANSLOCATION OF ANTIRETROVIRAL DRUGS INTO HIV-1
PERMISSIVE CELL LINES**

Thulile Khanyile



**A dissertation submitted to the Faculty of Health Sciences,
University of the Witwatersrand, Johannesburg, in fulfilment of the
requirements for the degree of Master of Science in Medicine.**

Johannesburg, 2015

DECLARATION

I, Thulile Khanyile declare that this dissertation is my own work. It is being submitted for the degree of Master of Science in Medicine in the University of the Witwatersrand, Johannesburg. It has not been submitted before for any degree or examination at this or any other University.

.....

.....day of June, 2015

DEDICATION

To my mom, dad and little brother...

I love you guys...

Conference proceedings

T. Khanyile, M. Papathanasopoulos, A. Forbes and P. Mthunzi. Optical delivery of ARV drugs into HIV-1 permissive cells. CSIR Emerging Researcher's Symposium; 2013 October 29-30; Pretoria, South Africa (*Oral presentation*).

T. Khanyile, M. Papathanasopoulos, A. Forbes and P. Mthunzi. Photo-translocation of anti-HIV-1 drugs into TZM-bl cells. Optics in Life Sciences Congress; 2013 April 14-18, Hawaii, United States of America (*Oral presentation*).

T. Khanyile and P. Mthunzi. Assessment of antiretroviral drug metabolism within optically treated cell populations. SPIE: Photonics West BiOS, 2015 February 7-12, San Francisco, California, United States of America (*Oral Presentation – Abstract accepted*).

T. Khanyile, M. Papathanasopoulos and P. Mthunzi. Selective delivery of antiretroviral drugs into live HIV-1 permissive cells using pulsed laser light. SPIE: Photonics West BiOS, 2015 February 7-12, San Francisco, California, United States of America (*Poster Presentation – Abstract accepted*).

Peer reviewed publications and conference papers

T. Khanyile, M. Papathanasopoulos and P. Mthunzi (2015). Photo-translocation of antiretroviral drugs into HIV-1 permissive cell lines (*In preparation*).

Abstract

Photo-translocation makes use of laser light to translocate exogenous materials into cells. Its applicability as a drug delivery systems (DDS) has not been explored. This proof-of-principle study evaluated the applicability of a home-built femtosecond (fs)-laser based photo-translocation system as a DDS, using human immunodeficiency virus type-1 (HIV-1) antiretroviral (ARV) drugs as a model. A tightly focused pulsed laser was integrated into a photo-translocation system which was set up, validated and used to facilitate the delivery of ARV drugs against a concentration gradient into TZM-bl cells. To ensure preservation of the cell's integrity, cell viability tests were carried out post laser treatment. An HIV-1 subtype C envelope-pseudovirus (ZM53) was generated and used in an *in vitro* phenotypic inhibition assay to measure the success of photo-translocation of three selected ARV drugs into TZM-bl cells.

The near infrared (NIR) photo-translocation setup was successfully assembled and validated, as shown by characterisation of the relevant parameters such as pulse duration (10 picoseconds), central wavelength (1063.8 nm) and beam quality (1.15). The optimal functionality of the newly built photo-translocation system, as determined by trypan-blue exclusion dye in TZM-bl cells, was 3 doses of laser treatment at a power level of 60 mW and an exposure time of 50 ms. These parameters were extrapolated to photo-translocation experiments using selected ARV drugs. Photo-translocation of tenofovir and nevirapine resulted in enhanced levels of approximately 25% viral inhibition against ZM53 pseudoviruses. By contrast, no detectable change in viral inhibition was observed

in the photo-translocation of efavirenz. Cell viability results confirmed that no toxicity existed within the laser irradiated cell population with cell viabilities greater than 70% at the tested drug concentrations. Tenofovir was not toxic to the cells at the administered concentration of 20 µg/ml. However, nevirapine (10 µg/ml) and efavirenz (14 µg/ml) showed high levels of toxicity after prolonged exposure to the cells (48 hours) while laser irradiation and brief (30 minutes) exposure to the drugs resulted in significant elevations of cell viability. Overall, this study demonstrated for the first time that laser technology is an efficient, targeted DDS which led to elevated therapeutic effects of ARV drugs against HIV-1 pseudoviruses with minimal damage to the treated cells *in vitro*.

Acknowledgements

I thank my supervisors Prof Maria Papathanasopoulos and Dr Patience Mthunzi for their invaluable academic support, guidance and all the extra efforts made towards my Masters. Prof, I could have not completed this without you.

I would like to acknowledge Dr Makobetsa Khati, Dr Dalu Ncama, Dr Hazel Mufhandu and Prof Andrew Forbes from the CSIR for the contributions made to the running and completion of this study in their respective roles. I would also like to acknowledge Dr Mark Killnick from the University of the Witwatersrand for his contribution to the study.

The Mathematical Optics group, Nico Marome, Dr Herman Uys, Nicolene Botha, Attie Heindriks, and Bathusile Masina; I appreciate all the efforts you all made in assisting me with the study.

My mates Thandeka Mhlanga and Fakazi Nhachissambe; much love guys.

Sindisiwe Nondaba; my partner in crime, thank you for being there at all times 'mngani'.

My mom, dad and little brother; without your support I am completely bare... You guys motivate me to be better. It is because of the three of you that I sometimes feel like there are no limits to my dreams and abilities.

I thank the CSIR and the DST (PISA) for their financial assistance. I thank the OSA for the travel grant awarded for the Photonics in Life Sciences Conference.

Finally, The Almighty Jehovah God through whom all things are possible...
Ngiyokudumisa njalo!

Table of Contents

DECLARATION.....	i
DEDICATION.....	ii
Conference proceedings.....	iii
Peer reviewed publications and conference papers.....	iv
Abstract.....	v
Acknowledgements.....	vii
Table of Contents.....	ix
List of Figures.....	xiv
List of Tables.....	xvii
List of Abbreviations.....	xviii
1. Literature Background.....	1
1.1 Introduction.....	1
1.2 Current drug delivery routes.....	5
1.3 Methods to deliver therapeutic agents <i>in vitro</i>	7
1.3.1 Delivery of nucleic acids by chemical methods.....	7
1.3.2 Physical methods.....	8
1.3.2.1 Electroporation.....	8
1.3.2.2 Particle bombardment.....	8
1.3.2.3 Microinjection.....	9
1.3.3 Viral methods.....	10
1.3.4 Nanoparticles as a drug delivery system.....	11

1.3.5 Laser assisted transfection	12
1.4 A brief introduction to lasers	12
1.5 Brief overview to Gaussian beams	15
1.5.1 Gaussian beam propagation	16
1.5.2 Gaussian beam Intensity	17
1.6 Application of lasers to delivering therapeutics in biomedical research	18
1.7 Mechanisms of fs photoporation	22
1.7.1 Laser induced optical breakdown	22
1.8 Mechanisms for laser effects on biological cells and tissues	24
1.9 Photo-translocation of drugs	26
1.10 Photo-translocation: It's application to the clinical setting	26
1.11 Photo-translocation: It's application to intracellular infections	28
1.11.1 Epidemiology of HIV-1	29
1.11.2 HIV-1 life cycle and potential ARV drug targets	30
1.11.3 Current HIV-1 treatment.....	32
1.11.3.1 HIV-1 disease progression	34
1.12 Research objectives.....	39
2. Materials and Methods	40
2.1 Reagents used in this study.....	40
2.1.1 Cell lines	40
2.1.2 Plasmids used for the generation of molecularly cloned <i>env</i> -pseudoviruses	40

2.1.3 ARV drugs used in the study	41
2.2 Mammalian cell culture.....	41
2.2.1 Passaging of HEK 293T and TZM-bl cells	41
2.2.2 Quantification of mammalian cells using a haemocytometer	42
2.2.3 Generation of molecularly cloned <i>env</i> -pseudoviruses.....	43
2.2.4 Preparation of competent <i>E.coli</i> Top 10 cells.....	43
2.2.5 Transformation of competent <i>E.coli</i> Top 10 cells	44
2.2.6 Isolation of DNA plasmids using the Qiagen Maxiprep kit.....	45
2.2.7 Co-transfection of HEK 293T cells	46
2.2.8 Harvesting of <i>Env</i> -pseudotyped virus	47
2.2.9 <i>Env</i> -pseudotyped virus titration.....	47
2.3 Assembly and characterisation of a home built photo-translocation system	48
2.3.1 Validation of laser pulse trains and measurement of the repetition rate...	49
2.3.2 Central wavelength and spectral bandwidth measurements.....	49
2.3.3 Pulse duration measurement	50
2.3.4 Beam quality measurement	52
2.3.5 Beam diameter measurements.....	53
2.4 Assembly of the photo-translocation setup	53
2.5 Evaluation of the photo-translocation system	56
2.5.1 Trypan blue photo-translocation into TZM-bl cells	56
2.5.2 Photo-translocation of ARV drugs into TZM-bl cells	57
2.5.3 HIV-1 inhibition assay	58

2.5.4 Cytotoxicity assay	59
2.6 Statistical analyses	61
3. Results	62
3.1 Laser beam characterisation.....	62
3.1.1 Validation of laser pulse trains and determination of pulse repetition rate	62
3.1.2 Central wavelength and spectral bandwidth measurements.....	63
3.1.3 Pulse duration measurement	64
3.1.4 Determination of the beam quality	67
3.1.5 Beam diameter measurements.....	71
3.2 Assembly of photo-translocation set up	77
3.3 Photo-translocation of trypan blue viability dye	80
3.4 Photo-translocation of ARV drugs into TZM-bl cells	83
3.5 Cytotoxicity assay	87
4. Discussions	93
4.1 Characterisation of the laser towards the assembly of a functional photo-translocation setup.....	93
4.1.1 Mode-locking nature of the Fianium FemtoPower laser.....	94
4.1.2 Laser pulse durations.....	94
4.1.3 Beam quality contribution to the efficiency of photo-translocation	95
4.1.4 Functionality of assembled photo-translocation setup	96
4.2 Establishment of an HIV-1 inhibition assay	96
4.2.1 Fate of the ARV drugs used in the study.....	98

4.3	Effects of ARV photo-translocation on the inhibition of ZM53 <i>env</i> -pseudotyped virus replication	100
4.4	Effects of laser irradiation and ARV photo-translocation on TZM-bl cell viability	103
4.5	ps versus fs laser sources	106
4.6	Limitations of the study.....	107
5.	Conclusions and Future perspectives	110
5.1	Conclusions.....	110
5.2	Future perspectives.....	110
	References	112
	Appendices	127
	Appendix A: Derivation of equations.....	127
1.	Derivation of beam radius polynomial	127
	Appendix B: Formulae	128
1.	Calculation of % viral inhibition	128
2.	Calculation of % viability	128
3.	Calculation of TCID ₅₀	128
	Appendix C: Clearance Certificate	129

List of Figures

Figure 1.1: Schematic representation of basic laser components and operation.	13
Figure 1.2: Three level laser energy showing spontaneous and stimulated decay.	14
Figure 1.3: Continuous wave (CW) and pulsed modes of laser operation.....	15
Figure 1.4: Gaussian beam propagation in the z direction.....	16
Figure 1.5: Intensity profile of a Gaussian beam.	18
Figure 1.6: Plasma formation through the interplay of multiphoton and cascade ionization.	23
Figure 1.7: Summary of physical breakdown phenomena on biological cells as induced by fs laser pulses.	25
Figure 1.8: Schematic representation of a sample chamber with adherent HIV-1 permissive cells in an ARV drug and growth medium solution.	29
Figure 1.9: Life cycle of HIV-1 and site of action of antiretroviral therapy (red text).	32
Figure 1.10: Graphical representation of HIV-1 disease progression	35
Figure 2.1: Arrangement of the FROG set up.....	51
Figure 2.2: Experimental setup of the beam quality.	53
Figure 2.3: Arrangement of the photo-translocation set up.	55
Figure 3.1: Validation of laser pulse trains.	63
Figure 3.2: Spectrum showing the measured central wavelength and bandwidth of the Fianium laser.....	64
Figure 3.3: Spectrum of the measured FROG signal where intensity was plotted against wavelength.....	65
Figure 3.4: Spectrograms showing the time it took to measure each pulse.	66

Figure 3.5: FROG traces of the pulse duration measurement.	67
Figure 3.6: Graph showing the calculation of the beam quality.	70
Figure 3.7: Images of the laser beam as it propagated along the z axis.	71
Figure 3.8: Beam diameter measurement at the laser output.....	72
Figure 3.9: Intensity distribution of the laser beam as a function of z, propagation distance (in mm).....	73
Figure 3.10: Beam diameter measurement after the beam was expanded.	74
Figure 3.11: Intensity distribution of the laser beam as a function of z, propagation distance (in mm).....	75
Figure 3.12: Beam diameter measurement after the beam was focused through the objective lens.....	76
Figure 3.13: Intensity distribution of the laser beam as a function of propagation distance.....	76
Figure 3.14: Image of the completed home-built photo-translocation setup.	77
Figure 3.15 (a) to (d): Images illustrating the expansion and collapsing of an airy disk during focusing. These images were taken using a 60X objective lens.	78
Figure 3.16: Image showing the focusing of an airy disc through collapsing and expanding.....	79
Figure 3.17: (a) Example of a focused, well aligned airy disc while (b) to (d) show examples of unwanted spherical aberrations.	80
Figure 3.18: Bright field images of TZM-bl cells photo-porated in the presence of a membrane impermeable viability dye, trypan blue.	81
Figure 3.19: Bar graph showing the RLU values of the laser assisted delivery of tenofovir.....	85

Figure 3.20: Bar graph showing the RLU values of the laser assisted delivery of nevirapine.....	85
Figure 3.21: Bar graph showing the RLU values of the laser assisted delivery of efavirenz.....	86
Figure 3.22: MTT assay for laser irradiated cells.....	88
Figure 3.23: MTT assay for the photo-translocation of tenofovir into TZM-bl cells.	89
Figure 3.24: MTT assay for the photo-translocation of nevirapine into TZM-bl cells.	90
Figure 3.25: MTT assay for the photo-translocation of efavirenz into TZM-bl cells.	91

List of Tables

Table 3.1: Measured beam parameters for the Fianium FemtoPower laser.....	70
Table 3.2: Measured spot size and beam radius of the Fianium FemtoPower laser against the theoretical estimate of the beam radius.	73
Table 3.3: Measurement of the magnification factor for the expansion of the beam spot size, as well as the measured and expected spot sizes following beam expansion.....	74
Table 3.4: Measured spot size and beam radius of the focused Fianium FemtoPower laser against the theoretical estimate of the beam radius.	77
Table 3.5: The percentage inhibition values of photo-translocated ARV drugs against drug taken up naturally by the cells with drug to cell exposure times of 30 minutes and 48 hours by measuring luciferase activity in HIV-1 infected TZM-bl cells.....	87
Table 3.6: Percentage viabilities of laser irradiated cells and ARV photo-translocated cells assessed using the MTT assay.	92

List of Abbreviations

$2\omega_0$	Beam diameter
AAV	Adenovirus-associated virus
ABC	Adenosine triphosphate (ATP) binding cassette
AIDS	Acquired immunodeficiency syndrome
ARV	Antiretroviral
ATP	Adenosine triphosphate
b	Beam depth of focus
BB	Bessel beam
BBO	β -barium borate crystal
BS	Beam splitter
Cat.	Catalogue
CC	Cell control
CCD	Charge coupled device
CCR5	C-C chemokine receptor type 5
CD4 ⁺	Cluster of differentiation 4 positive
CHO	Chinese hamster ovary
CTL(s)	Cytotoxic T lymphocyte(s)
CW	Continuous wave
CXCR4	Chemokine C-X-C motif receptor type 4
CYP(s)	Cytochrome(s)
D4 σ	Second moment

DC	Drug control
DDS	Drug delivery system
DEAE	2-(diethylamino)ether
DM	Dichroic mirror
DMEM	Dulbecco's Modified Eagle's Medium
DNA	Deoxyribonucleic acid
<i>E.coli</i>	<i>Escherichia coli</i>
EI(s)	Entry inhibitors
EM	Electromagnetic
Env	Envelope
EXP	Experimental
FBS	Fetal bovine serum
FDA	Food and drug administration
FROG	Frequency-resolved optical gating
Fs	Femtosecond
FWHM	Full width at half maximum
GFP	Green fluorescence protein
GIT	Gastrointestinal tract
GM	General medium
Gp120	Envelope glycoprotein 120
HAART	Highly active antiretroviral therapy
HEK	Human embryonic kidney

HeLa	Henrietta Lacks
HIV-1	Human immunodeficiency virus type 1
IC ₅₀	50% inhibitory concentration
IN(s)	Integrase inhibitor(s)
KTP	Potassium titanyl phosphate
L	Lens
LASER	Light Amplification by Stimulated Emission for Radiation
LB	Luria Bertani
LC	Laser control
LTR	Long terminal repeat
Luc	Luciferase
M	Mirror
M^2	Beam quality factor
MDR	Multidrug resistance
mRNA	Messenger ribonucleic acid
MTT	3-(4,5-dimethylthiazol-2-yl)-2,5-diphenyltetrazolium bromide
mV/div	Millivolts per division
NA	Numerical aperture
NG108	Neuroblastoma glioma
NIH	National Institutes of Health
NIR	Near-infrared
NNRTI(s)	Non-nucleoside reverse transcriptase inhibitor(s)

NRTI(s)	Nucleoside reverse transcriptase inhibitor(s)
Ns	Nanosecond
ns/div	Nanosecond per division
PBMC(s)	Peripheral blood mononuclear cell(s)
PBS	Phosphate Buffered Saline
PC	Positive control
PEST	Penicillin-streptomycin
P-g	P-glycoprotein
PI(s)	Protease inhibitor(s)
PIC	Pre-integration complex
Ps	Picosecond
PtK2	Rat-kangaroo kidney epithelial
<i>r</i>	Radial distance
RLU	Relative luminescence units
RNA	Ribonucleic acid
Rpm	Revolutions per minute
RPMI	Roswell Park Memorial Institute medium
RT	Reverse transcriptase
RTI(s)	Reverse transcriptase inhibitor(s)
SA	South Africa
siRNA	Small interfering ribonucleic acids
SMA	Sub-miniature version A

SNP(s)	Single nucleotide polymorphisms
SOC	Super optimal broth
Tat	Trans-activator of transcription
TB	Tuberculosis
TC	Triton X-100 control
TCID ₅₀	50% tissue culture infectious dose
TDF	Tenofovir disoproxil fumarate
TEM ₀₀	Transverse electromagnetic mode
TL	Tube lens
tRNA	Transfer ribonucleic acid
UNAIDS	Joint United Nations Programme on HIV/AIDS
US	United States
UV	Ultraviolet
VC	Virus control
WHO	World Health Organisation
z	Axial distance
z_R	Rayleigh range
$\omega(z)$	Beam width
ω_0	Beam waist

1. Literature Background

1.1 Introduction

In the medical sciences successful delivery of therapeutic, preventative and nutritional agents is imperative to the survival of humankind. There are generally a variety of therapeutic agents in the form of (but not limited to) hydrophilic agents (Glauser *et al.*, 2014, Patel *et al.*, 2001), nucleic acids including small interfering ribonucleic acids (siRNA) (Shen *et al.*, 2012, Chen *et al.*, 2010, Gomes *et al.*, 2014, Hyukjin Lee *et al.*, 2012), lipids (Szebeni *et al.*, 2011), proteins (van den Berg *et al.*, 2011), vaccines (Bolhassani *et al.*, 2011), and other macromolecules. Mostly, at molecular levels, these agents are not readily taken up by mammalian cells due to the presence of a generally non-permeable membrane lipid bilayer which is the outermost layer of all mammalian cells. The lipid bilayer serves to control the movement of molecules in and out of the cell. Therapeutic drugs have to penetrate the cell membrane in order to execute an appropriate therapeutic effect at the target site (Bally *et al.*, 1999, Belting *et al.*, 2005). In *in vivo* systems, drugs have to be transferred from the site of administration to the bloodstream before reaching respective target sites. The rate at which this transfer occurs as well as the efficiency of the drug is dependent on the route of administration or the drug delivery system (DDS). Depending on the DDS used, the drug may only be partially absorbed into the bloodstream leading to a low bioavailability of the drug at the target site (Muller *et al.*, 2004).

Drugs are absorbed into the circulatory system depending on their chemical properties. This process can occur either by passive or active diffusion. During passive diffusion drugs move from a region of high concentration to one of a lower concentration. The process of passive diffusion is governed by factors which include the size and shape of the molecule, the degree of ionization and the solubility of the drug (Levine, 1970). Active diffusion moves drugs against a concentration gradient from a region of low drug concentration to that of a high drug concentration (Lennernas *et al.*, 1996), where the transport of drugs is assisted by energy in the form of adenosine triphosphate (ATP). Other methods of drug absorption by target cells include, but are not limited to endocytosis, exocytosis and pinocytosis. These two drug transport systems occur in the case where large molecules have to cross the cell membrane. Contrarily, in the case of endocytosis the drug is engulfed by the cell membrane followed by the intracellular pinching off of the vesicle encasing the drug. The opposite is exocytosis where the cells usually secrete and release substances such as neurotransmitters (Farquhar, 1983, Bretscher, 1984, Battey *et al.*, 1999). Pinocytosis refers to the invagination of the cell membrane around a molecule in turn incorporating the drug inside the cell (Chillistone, 2014).

Factors that affect the absorption of drugs into the blood stream include product bioavailability which involves the speed and extent to which a drug is absorbed; the pharmacokinetics of the drug which consist of the metabolism, the distribution as well as the elimination of the compound. The formulation (whether the drug is a capsule or tablet etc.) of the drug may also affect its absorption, but when it has reached the circulatory system the initial formulation of the drug does not affect its

behaviour as it would usually already be in a dissolved state (Martinez *et al.*, 2002). Furthermore, the environmental conditions of the gastrointestinal tract (GIT) and the nature of the drug absorbing cell particularly the cells metabolic activity and the structure of the cells absorbing surface which also affect the absorption of the therapeutic agents (Levine, 1970).

Pharmacogenetics, the study of how the host genetic differences in the metabolic pathway of drugs contributes to how individuals respond to drugs must also be considered as a factor which contributes significantly to the efficacy of a drug. This becomes crucial as host genetic differences cause different individuals and populations to respond differently to medication even when administered in the same dosages (Lu, 1998). The human body has various drug targets such as receptors (Viola *et al.*, 2008), enzymes (Overall *et al.*, 2006) and proteins (Anishetty *et al.*, 2005). Drugs target these proteins which are involved in a variety of cellular events including signal transduction and cell cycle control to induce a pharmacological effect. The genes which code for these targets are genetically polymorphic (Chan *et al.*, 2004).

The ability of a drug to be absorbed, distributed and metabolised, and interact with its target can be investigated through an understanding of host genetic differences. Genetic factors account for the inter-individual differences observed in the variable manner to which individuals respond to drugs (Eichelbaum *et al.*, 2006). The majority of orally administered drugs available in the market are metabolised by various forms of polymorphic, membrane associated enzymes known as cytochromes P450 (CYP) (Evans *et al.*, 1999). The presence of single

nucleotide polymorphisms (SNPs) which are DNA sequence variations in genes encoding CYPs are the basis for the genetic variability found in different individuals. These variations alter the activity of the encoded protein compared to the wild type sequence. In such instances, the activity of the protein may be reduced due to the genetic polymorphisms while the variation can also result in elevated activities of the protein (Evans *et al.*, 1999).

The efficacy of drugs is also dependant on the drugs ability to cross physical barriers in order to reach their target site of action. Physical barriers in the GIT, in the form of plasma membrane contain adenosine triphosphate (ATP)-binding cassette (ABC) efflux proteins which mediate drug transport as this plays a major role in the absorption, bioavailability and elimination of drugs (Chan *et al.*, 2004). Genetic polymorphisms which interfere with the expression of these efflux proteins or which alter their affinity for substrates are able to result in phenotypic and pharmacological effects of the drugs (Eichelbaum *et al.*, 2006). Host genetic effects of how a drug is metabolised, absorbed and eliminated are an important factor as they can result in negative clinical effects on individuals being treated as the therapeutic doses being administered may not be ideal for the desired therapeutic effect with minimal side effects (Shastri, 2005).

In order to achieve high drug bioavailability at specific target sites, there has been a shift in the drug development arena towards focusing more on the systems governing drug delivery. Researchers are investigating various DDS to enhance the bioavailability of drugs and to decrease the occurrence of unwanted side effects by more accurately depositing drugs directly to the target sites.

1.2 Current drug delivery routes

The methods of drug delivery most frequently used in the clinic include enteral and parenteral systems. Enteral drug delivery includes oral and sublingual administration of drugs. In oral delivery a drug is given by the mouth and ingested as opposed to sublingual administration where a drug is placed beneath the tongue and allowed to diffuse into the capillary network and subsequently enter the systemic circulation directly (Thanou *et al.*, 2001).

Oral administration is the most preferred route as it is painless and self-administered (Plapied *et al.*, 2011). Orally administered drugs are normally absorbed into the blood stream via passive intracellular diffusion where the intestinal epithelium provides a physical barrier to the absorption of drugs. This in turn presents a challenge to the absorption of drugs by the circulatory system (Plapied *et al.*, 2011). Furthermore, chemical and enzymatic fluids in the GIT contribute to drug degradation which prohibits the administration of macromolecules (Plapied *et al.*, 2011). Another disadvantage of oral drug administration is the time required for the drug to travel through the intestine as it can result in incomplete drug release which then leads to a diminished efficacy of the administered dosage (Singh *et al.*, 2000).

Additional routes of administration are parenteral which involve the use of a needle, injection or catheter to introduce drugs directly across the body's barrier defences into the systemic circulation. This route allows for the delivery of drugs that are poorly absorbed or unstable in the GIT (Kumar *et al.*, 2007). Administration of drugs using this method is painful, generates dangerous medical

waste and may cause an increased risk of infection at the injection site (Prausnitz *et al.*, 2008).

Transdermal drug delivery employs a patch which applies the drugs into the circulatory system through the skin (Kumar *et al.*, 2007). The method is non-invasive, easy to self-medicate and the drug is not exposed to the harsh environment of the GIT (Naik *et al.*, 2000). Transdermal patches are however not able to deliver macromolecules with molecular weights greater than 1000 Da (Naik *et al.*, 2000a).

Although the above DDSs are the most widely used they have various limitations as they are designed to disseminate the drug into the body through the circulatory system (McAllister *et al.*, 2003). The drugs are subsequently able to interfere with body systems that are not infected or diseased leading to unwanted side effects where harmful and unpleasant reactions occur in the body as drugs accumulate in unaffected tissues and organs (Vasir *et al.*, 2005). This also results in the dosages being administered not reaching the sites of infection in concentrations that lead to effective efficacy levels (Torchilin, 2000). To mitigate the host of limitations presented by these delivery systems, researchers have put much focus into the development of new DDSs with the ability to deliver exogenous and therapeutic agents to target sites in relevant therapeutic concentrations (Allen *et al.*, 2004). The applicability of DDS to move drugs across a membrane are first investigated at an *in vitro* level after which respective pre-clinical animal studies are carried out (Illum, 2003, Illum *et al.*, 1994, He *et al.*, 1998). There are a variety of methods that have been explored for targeted delivery of therapeutic drugs and

genetic materials into mammalian cells at an *in vitro* level, and some of these methods are discussed in more detail below.

1.3 Methods to deliver therapeutic agents *in vitro*

The progression and development of therapeutic agents relies on the ability of these agents to penetrate the cell membrane. Over the years a variety of methods such as electroporation (Lundkvist *et al.*, 2003), biodegradable nanoparticles (Panyam *et al.*, 2003), cell-penetrating proteins and peptides (Gupta *et al.*, 2005), folate mediated delivery (Lu *et al.*, 2012), protein transduction (van den Berg *et al.*, 2011), ultrasonic magnetic nanoparticles by magnetic resonance monitoring (Liu *et al.*, 2010) and the use of theranostics with spatiotemporal imaging (Knipe *et al.*, 2013) have been utilized to achieve intracellular delivery of therapeutic agents. Additionally, and briefly highlighted below is the use of chemical agents, physical methods, viral vectors, and nanoparticles.

1.3.1 Delivery of nucleic acids by chemical methods

Chemical methods of delivery, particularly during transfection procedures, have been utilized extensively in various studies as they are easy, versatile and have proved effective in the delivery of nucleic acids (Marivin *et al.*, 2015). Examples of chemicals usually used are calcium phosphate (Jordan *et al.*, 1996, Jordan *et al.*, 2004), 2-(diethylamino)ether (DEAE)-dextran (Mack *et al.*, 1998), artificial lipids (Zhi *et al.*, 2010, Shiraishi *et al.*, 2012) and proteins to name a few. With all its advantages, chemical transfections may be limited by their toxic effects as well as a difficulty to adapt to *in vivo* studies (Luo *et al.*, 2000).

1.3.2 Physical methods

1.3.2.1 Electroporation

Electroporation uses short and intense electric pulses to increase the permeability of the lipid bilayer of mammalian cells (Gehl *et al.*, 1999), ultimately creating hydrophilic pores and temporary damage to the membrane (Wang, 2013). The generated pores allow passage of non-permeating molecules to enter into the cytosol via diffusion (Pucihar *et al.*, 2008). Electroporation has been used in delivering various macromolecules such as proteins and nucleic acids both *in vitro* and *in vivo* (Choi, 2012). Examples of *in vivo* studies include the transfer of plasmid DNA and siRNA into dental tissues of rats (Yao *et al.*, 2014) and in the study of nucleic acid transfer into rodent brains in turn facilitating an understanding of brain disorders in gene therapeutics studies (Ding *et al.*, 2014). However, the high mortality of cells after exposure to high voltages renders electroporation unfavourable as it leads to tissue damage (Luo *et al.*, 2000). Additionally, during *in vivo* electric field application, pain and muscle twitching in large animals and humans have been reported and attributed to nerve stimulation (Tjelle *et al.*, 2006).

1.3.2.2 Particle bombardment

Particle bombardment or biolistics is a method where exogenous materials are coated into heavy metal particles (tungsten or gold) (Davis *et al.*, 1999). The micron-size metal particles are loaded into a macrocarrier where a gas, most commonly helium (He), is applied with high pressure causing the macrocarrier to be propelled forward and upon sudden stopping the microparticles are projected

by the principle of inertia into the target cells (Zilony *et al.*, 2013, Klein *et al.*, 1987).

The transfection efficiency of treated cell populations is determined by particle size and target distance (Tanner *et al.*, 1997). Biolistics have been used in a variety of studies involving transfection of genes into plant cells (Klein *et al.*, 1987), gene silencing (Shefi *et al.*, 2006), *in vitro* delivery of cancer therapeutics (Zilony *et al.*, 2013), and expression of deoxyribonucleic acid (DNA) and ribonucleic acid (RNA) in parasitic helminths (Davis *et al.*, 1999). Biolistics has however been reported to have limited accuracy and reproducibility (Shefi *et al.*, 2006).

1.3.2.3 Microinjection

Microinjection is a physical method where a glass needle (such as a microcapillary pipette or injection) is employed to directly inject exogenous materials into the nucleus or cytoplasm of the cell with high efficiency (Nelson *et al.*, 2002), through hydrostatic pressure (Mehier-Humbert *et al.*, 2005).

Microinjection allows single cells to be micromanipulated one at a time which proved advantageous in various studies where the manipulation of neuronal cells was carried out (Lappe-Siefke *et al.*, 2008, Wong *et al.*, 2014, Guo *et al.*, 2010). The single cell treatment aspect of microinjection has also been shown to enhance the development of mouse models for the investigation of disease mechanisms and the production of therapeutic agents; for example, (Wefers *et al.*, 2013)

successfully microinjected transcription activator like effector nucleases into single-cell embryos.

1.3.3 Viral methods

Viral mediated gene delivery is the most efficient method of intracellular delivery, where adenoviruses and lentiviruses are the most commonly used viral vectors (Sugiyama *et al.*, 2005). An optimal viral vector is one which is able to transduce into both dividing and nondividing cells. The transduced cell must consequently have the ability to produce sufficient quantities of the inserted target gene (Sugiyama *et al.*, 2005). Both adenoviruses and retroviruses are able to infect dividing and nondividing cells but adenoviruses do not allow for integration into the host cell genome while retroviruses are incorporated stably into host genome resulting in prolonged gene expression (Sugiyama *et al.*, 2005, Price *et al.*, 1987).

While viral mediated delivery may be efficient for gene delivery (An *et al.*, 2003) it may present un-wanted immune responses in immunocompetent animals and humans. For example, great promise in the correction of haemophilia B using an adenovirus-associated virus (AAV) was demonstrated in a clinical setting however, unwanted cytotoxic T-lymphocyte responses against the transduced hepatocytes were still observed (Manno *et al.*, 2006, Mingozzi *et al.*, 2007). In a later study, no acute or long-lasting toxicities were observed in severe haemophilia B patients where an enhanced AAV version was used. However, elevated levels of aminotransferases induced by the AAV-capsids mediated an immune response especially when higher prophylactic injections were administered (Nathwani *et al.*, 2011).

1.3.4 Nanoparticles as a drug delivery system

Nanoparticles (particles with sizes ranging from 1-100 nanometers) have been reported to hold great potential in overcoming physiological barriers and guide therapeutic drugs to specific cells either by passive or ligand-mediated or active targeting mechanisms (Mallipeddi *et al.*, 2010). Passive targeting, which requires that the nanoparticles circulate continuously in the blood stream to ensure that they are exposed to the target site, is a mechanism which takes place as nanoparticles encounter extravasation at the target site. This presents a challenge as the half-lives of nanoparticles may be relatively short due to host natural defence mechanisms which eliminate them from the body (Koo *et al.*, 2005). This challenge can be dealt with by ligand-mediated active targeting where a target ligand such as an antibody (Kim *et al.*, 2009), bacteriophage (Li *et al.*, 2011) or ARV drugs (Govender *et al.*, 2008) drugs is included in the nanoparticle. Active targeting therefore allows the ligand to bind to a specific cell-surface antigen and/or reporter in the target site (Cho *et al.*, 2008).

Nanoparticles are classified into various groups based on the material used during manufacturing, such as liposomes (Al-Jamal *et al.*, 2011), dendrimers (Kesharwani *et al.*, 2014), polymeric nanoparticles (Ensign *et al.*, 2012), solid lipid nanoparticles (Kakkar *et al.*, 2011) and metal nanoparticles (Kumar *et al.*, 2011, Rasmussen *et al.*, 2010).

1.3.5 Laser assisted transfection

First demonstrated in 1984, a laser based method to introduce exogenous genetic materials into mammalian cells was developed (Tsukakoshi *et al.*, 1984). This technique employs either continuous wave (CW) or pulsed laser sources of different wavelengths to deliver exogenous matter into mammalian cells (Palumbo *et al.*, 1996, Paterson *et al.*, 2005). To achieve this, a tightly focused laser beam spot is tailored and employed to generate a high precision “self-healing” pore on the cell plasma membrane (photoporation). Through the generated pore, exogenous materials contained in the medium to which the cells are submerged are taken up (Tsukakoshi *et al.*, 1984). Laser assisted delivery of exogenous materials into cells, which is the focus of this dissertation, is discussed in more detail in section 1.6.

1.4 A brief introduction to lasers

A laser is a device which emits directional, coherent and monochromatic light commonly referred to as a laser beam. The term LASER is an acronym which stands for Light Amplification by Stimulated Emission for Radiation. As suggested by the term, the action of a laser is governed by the process of stimulated emission. A laser is composed of a lasing material (crystal, gas, dye, etc), a pump source which adds energy to the lasing material (flash lamp, electrical current, etc) and an optical cavity. The optical cavity consists of a totally reflective mirror and a partially reflective mirror (Figure 1.1) (Milonni *et al.*, 2010).

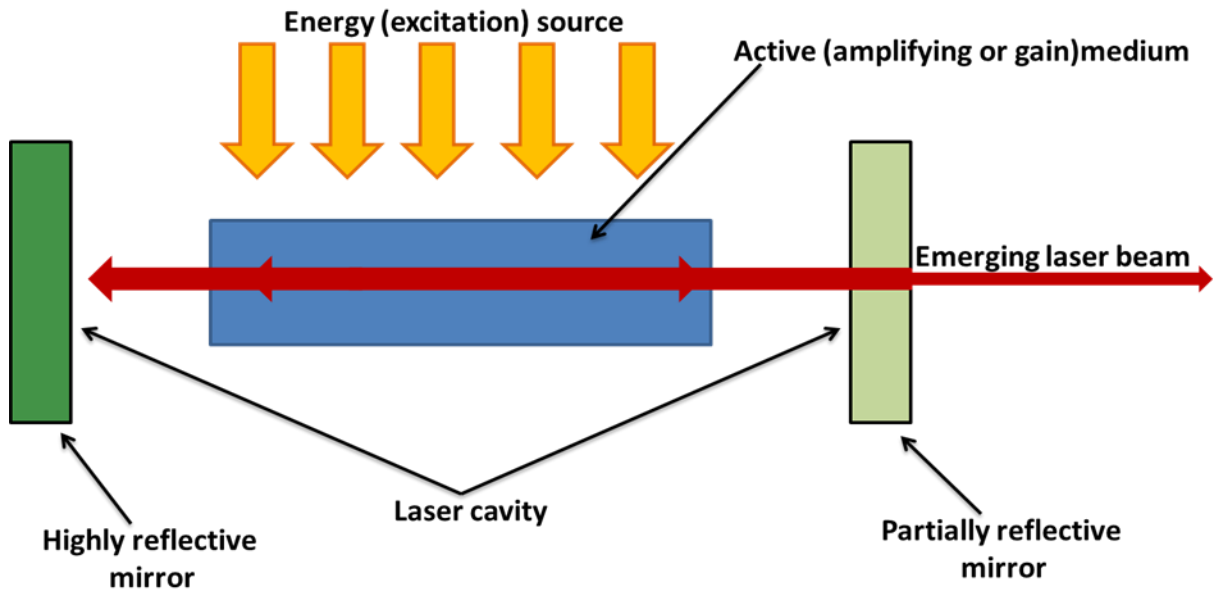


Figure 1.1: Schematic representation of basic laser components and operation.

In the lasing material are atoms to which electrons are contained. Electrons are normally in a steady state lower energy level. Energy is added to the active medium resulting in the excitation of electrons to a higher energy state. Here the electrons are in an unstable state and will stay at this energy level for a brief period of time. The electrons therefore decay back to their original energy state in one of two ways, either by spontaneous decay or by stimulated decay (Milonni *et al.*, 2010). A diagram depicting spontaneous and stimulated decay is shown in Figure 1.2.

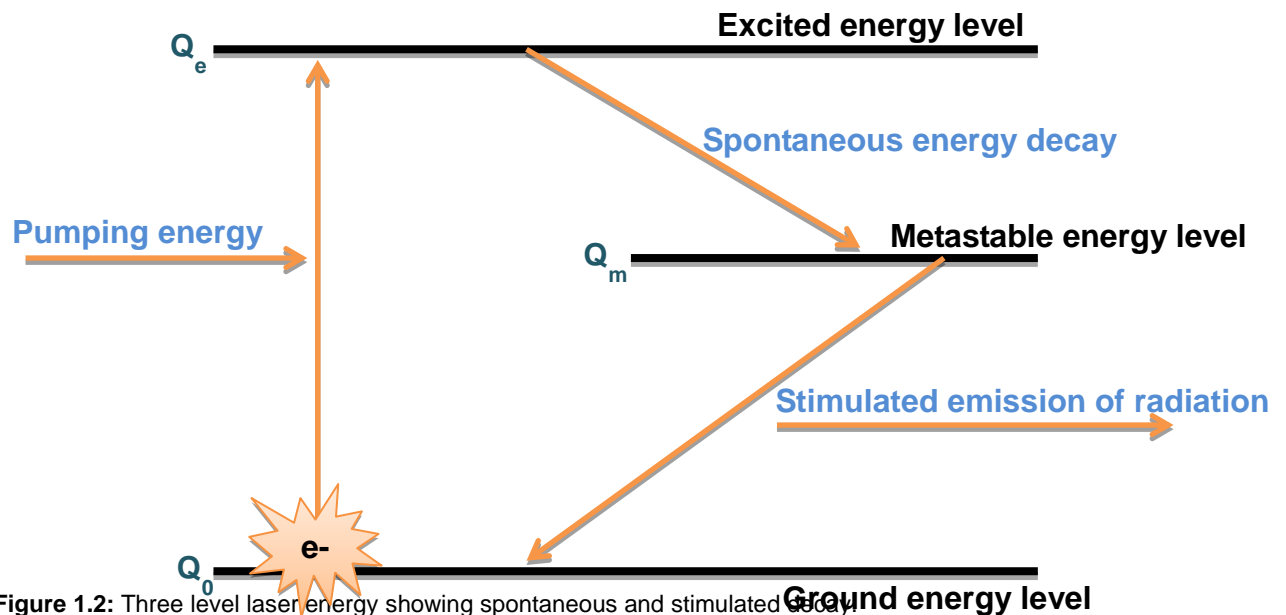


Figure 1.2: Three level laser energy showing spontaneous and stimulated decay.

Q_e , excited energy level; Q_m , metastable energy level; Q_0 , ground energy level; e^- , electron.

During spontaneous decay the electrons fall to the ground state while randomly directed photons are emitted. In stimulated decay, photons from spontaneously decaying electrons strike excited electrons causing them to fall to the ground state. Energy is released in the form of photons of light which travel in phase at the same wavelength and in the same direction as the incident photon. In a case where the direction of the photons is parallel to the optical axis, the emitted photons travel back and forth in the optical cavity through the lasing material as depicted in Figure 1.1. The lasing material is situated in between a totally reflective mirror and a partially reflective mirror (Milonni *et al.*, 2010).

Lasers can either operate in a continuous wave (CW) mode where the power output remains the same irrespective of time or in a pulsed manner. By contrast,

pulsed lasers operate such that the power varies with respect to time at a repetitive rate as shown in Figure 1.3 (Lackner, 2008).

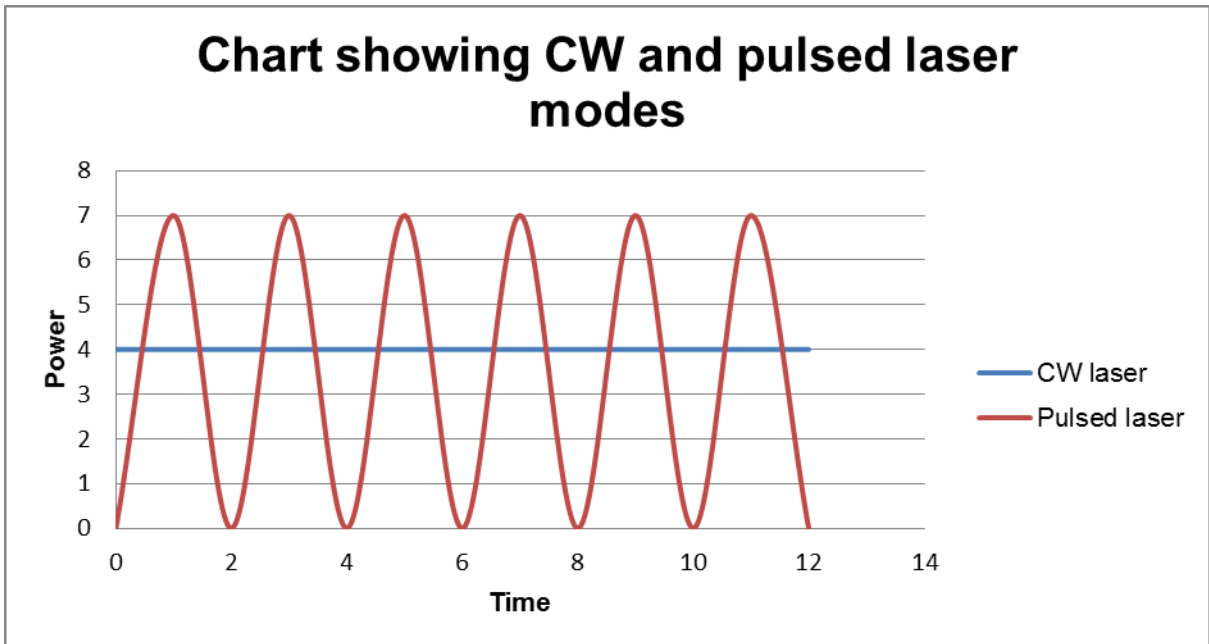


Figure 1.3: Continuous wave (CW) and pulsed modes of laser operation.

CW power levels (in watts) remain constant over time (in seconds; blue) whilst pulsed laser modes (red) experience varying power levels with respect to time.

The output power of pulsed lasers is stored in the power supply of the laser where the stored energy is capable of reaching very high levels. High-intensity laser pulses result from a discharge of the stored energy into the laser whilst the peak power levels of the pulses exceed the power levels attainable with a CW laser beam (Al-Watban *et al.*, 2004).

1.5 Brief overview to Gaussian beams

A variety of lasers exist with different characteristics and specifications, allowing different lasers to be used for different functions. This section of this dissertation

therefore gives a brief background on the propagation of lasers with a Gaussian profile so as to bring to light the functionality of the laser used in this study.

1.5.1 Gaussian beam propagation

Although lasers propagate in a coherent manner, in reality they diverge slightly as they propagate by an angle theta (Θ , see Figure 1.4) away from the beam waist, ω_0 . Angle Θ which describes the angular spread (divergence) from the beam diameter ($2\omega_0$) is given by:

$$\Theta = \frac{\lambda}{\pi\omega_0} \quad (1.1)$$

where λ is the wavelength of the laser light (Saleh *et al.*, 1991). The Rayleigh range, Z_R of a Gaussian beam refers to the distance from the ω_0 where the radius is increased by a factor of $\sqrt{2}$. The Z_R is essentially the standard length used to measure the divergence of the beam and is depicted as:

$$Z_R = \frac{\pi\omega_0^2}{\lambda} \quad (1.2)$$

Both the divergence angle and the Rayleigh range are depicted in Figure 1.4.

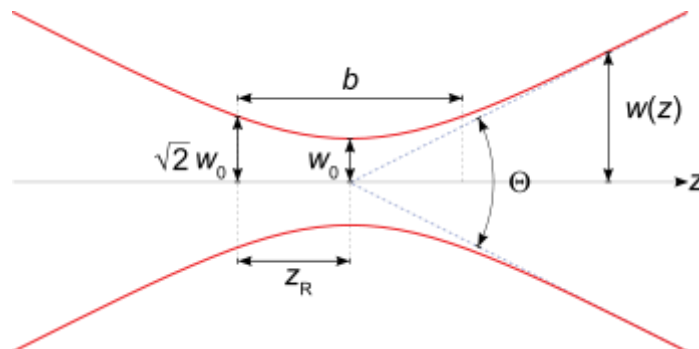


Figure 1.4: Gaussian beam propagation in the Z direction.

The Gaussian beam width $\omega(z)$ changes as a function of distance along the beam. ω_0 : Beam waist; b : depth of focus; Z_R : Rayleigh range; Θ : total angular spread.

The beam depth of focus, b , refers to the axial distance where the beam radius lies within a factor $\sqrt{2}$ of its minimum value. The beam has its minimum width at a propagation distance of $z = 0$ so the best focus of the laser is at the plane $z = 0$. On either sides of this position the beam gradually goes out of focus and the beam waist subsequently increases away from this position (Saleh *et al.*, 1991).

1.5.2 Gaussian beam Intensity

The intensity of any laser is given by $I(r) = |E(r)|^2$ and is a function of the axial and radial distances z and r respectively where r is given as:

$$r = (x^2 + y^2)^{\frac{1}{2}}. \quad (1.3)$$

The intensity of a Gaussian beam can then be expressed as:

$$I(r, z) = I_0 \left[\frac{\omega_0}{\omega(z)} \right]^2 \exp \left[\frac{-2r^2}{\omega^2(z)} \right] \quad (1.4)$$

where the peak intensity is $I_0 = |E_0|^2$. The Gaussian function has its peak at $r = 0$ and decreases monotonically as r increases. A Gaussian beam has its greatest intensity at the position of the beam waist where the peak intensity is at the centre of the beam ($r = 0, z = 0$). The intensity profile of a Gaussian beam is shown in Figure 1.5.

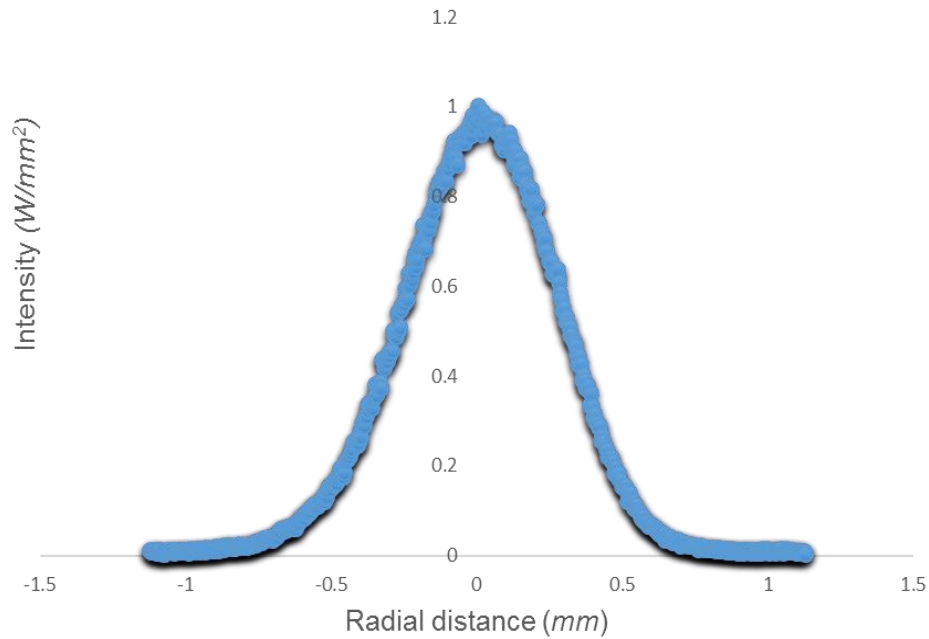


Figure 1.5: Intensity profile of a Gaussian beam.

1.6 Application of lasers to delivering therapeutics in biomedical research

Various types of laser sources have been used in the biomedical research arena for successful introduction of exogenous agents in *in vitro* transfections. When first demonstrated, Tsukakoshi *et al.*, (1984) used a nanosecond (ns), pulsed laser in the ultraviolet (UV) region of the electromagnetic (EM) spectrum (Tsukakoshi *et al.*, 1984). Since then, utilized laser sources have varied from CW lasers within the visible range of the EM spectrum (Palumbo *et al.*, 1996, Schneckenburger *et al.*, 2002, Paterson *et al.*, 2005) to pulsed laser sources in the near-infrared (NIR) spectral region (Tirlapur *et al.*, 2002, Stevenson *et al.*, 2006, Uchugonova *et al.*, 2008). The mechanism of CW laser based photo-transfection is based on single photon absorption and photochemical effects (Schneckenburger *et al.*, 2002). The highest transfection efficiencies obtained through this mechanism are in the range of 30% (Schneckenburger *et al.*, 2002) however, due to the high irradiance

thresholds required for CW membrane permeabilisation, ablative effects and subsequent cell damage follows laser irradiation.

In the case of pulsed laser sources, the delivery of exogenous materials into the cells has been achieved using ns, picosecond (ps) and femtosecond (fs) pulse durations. Nanosecond pulses have been utilised in various studies, as mentioned earlier when the technique was first introduced by (Tsukakoshi *et al.*, 1984), a laser with a 5 ns pulse duration was employed. In a study by Venugopalan *et al.*, (2002), ns lasers at 532 and 1064 nm were employed to investigate the physical processes involved in cell micromanipulation where water was employed to investigate the respective physical mechanisms. This follows results reported by Docchio *et al.*, (1986) where it was shown that in water, ocular and other biological media, the optical breakdown threshold is similar. The results of the study by Venugopalan *et al.*, (2002) indicated that harmful effects such as cavitation bubbles and shock wave dynamics were associated with the use of ns laser pulse durations. From this study it was deduced that employing laser sources with shorter durations would be advantageous as optical breakdown is understood to decrease with decreasing pulse durations (Venugopalan *et al.*, 2002). Picosecond pulses which lie in between ns and fs pulse durations also induce harmful effects in cells but at a milder level than that observed in the case of ns pulses.

First demonstrated by Tirlapur *et al.*, (2002), fs laser sources in the NIR spectral region have become the most understood and most commonly utilised laser source for photoporation and photo-transfection. In their study, Tirlapur *et al.*,

(2002) reported being able to achieve transfection efficiencies of 100% irrespective of which cell line they used for their experiments. Furthermore they reported that no harmful effects were detected within the treated cell populations. Compared to the ns laser used by Tsukakoshi *et al.*, (1984), Tirlapur *et al.*, (2002) used a fs pulsed titanium sapphire laser with a repetition rate of 80 MHz and a wavelength of 800 nm. Here the viability of the transfected Chinese hamster ovary (CHO-K1) and the rat-kangaroo kidney epithelial (PtK2) cells remained intact. This comparison between the two laser modes used in these studies was further investigated by Zeigler *et al.*, (2009) when they showed that using a ns pulsed laser source at the UV spectral region (337 nm) yielded a 36% cell viability in NG-108 (neuroblastoma glioma) cells as opposed to a 79% viability when a fs pulsed laser source in the NIR spectral region (770 nm) was used for the transfection experiments.

Femtosecond laser sources in the NIR spectral region have been demonstrated where fluorescent plasmids were delivered into a variety of cell lines such as HeLa (Henrietta Lacks) (Nioka *et al.*, 2008), HEK (human embryonic kidney) (Mthunzi *et al.*, 2010), CHO (Tirlapur *et al.*, 2002) as well as in stem (Uchugonova *et al.*, 2008) and neuronal cells (Barrett *et al.*, 2006), of which the latter cells have both been reported as difficult cells to transfect. Photoporation has shown successful delivery of fluorescent markers Lucifer yellow (Mallipeddi *et al.*, 2010), green fluorescence protein (GFP) (Mthunzi *et al.*, 2010) and the transcription factor *Elk1* messenger RNA (mRNA) (Barrett *et al.*, 2006). Photoporation is a selective method as it allows targeted treatment of individual cells in a population (Stevenson *et al.*, 2010). The technique has also shown sub-cellular accuracy

where different regions of cells can be targeted preferentially (Barrett *et al.*, 2006). In addition to the fact that fs laser assisted delivery of exogenous material offers higher transfection efficiencies than conventional methods (e.g. 100% (Tirlapur *et al.*, 2002) versus 30% for chemical transfections), the technique is advantageous over the other methods that have been discussed thus far as it offers reproducible results and no direct physical contact with the cell takes place.

Although great strides have been made towards the development of DDS, major drawbacks are their applicability in the clinical setting. In a study by Zeira *et al.*, (2003), energy pulses from a fs titanium sapphire NIR laser were used to deliver plasmids expressing a murine erythropoietin gene into the tibial muscle of mice. Following DNA injection, cells beneath the skin were illuminated by the laser resulting in gentle cell poration. This led to high murine erythropoietin expression with negligible tissue damage in the mice (Zeira *et al.*, 2003). Following that study, Zeira *et al.*, (2007) further modified the fs laser delivery system reported in 2003 such that it included an articulated arm. This modification allowed for precise guided targeting of the laser to desired sites of injection (Zeira *et al.*, 2007). The collaboration of lasers and an articulated arm has also been shown to be effective for *in vivo* use (Chen *et al.*, 2012). Here the articulated arm was employed to optically translocate a hydrophilic model drug sulforhodamine B, methyl blue and a model vaccine antigen ovalbumin into male BALB/c mice models (Chen *et al.*, 2012). With their ability to be precisely focused to the site of injection together with the flexibility of the arm, the technology has potential for gene and drug delivery into larger animals as well as humans (Zeira *et al.*, 2007). A further advantage of laser technologies is that they can be integrated with surgical or

medical devices like endoscopes to reach areas that are non-approachable treatment sites during medical operations or interventions in the clinic (Menezes *et al.*, 2012). There is no literature on the use of fs photo-poration to assist in the delivery of drugs into mammalian cells.

1.7 Mechanisms of fs photoporation

It is essential to understand the physical principals which govern fs photoporation in order to achieve usefulness of the technique and increased efficiencies during experiments.

1.7.1 Laser induced optical breakdown

Laser induced optical breakdown refers to the formation of a plasma in transparent media such as water or biological materials such as cells (Docchio *et al.*, 1988). A plasma is generated in transparent biological media through the formation of quasi-free electrons as a result of an interplay of multiphoton and cascade ionization when high intensity laser pulses are focused onto the transparent medium (Noack *et al.*, 1998). A diagram showing the generation of a plasma through laser induced breakdown is depicted in Figure 1.6.

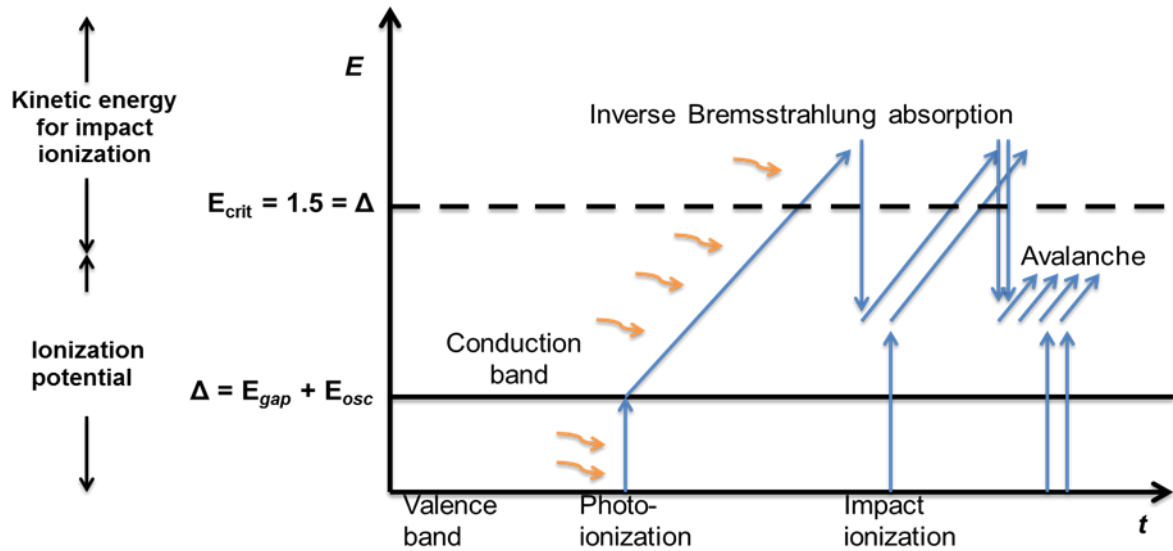


Figure 1.6: Plasma formation through the interplay of multiphoton and cascade ionization.

Repeat cycles of inverse Bremsstrahlung absorption and impact ionization result in the avalanche growth of the number of free electrons. t : time, E : energy, E_{crit} : critical energy, E_{gap} : band gap energy, E_{osc} : oscillation energy and Δ : excitation energy (Redrawn from (Vogel *et al.*, 2005)).

A free electron produced in the active medium absorbs photons in a process known as inverse Bremsstrahlung absorption which refers to the mechanisms involved in the transfer of energy from laser light in matter (Schlessinger *et al.*, 1979). As the photons are being absorbed the electron gains kinetic energy. Absorption by inverse Bremsstrahlung takes place several times after which the gained kinetic energy is large enough to produce another free electron through impact ionization. As a result, two free electrons with slow movement (low kinetic energy) become available. Repetitive cycles of inverse Bremsstrahlung absorption and impact ionization take place and result in the avalanche growth of free electrons (Rudd *et al.*, 1992). It is important to note that the electrons will also collide with heavy charged particles such as ions and atoms at which time a fraction of energy is lost (Rudd *et al.*, 1992). For the avalanche growth in the number of electrons to take place, the irradiance must be high enough to

overcome the losses in free electrons which may have been experienced through the diffusion of electrons from the focal volume (Stuart *et al.*, 1996). Also, the energy gained through inverse Bremsstrahlung must be rapid compared to that lost during collisions with heavy particles. This whole process is referred to as avalanche ionization or cascade ionization (Vogel *et al.*, 2005).

1.8 Mechanisms for laser effects on biological cells and tissues

Femtosecond laser induced cell permeabilization research has come a long way in understanding the mechanisms involved in the functionality of the technique. The majority of the studies that have been reported (Mthunzi *et al.*, 2010, Tirlapur *et al.*, 2002, Uchugonova *et al.*, 2008, Zeira *et al.*, 2003) have made use of lasers with high laser oscillation repetition rates in the range of 80 MHz and pulse energies below the optical breakdown threshold (Vogel *et al.*, 2005). This however only accounts for one of the treatment regimens available for photoporation. The other employs laser oscillators which emit low repetition rates of 1-kHz. These are not commonly used in studies due to the fact that they result in bubble formation as they are slightly above the optical breakdown threshold (Vogel *et al.*, 2005).

Using the 80 MHz regime, 40 000 to several million pulses have been utilised at one spot of the cell membrane to induce permeability (Koenig *et al.*, 2002). On the other hand, 30 to several hundred pulses have been used for the same purpose using 1-kHz repetition rates (Heisterkamp *et al.*, 2005, Maxwell *et al.*, 2005). Using low repetition rate oscillators, cavitation bubbles which are known to induce damage on the cell's integrity have been reported. In Figure 1.7 below an

overview of experimental damage, transfection and dissection thresholds on biological cells is shown. These are shown in conjunction with different low-density plasma effects and physical breakdown phenomena (Vogel *et al.*, 2005).

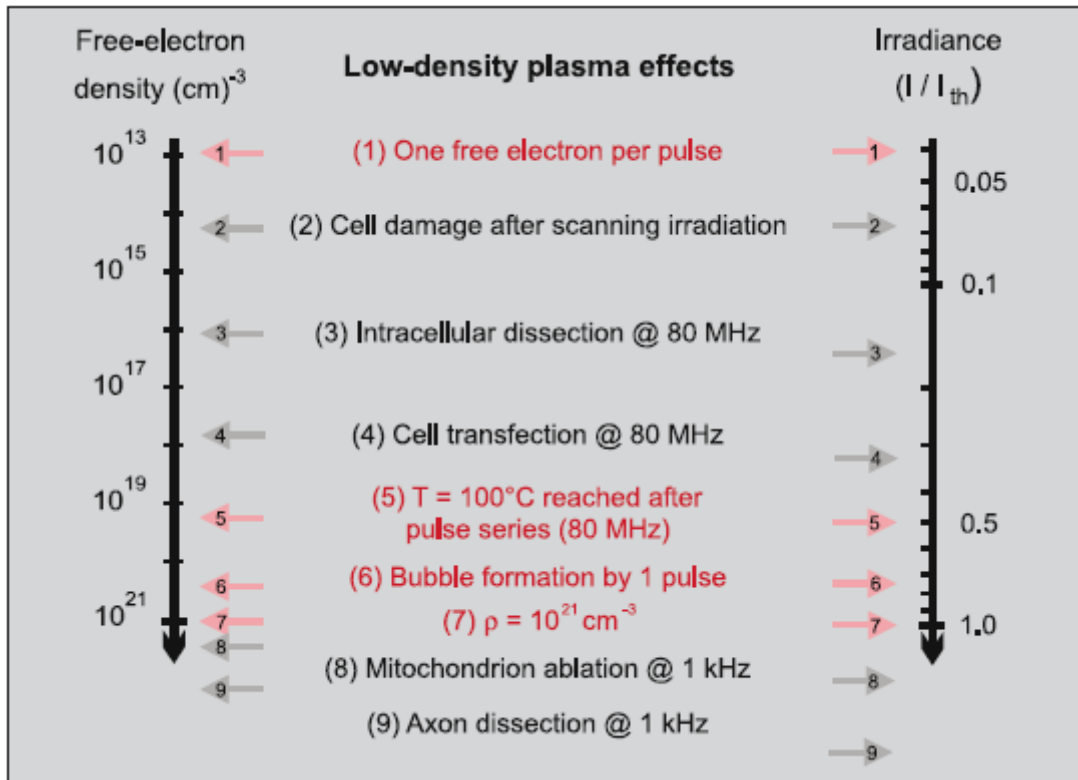


Figure 1.7: Summary of physical breakdown phenomena on biological cells as induced by fs laser pulses.

The different effects are shown alongside corresponding values of free electron densities and irradiances where the values are normalised to the optical breakdown threshold I_{th} . I_{th} is defined by a critical electron density of $Q_{cr}=10^{21} \text{ cm}^{-3}$. Copied from (Vogel *et al.*, 2005).

Overall, where the choice of which type of laser source is optimal to achieve enhanced permeability of biological cells with the aim to enable cells to take up exogenous materials is in question, fs pulsed laser sources take precedence over ns, ps and CW laser sources. Also, repetition rates of 80 MHz are preferred over 1-kHz as they do not often result in negative effects such as bubble formation. The photochemical effects induced by fs lasers through the generation of free electrons are spatially confined to precisely the exposed spot on the cell

membrane. Furthermore, the energy levels required to achieve cell ablation are very low thereby shielding the cells from detrimental effects such as cavitation bubbles and shockwaves which are kept to an absolute minimum in the case of fs laser sources at high repetition rates.

1.9 Photo-translocation of drugs

Femtosecond photoporation is a high precision technique whose applicability to various cell lines to deliver various exogenous materials is discussed in section 1.6. The concept of the technique is described in section 1.3.5. To date, the laser based technique discussed here has not yet been used to deliver drugs into target cells (photo-translocation). Since the use of current DDS lead to unwanted side effects as drugs are able to accumulate in unaffected tissues and organs, a DDS involving the use of a laser is an attractive alternative to the safe delivery of drugs directly into target sites.

1.10 Photo-translocation: It's application to the clinical setting

Although demonstrated at a cellular and *in vitro* level, photo-translocation of drugs would also be suited *in vivo* for drug delivery into tissues, organs, bones and muscles. This technology has applicability in assisting with the delivery of therapeutic agents of various diseases including but not limited to non-communicable diseases such as cancer and cardiovascular diseases as well as communicable diseases such as *Mycobacterium tuberculosis* (TB), human immunodeficiency virus type 1 (HIV-1) and the Ebola virus. The technology could also be used in targeting difficult to reach areas where drug penetration is limited by the presence of physiological barriers (such as the blood brain barrier (BBB)).

The application of laser sources to the delivery of exogenous material such as fluorescent plasmids has been demonstrated *in vitro* by various studies (Mthunzi *et al.*, 2010, Tirlapur *et al.*, 2002, Uchugonova *et al.*, 2008, Zeira *et al.*, 2003) and the potential of lasers as a DDS to reach the clinical setting has been one of the major concerns of this technology. In a patent, US Pat No 5 925 012 issued on July 20, 1999 to Murphy-Chutorian, they showed that they developed an apparatus with the ability to dispense predetermined amounts of therapeutic agents into target areas of the human body. The application of the apparatus is disclosed in the patent where the apparatus is described in detail. The administration of the drug is suggested to be possible through administration in an opening (such as a cut) in the human body. The described apparatus consists of a laser inlet and a drug inlet. The laser inlet is used to guide a means to deliver the laser light such as an optical fibre to the target body structure where an opening will be generated. The drug inlet is designed to receive and transmit the drug to the created opening. Daniel *et al.*, (1999) describes that the administration of the drug would be by manual or automated actuation of a piston or syringe element. Although these studies were done to demonstrate the use of a laser as a DDS, the application of the apparatus to deliver the drugs *in vitro* and *in vivo* have not yet been demonstrated.

By using such an apparatus and incorporating an articulated arm for better direction as well as a camera as in the case of endoscopy as suggested by Zeira *et al.*, (2007) the administration of drugs in a localised manner may be achievable in the clinical setting. A DDS of this nature would allow drug administration into tissues thus minimizing the amount of drug required, minimizing dosing periods

and in turn decreasing the costs of treatments. Confining administration of therapeutics to defined target locations of the body would also enable otherwise toxic drugs to be delivered in a controlled manner.

1.11 Photo-translocation: It's application to intracellular infections

Intracellular infections such as mycobacterial infections, malaria and HIV-1 are some examples where the antimicrobial treatment requires delivery of drugs directly into infected cells, tissues or organs (Briones *et al.*, 2008). For the purposes of this proof-of-principle study we will only focus on HIV-1 infection.

In this study, the use of lasers is employed to assess whether antiretroviral (ARV) drugs which already exist in the pharmaceutical market for treating HIV-1 can be more efficiently delivered into target cells by photo-translocation. Photo-translocation is therefore defined as a laser based technique that utilizes laser light sources as a means to facilitate or improve on the intracellular delivery of exogenous materials such as ARV drugs (Figure 1.8).

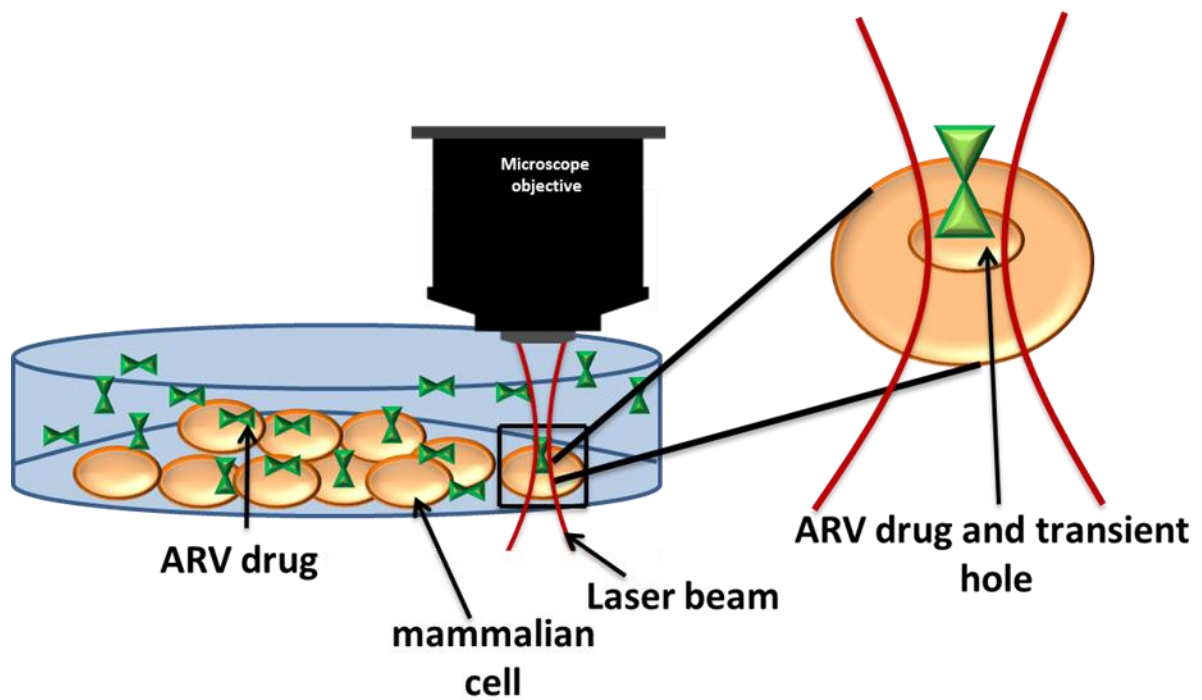


Figure 1.8: Schematic representation of a sample chamber with adherent HIV-1 permissive cells in an ARV drug and growth medium solution.

A focused laser is shown during the process of cell membrane poration where subsequent diffusion of the ARV drug through the generated pore takes place.

Additional advantages making laser based techniques desirable for drug delivery are that the technique can be coupled with various optical techniques such as microscopy (Stevenson *et al.*, 2010) that permit real time viewing of *in vitro* drug delivery studies.

1.11.1 Epidemiology of HIV-1

HIV-1, the causative agent for acquired immunodeficiency syndrome (AIDS) infects clusters of differentiation 4 positive (CD4⁺) T lymphocytes of the human immune system (Ratner *et al.*, 1985, Barre-Sinoussi *et al.*, 1983). By depleting CD4⁺ T lymphocytes the virus progressively reduces the effectiveness of the immune system leaving infected individuals susceptible to opportunistic infections

and tumors, ultimately leading to death (Klatzmann *et al.*, 1984, Lifson *et al.*, 1986).

1.11.2 HIV-1 life cycle and potential ARV drug targets

Several steps in the HIV-1 replication cycle are potential targets for therapeutic interventions. The first step of the cycle is the attachment of the virus using surface envelope (env) glycoprotein, gp120, to the host cell surface receptor (CD4) (Maddon *et al.*, 1986). This step is followed by a conformational change in env which enables gp120 to bind to a cellular chemokine co-receptor (C-X-C motif receptor type 4 (CXCR4) or C-C chemokine receptor type 5 (CCR5)) (Alkhatib *et al.*, 1996). The env glycoprotein gp41 then interacts with the host cell plasma membrane which results in the fusion of the membranes of the virus and the host cell (Kowalski *et al.*, 1987, Eckert *et al.*, 2001). Currently United States (US) Food and Drug Administration (FDA) approved entry inhibitors bind to either env proteins or to chemokine coreceptors to prevent the virus from entering the cell (Este *et al.*, 2007).

Following fusion, the conical shaped viral core (p24) is deposited into the host cell's cytoplasm. The viral core contains two copies of single stranded RNA, viral proteins and primer transporter RNA (tRNA) (Ganser *et al.*, 1999). The viral core is then uncoated to enable the viral genetic material to be reverse transcribed into cDNA by the reverse transcriptase (RT) enzyme (Bukrinsky *et al.*, 1993). Nucleoside reverse transcriptase inhibitors (NRTIs) can inhibit this step by being preferentially incorporated into viral DNA to act as chain terminators (Furman *et al.*, 1988). Non-nucleoside RTIs (NNRTIs) are also able to inhibit this conversion

by directly binding to RT. The newly synthesized viral DNA binds to HIV-1 integrase, and a range of other viral and host proteins to form of a pre-integration complex (PIC) which is then translocated into the nucleus of the host cell (Bowerman *et al.*, 1989). The viral DNA is irreversibly inserted into the host's genome by viral integrase, and the integration process is completed by the host DNA repair elements to form a provirus (Goff, 1992, Bowerman *et al.*, 1989). Strand transfer integrase inhibitors prevent the integration process in the nucleus. The provirus then follows one if two possible routes. It can either be transcribed to ultimately form new progeny virions or can lie dormant in a state of latency (Siliciano *et al.*, 2004). Viral proteins are transcribed, and a range of viral mRNA's (singly, multiply spliced and unspliced) are translated in the cytoplasm to generate all the necessary viral proteins. The envelope glycoproteins (gp160) is cleaved by cellular proteases into gp120 and gp41 components, and the gag-pol polyprotein is cleaved by the viral protease enzyme (Sodroski *et al.*, 1986).

The final steps of the HIV-1 life cycle are viral assembly, budding and maturation. Assembly involves the packaging and creation of the virus where HIV proteins are recruited to the cell membrane. The budding process encompasses the immature virus budding out of the cell with the host plasma membrane components within which the viral envelope glycoproteins are embedded. The final step which is maturation involves completion of the gag-pol polyprotein cleavage, which permits the virus to be able to infect subsequent cells. HIV-1 protease is the enzyme responsible for the maturation process (Warnke *et al.*, 2007). Protease inhibitors prevent gag-pol polyprotein cleavage, resulting in immature, non-infectious virions. An illustration of the viral life cycle is shown in Figure 1.9.

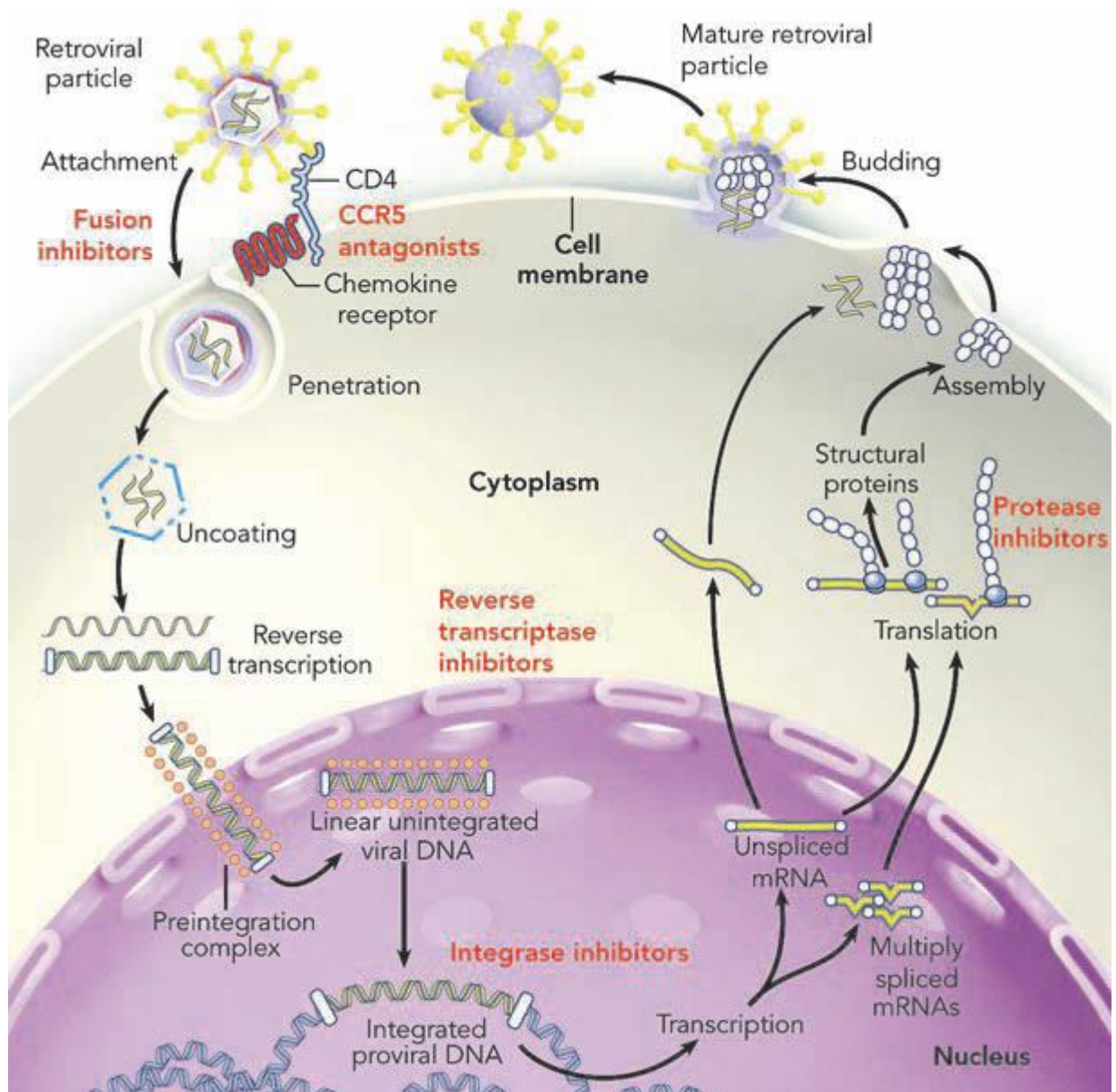


Figure 1.9: Life cycle of HIV-1 and site of action of antiretroviral therapy (red text).

Adapted from (Furtado *et al.*, 1999).

1.11.3 Current HIV-1 treatment

The current treatment for HIV-1 infection, termed highly active antiretroviral therapy (HAART), involves the oral administration of a combination of a minimum of three US food and drug administration (FDA) approved ARV drugs. The drugs prevent progression of HIV-1 infection to AIDS by blocking or interfering with specific parts of the viral life cycle (Martinez *et al.*, 2002a, Warnke *et al.*, 2007).

FDA approved ARVs are grouped into four categories according to their mechanism of action, namely entry inhibitors (EI, e.g. maraviroc), RTIs (nucleoside RTIs (NRTI, e.g. tenofovir) and NNRTI (e.g. efavirenz)), integrase inhibitors (INs, e.g. raltegravir) and protease inhibitors (PI, e.g. ritonavir) (Arts, 2012).

The introduction of HAART has over the years decreased AIDS related mortalities subsequently increasing the life expectancy of HIV-1 infected persons (Sharma *et al.*, 2010). However, HAART faces challenges and limitations that are cause for concern. Once HAART is initiated, treatment is lifelong, which can result in toxicities, as well as the inevitable emergence of ARV drug resistance (Este *et al.*, 2010). Host genetics, which impact on plasma and intracellular concentrations of ARVs is an additional concern. Furthermore, since HAART cannot target the latent viral reservoirs there is currently no cure for HIV-1 infection (Katlama *et al.*, 2013). ARV drugs possess a poor targeting ability to latent sites of infection including the CD4⁺ memory T cells, lymphatic system, macrophages, the central nervous system and the lungs (Sharma *et al.*, 2010, Reviewed by Alexaki *et al.* (2008)). More specifically, in the lungs and brain HIV-1 is contained in alveolar macrophages and microglia respectively, to which the drugs are not able to penetrate (Von Briesen *et al.*, 2000, Hu *et al.*, 2000). Since the existing US FDA approved ARV drugs are not able to eradicate latent virus, novel drugs and DDS to target this integrated provirus are required.

Worldwide, there is a major drive to understand and try eradicate HIV-1 from the latent reservoirs, resulting in a “functional” cure or cure. A DDS with the future ability to deliver therapeutic concentrations of novel ARV drugs which specifically

target integrated proviruses in latent sites in patients on HAART with undetectable viral loads presents a novel approach towards eradication of HIV-1. Viral reservoirs are established early in HIV-1 infection and they hinder sterilizing immunity while also hindering possibilities of curing the infection with the potent ARV drug regimens currently in use (Dahl *et al.*, 2010, Shen *et al.*, 2008). Following successful ARV therapy, virus levels in the plasma of many patients becomes undetectable. The long term persistence of HIV-1 is due to the presence of cellular and anatomical reservoirs. Of the known reservoirs the most alarming is that consisting of latently infected resting memory CD4⁺ T cells which carry integrated HIV-1 DNA (Pierson *et al.*, 2000). HIV-1 latency can be described as integrated provirus with no active transcription and therefore no replication (Kulkosky *et al.*, 2002). Since the existing US FDA approved ARV drugs are not able to eradicate latent virus, novel drugs to target this integrated provirus are required. The majority of the latent virus is found in CD4⁺ T cells of the memory phenotype where the half-life is a long period of up to 44 months (Blankson *et al.*, 2002).

1.11.3.1 HIV-1 disease progression

The clinical course of HIV-1 infection is made up of three phases namely; acute primary infection, clinically asymptomatic infection and the symptomatic HIV-1 infection, and progression to AIDS phase (Cohen *et al.*, 2010).

The acute primary infection phase which can last up to 6 months, until the patient seroconverts, and is when HIV-1 infection is established (Lyles *et al.*, 2000). This phase is characterised by a rise in viral levels in the plasma as the virus is allowed

to replicate uncontrollably (Clark *et al.*, 1991) and allowed to spread to lymph nodes and then into the bloodstream. Infected cells can be lysed or they can manifest into latent infection where macrophages and resting CD4⁺ T cells establish themselves as viral reservoirs (Zack *et al.*, 1988). Following a rise in viral levels an immune response is elicited by cytotoxic T lymphocytes (CTLs). A decrease in the viral levels in the plasma is subsequently observed, reaching a set point (Ogg *et al.*, 1998). A graphical representation of HIV-1 disease progression to AIDS is shown in Figure 1.10.

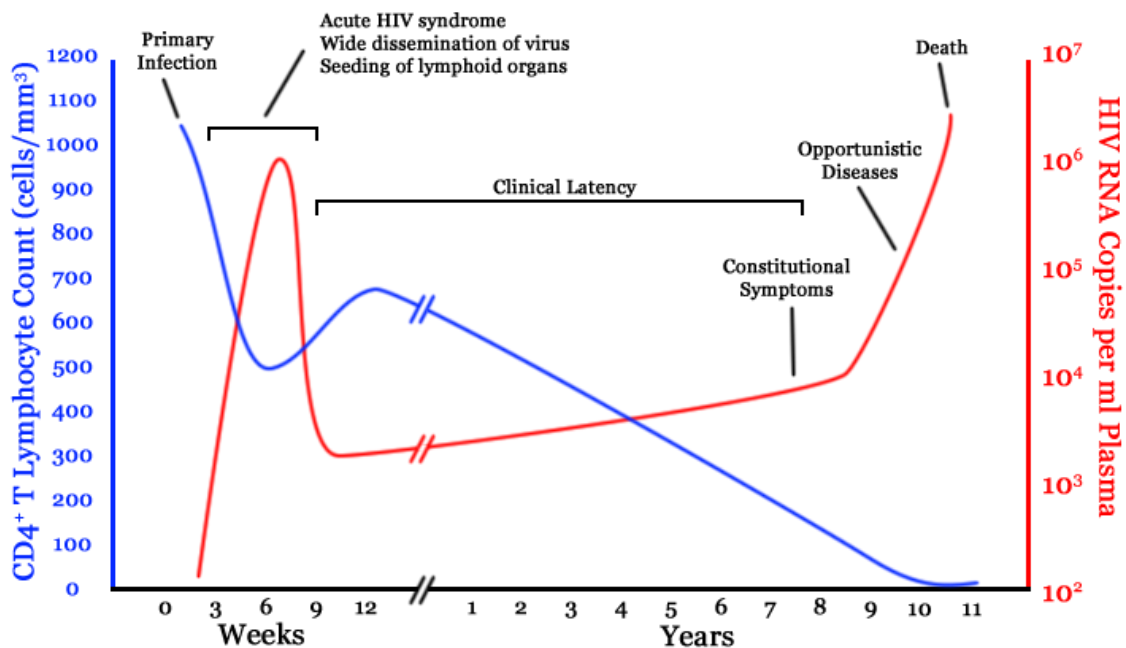


Figure 1.10: Graphical representation of HIV-1 disease progression

HIV-1 disease progression as a relationship between the changing levels of the CD4⁺ T cell count (cells/ μ l) and the HIV RNA copies (per ml) in the plasma. The blue line represents the CD4⁺ T cell count while the red line represents the HIV RNA copies/mL of plasma. Obtained from http://en.wikipedia.org/wiki/HIV#mediaviewer/File:Hiv-timecourse_copy.svg (Access date: 10 September 2014).

The second phase is the asymptomatic phase where there is an absence of symptoms. This period which can last for up to 10 years is characterised

maintenance of the viral load set point in the plasma (Iwami *et al.*, 2008). This decline in viral load is due to the innate and adaptive immune responses of the host where antibodies bind to viral particles or cause the elimination of infected cells (Stamatatos *et al.*, 2009). During this period infected cells are eliminated as T-lymphocytes which are specific to HIV-1 recognise the virus antigens that are presented on the surface of infected cells. While this elimination process occurs the HIV-1 continues to replicate and counteract the effects of the host's immune responses while establishing a stage of chronic systemic inflammations (Fauci, 1993). The final stages of the asymptomatic phase sees the infected persons undergo a slow but progressive loss of CD4⁺ T cells where the immune system is subsequently led to its detriment (McCune, 2001). The CD4⁺ T cell depletion occurs predominantly in the GIT (Brenchley *et al.*, 2004) and sees the architecture of the lymphoid tissue go through a destruction which renders it permeable to viral diffusion to surrounding CD4⁺ T cells. In turn, the virus is allowed to spread within the local, regional and whole lymphoid environments ultimately leading to a speedier progression to AIDS (Brenchley *et al.*, 2004, Mehandru *et al.*, 2004).

Symptomatic HIV-1 infection and progression to AIDS is the final phase of disease progression and is characterised by the weakening of the immune system. This is caused by a further decline in CD4⁺ T cells to levels lower than 200 cells/ μ l in the blood. Consequently the body is left susceptible to opportunistic infections (Brooks *et al.*, 2009). Some infections which are prevalent among AIDS patients and often display limited clinical infection in healthy individuals include *Candida albicans*, *Pneumocystis carinii*, *Cryptosporidium parvum* and *Toxoplasma gondii* (Kasper *et al.*, 1998). During this AIDS phase patients present with symptoms

such as a reduction in body weight, respiratory and GIT symptoms while anemia and lymphopenia are normally detected during this phase (Revicki *et al.*, 1995, Lucas, 1990). In the absence of treatment regimens, the Joint United Nations Programme for HIV/AIDS (UNAIDS) and the World Health Organisation (WHO) predict that a person infected with HIV-1 should live a period of approximately 11 years before perishing from AIDS-related illnesses.

During 2012 there were 2.1 million new infections with 35 million persons already infected with HIV-1 worldwide (UNAIDS, 2014). South Africa (SA) currently has approximately 6.3 million HIV-1 infected individuals, of which over 2.4 million people are receiving HAART. In addition, there were approximately 370 000 new infections in 2012 (UNAIDS, 2014). The high numbers of South Africans that will require HAART for their lifetime highlights the severity of the problem. The long term toxicities associated with ARV combination therapy and the substantial financial implications necessary to treat all the patients that will still need treatment for their lifetime calls for urgent and novel approaches to eradicate latent reservoir sites (Pierson *et al.*, 2000). ARV therapy is vital to the treatment of HIV-1 however, in its present form it is not likely to eradicate HIV-1 from infected persons. Novel strategies and approaches should therefore focus on eradicating latent reservoir sites following effective usage of ARV therapy as induction therapy to enable undetectable viral levels to be achieved in the plasma (Kulkosky *et al.*, 2002).

There is currently a major search in the research community for the acquisition of a “functional cure” to eradicate HIV-1 from reservoir sites (Katlama *et al.*, 2013). The major priority of the majority of the studies is the discovery of new molecules with the ability to work safely on their own or in conjunction with other drugs to reactivate viral transcription with high efficiency in latently infected cells (Katlama *et al.*, 2013). This is widely referred to as drug infestation. Continuous rounds of activated viral infection would in this case be blocked by ARV therapy and the productively infected cells would subsequently be destroyed (Lewin *et al.*, 2011, Shan *et al.*, 2012).

This dissertation reports on a proof-of-principle study where a fs laser based DDS is demonstrated by delivering selected ARV drugs into HIV-1 permissive cells. The currently available ARV drugs used for the treatment of HIV-1 are not able to eradicate integrated HIV-1 provirus from reservoir sites. While studies to purge HIV-1 from these sites and other studies continuing to search for and discover novel drugs to target integrated HIV-1 provirus, this study focuses on exploring pulsed fs laser sources for their use as a DDS. This study therefore aims to show that it is possible to facilitate the more efficient delivery of therapeutic drugs (ARVs) into target, TZM-bl cells without compromising their viability. As discussed previously, the technology has been utilized to deliver impermeable fluorescent dyes but has not yet been applied to the delivery of drugs as demonstrated in this study.

1.12 Research objectives

The overall aim of the study was to set up a photo-translocation system to test its applicability in selectively and non-invasively delivering ARV drugs into HIV-1 permissive cells.

This was achieved by the following objectives:

1. To assemble and characterize a photo-translocation set up (in-house).
2. To assess the ability of the in-house photo-translocation setup which contains a fs laser, to deliver ARV drugs into TZM-bl cells and inhibit viral replication.
3. To assess the viability of TZM-bl cells post treatment with the laser as well as ARV drugs.

2. Materials and Methods

2.1 Reagents used in this study

2.1.1 Cell lines

TZM-bl cells, also called JC57BL-13, were obtained from the National Institutes of Health (NIH) AIDS Research and Reference Program ((catalogue (cat.) no. 8129). TZM-bl cells are a HeLa derived, genetically engineered cell line which expresses endogenous CXCR4 and transgenic CD4 and CCR5 on their cell membrane. The HIV-1 permissive cell line also contains Tat-responsive reporter genes for firefly luciferase (*Luc*) and *Escherichia coli* (*E.coli*) β -galactosidase under the control of an HIV-1 (LTR). These cells are highly permissive to infection by various HIV-1 strains including primary and molecularly cloned *Env*-pseudotyped viruses (Brass *et al.*, 2008). TZM-bl cells were used in the laser treatment and in vitro phenotypic inhibition assay experiments. HEK 293T cells were available in our laboratory and used in transfection studies to generate pseudoviruses.

2.1.2 Plasmids used for the generation of molecularly cloned *env*-pseudoviruses

In this study an *Env*-pseudotyped virus, ZM53, which was originally acquired from a Zambian, male patient in the acute or early stage of infection was used (Derdeyn *et al.*, 2004). The HIV-1 *env* expressing ZM53 plasmid (cat. no. 11313) and the HIV-1 backbone plasmid pSG3 Δenv (cat. no. 11051) which contains a defective *env* gene were both obtained from the NIH AIDS Research and Reference Reagent Programme.

2.1.3 ARV drugs used in the study

A NRTI (tenofovir, cat. no. 10199) and two NNRTIs, efavirenz (cat. no. 4624) and nevirapine (cat. no. 4666) were selected for use in this study and obtained from the NIH AIDS Research and Reference Reagent Programme.

2.2 Mammalian cell culture

Both TZM-bl and HEK 293T cells were cultured in a 37°C, 5% carbon dioxide and 85% humidity incubator. The cells were grown routinely in a T-75 vented top culture flask (Nunc™, The Scientific Group, SA). Cells were grown in general medium (GM) containing Dulbecco's Modified Eagle's Medium (DMEM, Sigma Aldrich, SA), 10% fetal bovine serum (FBS, Sigma Aldrich, SA) and supplemented with 1% penicillin-streptomycin (PEST, Sigma Aldrich, SA). The cells were trypsinised routinely at 70-80% confluency and passage numbers were recorded accordingly on the culture flask.

2.2.1 Passaging of HEK 293T and TZM-bl cells

Upon reaching 70-80% confluency, which means that 70-80% of the bottom surface of a T75 tissue culture flask (Nunc, The Scientific Group, SA) was covered by the cell monolayer, the cells were passaged. Working in sterile conditions in a 70 % ethanol disinfected biosafety level 2 hood, the GM in the flask was aspirated. The cell monolayer was washed with pre-warmed 1 × phosphate buffered saline (PBS, Sigma Aldrich, SA) to remove residual FBS. The monolayer was bathed in 0.25 % trypsin EDTA (Sigma Aldrich, SA) and left to stand briefly. The trypsin was aspirated and the flask of cells was incubated in normal cell growth conditions for less than 5 minutes to allow trypsinization and lifting of the cell monolayer. The

cells were then resuspended in GM, quantified (as described in section 2.2.2 below) and 1×10^6 cells returned to the flask (or transferred to a fresh flask) and topped up with an appropriate amount of GM.

2.2.2 Quantification of mammalian cells using a haemocytometer

Cells were resuspended in GM after the process of trypsinisation, and 10 μ l cell suspension was diluted in 40 μ l of trypan blue viability dye (Sigma Aldrich, SA) to make up a 5 times dilution. After gentle mixing, 10 μ l of the sample was loaded onto the counting chamber of a haemocytometer by capillary action. The counting chamber of a haemocytometer is engraved with a laser-etched grid of perpendicular lines consisting of nine 1 \times 1 mm squares. The 0.1 mm depth of the chamber gives each square a defined volume. As such, each of the squares contains a volume of 10^{-4} μ l. The area bounded by the lines and the depth of the counting chamber are known thus making it possible to count the number of cells in a specific volume.

Using a light microscope and focusing onto the grid of the counting chamber, the number of white cells in the four corner quadrants of the grid were quantified. The total number of cells in the four quadrants was averaged by dividing the sum by four. This value was multiplied by the dilution factor (i.e. 5) and by 10^4 . The resultant value gave an approximation of the number of cells per ml which made it possible to seed the required number of cells in an experiment as required.

2.2.3 Generation of molecularly cloned *env*-pseudoviruses

The pSG3^{Δ*env*} and ZM53 plasmids were transformed into competent *E.coli* Top 10 cells. Due to the incomplete genome of *Env*-pseudotyped viruses they are generally incapable of generating infectious progeny virions. The *Env*-pseudotyped viruses are therefore said to be capable of only a single round of infection. The original plasmids were isolated using the Qiagen Maxiprep kit (Invitrogen) according to the manufacturer's instructions (see section 2.2.6 below).

2.2.4 Preparation of competent *E.coli* Top 10 cells

To introduce DNA into bacterial *E.coli* cells (transformation) which are not naturally transformable, the cells have to gain competency. This process which is induced by chemical methods ultimately allows the *E.coli* bacterial cells to take up DNA. The chemical, calcium chloride (CaCl₂, Sigma Aldrich, SA), alters the permeability of the cell membrane thereby allowing DNA to cross the cell membrane.

Luria Bertani broth (LB, 5 ml, Sigma Aldrich, SA) medium (10 g/L bacto-tryptone, 5 g/L yeast extract, 5 g/L sodium chloride in distilled water and autoclaved at 120°C for 25 minutes) was inoculated with *E.coli* Top 10 and grown overnight at 37°C in a shaking incubator set at 200 revolutions per minute (rpm). The overnight culture (1 ml) was used to inoculate 100 ml of LB medium. The culture was shaken in a 37°C water bath until the cell density reached mid-log growth phase (approximately 5×10^7 cells/ml). The growth rate of the culture was determined by removing 1 ml aliquots of culture at various intervals after which the optical density was read at a 550 nm wavelength using a spectrometer. The culture was chilled on ice for 10 minutes and the cell suspension spun at 4000 g in a centrifuge for 5

minutes at 4°C. The supernatant was discarded ensuring that the pellet was not dislodged. The pellet was resuspended in 50 ml of the original culture that contained 60 ml of sterile CaCl₂ and 15% glycerol. The cell suspension was placed in an ice bath for 30 minutes and then centrifuged at 4000 g for 5 minutes at 4°C after which the supernatant was discarded. The pellet was gently resuspended in 5 ml of sterile ice-cold CaCl₂ using pre-chilled pipettes. Aliquots of 50 µl were prepared and the competent *E.coli* Top 10 cells were stored for long term usage at -80°C.

2.2.5 Transformation of competent *E.coli* Top 10 cells

Competent *E.coli* Top 10 cells were thawed and kept on ice throughout the duration of the experiment to ensure that loss of competency was minimised. *Env* pseudotyped viral plasmid (1 µl, ZM53 and pSG3^{Δ*env*}) was transferred to eppendorf tubes that contained 25 µl of thawed competent *E.coli* Top 10 cells. A negative control was prepared by transferring 26 µl of the cells into a separate eppendorf tube. The tubes were incubated on ice for 30 minutes. Following that, the samples were heat shocked at 42°C for 45 seconds and immediately kept on ice for 2 minutes. The temperature shift enabled the cells to take up the ligation mixture. Super optimal broth (SOC, Sigma Aldrich, SA) medium (250 µl) was added to the cells and incubated at 37°C in a shaking incubator at 200 rpm for 30 minutes. An additional 1 ml of SOC was added to the cell mixture and 25 µl plated aseptically on LB agar (10 g/L bacto-tryptone, 5 g/L yeast extract, 10 g/L sodium chloride in distilled water and autoclaved at 120°C for 25 minutes) supplemented with 100 µg/ml of ampicillin (Fermentas). The agar plates were incubated overnight in a 37°C incubator. A colony was aseptically inoculated into a 50 ml

falcon tube that contained 5 ml of LB broth supplemented with 100 µg/ml of ampicillin. The inoculated medium was incubated in a shaking incubator at 37°C, 200 rpm for 8 hours. The 5 ml culture was transferred to 200 ml of LB supplemented with 100 µg/ml of ampicillin and then incubated at 37°C, 200 rpm for 16 hours.

2.2.6 Isolation of DNA plasmids using the Qiagen Maxiprep kit

The Qiagen plasmid purification kits (Whitehead Scientific, SA), used in this study are based on a modification of an alkaline lysis procedure and the subsequent binding of plasmid DNA to an anionic-exchange resin in low salt and pH conditions. DNA is eluted with a high-salt solution, and the purified DNA is concentrated and desalted by precipitation using isopropanol.

The overnight culture that was obtained as the final product of *E.coli* transformation was retrieved from the shaking incubator and the bacterial cells were harvested by centrifugation at 6000 × g for 15 minutes at 4°C. The bacterial pellet was resuspended in 10 ml of resuspension buffer P1 (50 mM Tris-Cl, pH 8.0, 10 mM EDTA, 100 µg/ml RNase A). Lysis buffer P2 (10 ml; 200 mM NaOH, 1% SOS (w/v) was added and mixed gently by inverting 4-6 times followed by an incubation period of 5 minutes at room temperature. Chilled neutralisation buffer P3 (10 ml; 3.0 mM potassium acetate, pH 5.5) was added, the solution was mixed immediately by gentle inversion and incubated on ice for 20 minutes. The solution was centrifuged at 4°C, at 2000 × g for 30 minutes. The DNA plasmid containing supernatant was removed immediately and centrifuged once more under the same conditions. A Qiagen-tip 500 was equilibrated by applying 10 ml of equilibration

buffer QBT (750 mM NaCl, 50 mM MOPS, pH 7.0, 15% isopropanol (v/v); 0.15% Triton X-100 (v/v)) where the column was allowed to empty completely by gravity flow. The supernatant was then applied to a Qiagen-tip and allowed to enter the resin by gravity flow. The Qiagen-tip was washed twice with 30 ml of wash buffer QC (1.0 M NaCl, 50 mM MOPS, pH 7.0, 15 % isopropanol) and then the DNA was eluted with elution buffer QF (1.25 M NaCl; 50 mM Tris-Cl, pH 8.5, 15 % isopropanol (v/v)). The DNA was precipitated by adding 10.5 ml of room temperature isopropanol to the eluted DNA. The DNA solution was immediately pelleted by centrifugation at 15 000 × g for 30 minutes at 4°C. The supernatant was carefully decanted and the DNA pellet washed with 5 ml of 70% ethanol and further pelleted at 15 000 × g for 10 minutes. The supernatant was decanted ensuring that the pellet was not dislodged. The DNA pellet was air-dried for 5-10 minutes and redissolved in a suitable volume of distilled water. The DNA was stored at -20°C.

2.2.7 Co-transfection of HEK 293T cells

The *Env*-pseudotyped virus was generated by co-transfecting HEK 293T cells with the *env*-expressing ZM53 plasmid and the backbone plasmid pSG3^{Δ*env*}. Here 2.8 × 10⁶ HEK 293T cells were pre-seeded in a 6 cm tissue culture treated petri dish which contained 10 ml GM and incubated in appropriate growth conditions. A DNA mix was prepared by adding 10 µg of the ZM53 plasmid and 10 µg of pSG3^{Δ*env*}. The mix was filled up to a final volume of 300 µl with serum and antibiotic starved GM. Superfect (60 µl, Invitrogen, SA) was added to the DNA, mixed by vortexing and incubated for 15 minutes at room temperature. The cells were retrieved from the incubator and the cell monolayer was washed with 5 ml of

PBS (Sigma Aldrich, SA). GM (3 ml) was added to the DNA-Superfect solution and transferred to the cell monolayer. The cells were incubated for 3 hours under normal growth conditions. The medium was aspirated and the cell monolayer washed with PBS (5 ml) to remove residual DNA and transfection reagent. The cells were fed with GM (10 ml) and incubated for 48 hours under normal growth conditions.

2.2.8 Harvesting of *Env*-pseudotyped virus

Forty eight hours post transfection, the culture supernatant containing the pseudovirus was clarified from cells by filtration using a 0.45 µm filter. Aliquots were made and stored at -80°C.

2.2.9 *Env*-pseudotyped virus titration

The titration of *env*-pseudotyped viruses is imperative for the optimal performance of HIV-1 inhibition assays that were carried out in this study. The dosage of *Env*-pseudotyped virus to use in the inhibition assay was determined using the 50% tissue culture infectious dose (TCID₅₀) method. The TCID₅₀ refers to the amount of *Env*-pseudotyped virus with the ability to infect 50% of the inoculated cultures of TZM-bl cells.

The TCID₅₀ was determined by adding 100 µl of GM into all wells of a 96-well, flat bottom tissue culture treated plate (The Scientific Group, SA). *Env*-pseudotyped virus (25 µl) was added to the first four wells (column 1, rows A-D) of the 96-well plate where 5-fold serial dilutions were carried out by the transfer of 25 µl of the

pseudovirus to upper wells for a total of 11 dilutions. Column 12 of the 96-well plate was used for the cell control where no *Env*-pseudotyped virus was added. TZM-bl cells (10^4 cells/100 μ l in GM containing DEAE dextran (Sigma Aldrich, SA) to a final concentration of 20 μ g/ml in each well) were added to all wells of the 96-well plate. The plate was incubated for 48 hours in a 37°C, 5% CO₂ and 85% humidity environment. The detection system that was used for the assay was the Bright Glo luciferase substrate (Anatech Instruments, SA). Here the infectivity of the *Env*-pseudotyped virus was measured according to the expression of the *Luc* reporter gene in the TZM-bl cells after a single round of viral infection. The substrate functions to lyse the cells and cause luminescence of successfully infected cells. The relative luminescence units (RLU) were quantified using the Tecan Infinite F500 microplate reader. The TCID₅₀ dose that was used was calculated using Assay Excel Macros provided online by (Montefiori, 2009). Here the TCID₅₀ dosage is calculated based on the Reed and Muench formula (shown in Appendix B-3) where a cut-off value of RLU < 2.5 times the background was considered negative for the calculation (Reed, 1938). The *Env*-pseudotyped viruses that yielded between 15 000 and 150 000 RLU equivalents was selected.

2.3 Assembly and characterisation of a home built photo-translocation system

A commercial Fianium FemtoPower 1060-fs laser (Fianium, UK) and additional components were used to assemble a photo-translocation setup (described in section 2.4) with the ability to facilitate the targeted delivery of ARV drugs into TZM-bl cells. Extensive characterisation of the laser beam was undertaken to ensure that the laser specifications obtained in our laboratory matched those

reported by the manufacturer. The characterisation experiments which were investigated namely; the repetition rate, central wavelength, pulse duration, beam quality and beam diameter of the laser beam were crucial for the accurate assembly of the photo-translocation setup. Optimal functionality of the laser and assembled setup would facilitate successful ARV drug delivery in the planned experiments.

2.3.1 Validation of laser pulse trains and measurement of the repetition rate

To confirm the consistency of the pulses emitted by the laser, the laser pulse trains were observed and their repetition rates determined. Using an oscilloscope (Tektronix), the constantly varying signal voltages of the laser were observed. Here a sub-miniature version A (SMA) cable was used to connect the laser oscillator to the oscilloscope. The oscilloscope was set at a frequency of 150 MHz and a current of 50 Ohms. Pulse trains were taken on 5, 50 and 20 nanosecond per division (ns/div) time scale and 50, 50 and 200 millivolts per division (mV/div) amplitude, respectively.

2.3.2 Central wavelength and spectral bandwidth measurements

The central wavelength and spectral bandwidth of the Fianium laser were measured to validate that the peak intensity of the laser pulses was at a wavelength of 1064 nm as specified by the manufacturer. This was done by aligning an ocean optics spectrometer in the path of the laser beam. The spectrometer was connected to a computer to allow capturing of the output data. Subsequently the data was plotted on Excel and the resultant spectrum was used

to calculate the bandwidth of the laser at full width half maximum (FWHM). FWHM is where the full width of the laser and half of the laser intensity resides.

2.3.3 Pulse duration measurement

The success of photoporation as discussed earlier is affected by the pulse duration of the laser. The most commonly employed method for such a measurement is frequency-resolved optical gating (FROG) which involves spectrally resolving the signal beam of an autocorrelation measurement (Trebino *et al.*, 1997). However, in this study a home built autocorrelator was assembled and consisted of a beam splitter (BS), mirrors M_1 , M_2 and M_3 , a nonlinear crystal, a lens with a known focal length and finally a spectrometer that was connected to a computer to enable capturing of the FROG trace. All lenses and mirrors used in this study were obtained from Comar, UK. Figure 2.1 shows the self-assembled FROG experimental setup.

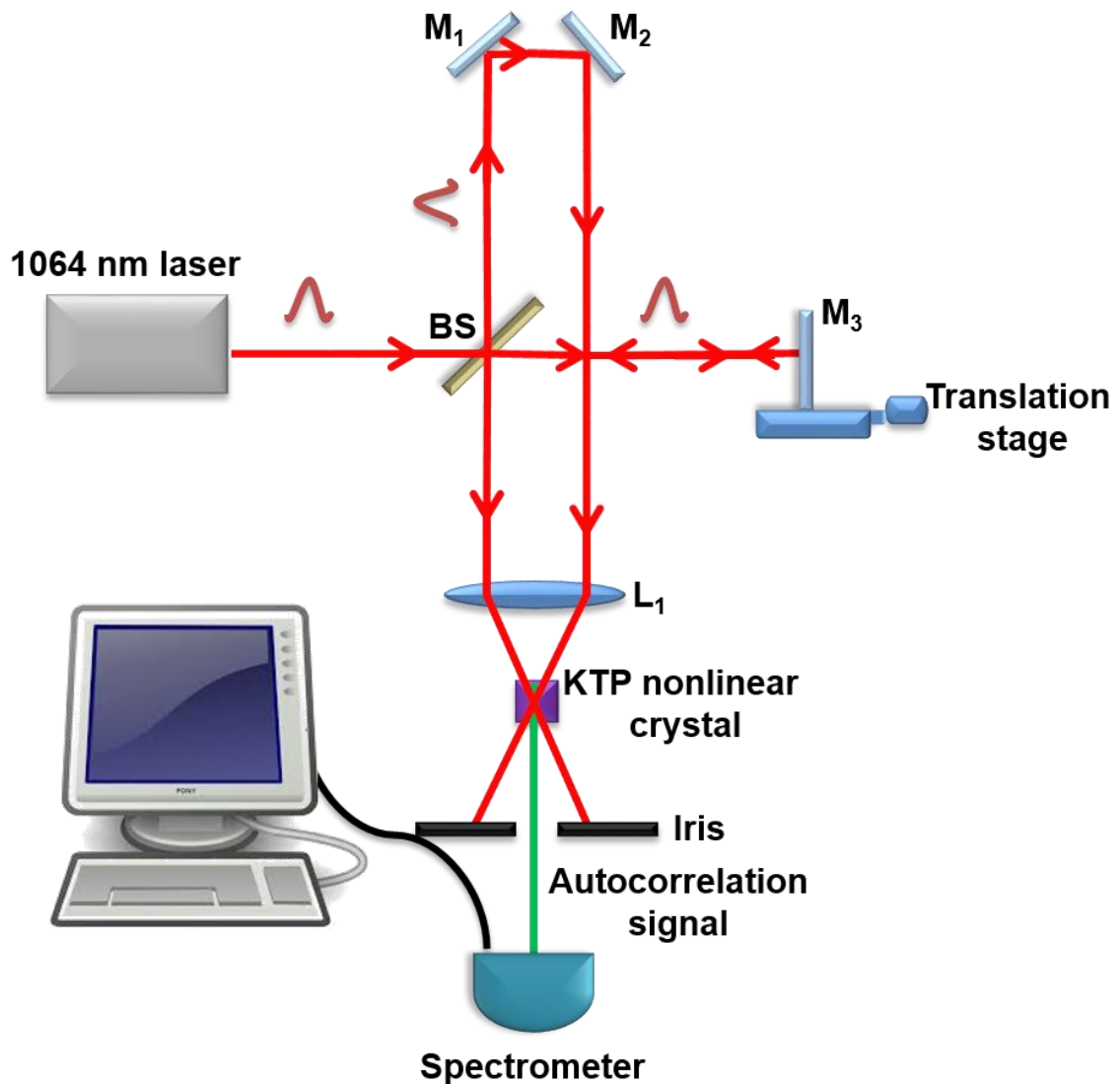


Figure 2.1: Arrangement of the FROG set up.

The NIR Gaussian beam was emitted by a Fianium FemtoPower laser where two pulses of the beam were created by a beam splitter. The red arrows indicate the path that was taken by each of the created beams. BS, beam splitter; M, mirror; and L, lens.

The BS separates the incoming pulse into two identical pulses which take different paths. The pulse that is refracted by the BS is further refracted by M_1 and M_2 . The path length of this pulse remains constant while the path length of the second pulse is adjustable. After the pulse is transmitted by the BS, the pulse is refracted back to the BS by M_3 which is mounted on an electronically movable stage (Newport, SA). The pulse is refracted by the BS and both pulses are focused by a

lens, L_1 , with a focal length of 100 mm onto the nonlinear β -Barium Borate crystal (BBO, CASIX, UK). When the two pulses overlap spatially and temporarily in the BBO crystal, a FROG signal with double the frequency of the incoming pulses is generated. A high repetition HR4000 spectrometer (Ocean optics) was placed in the path of the autocorrelation signal and multiple measurements of the pulses are taken over a wide range of pulse lengths and captured on the computer.

2.3.4 Beam quality measurement

The propagation of a laser can be approximated by assuming that the beam has an ideal Gaussian intensity profile which generally corresponds to the theoretical transverse electromagnetic mode (TEM_{00}). Real life lasers are however not truly Gaussian and to accommodate the variance a beam quality factor, M^2 , has to be defined. M^2 allows us to measure the amount of deviation of a laser beam from a theoretical Gaussian. This is done using a technique that incorporates a positive lens with known focal length and a charge coupled device (CCD) camera. The laser beam was focused through a lens with a focal length of 300 mm. Using the BeamGage laser profiler the diameter of the beam was measured at equal distance intervals (30 mm) from the lens (Figure 2.2).

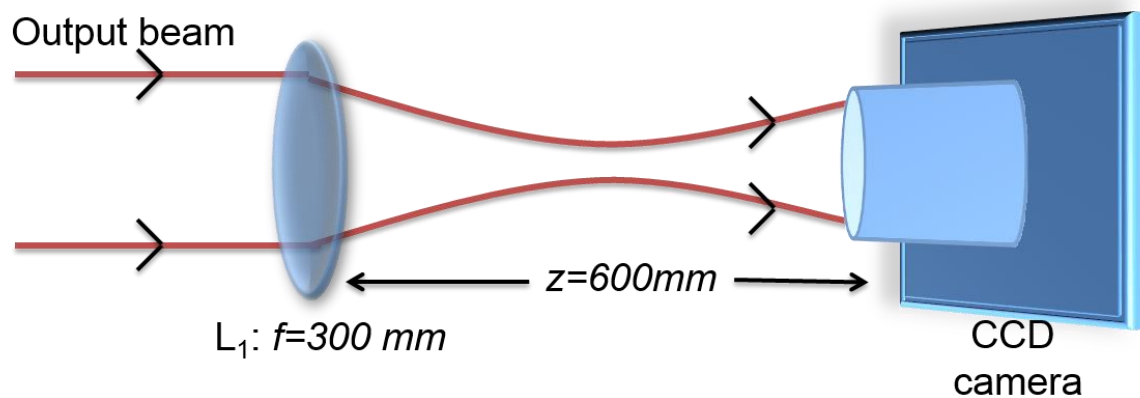


Figure 2.2: Experimental setup of the beam quality.

The output beam was focused through lens L_1 with a focal length (f) of 300 mm. A CCD camera was positioned at 30 mm distance intervals along the beam's axis of propagation (z) when beam diameter measurements were captured.

2.3.5 Beam diameter measurements

To ensure that a diffraction limited spot required for the photo-translocation of drugs was generated successfully, beam diameter measurements were taken at different points of the photo-translocation setup. For the measurement a USBSP206U CCD camera was utilised and placed along the path of the beam. Using BeamGage software (Spiricon Laser Beam Diagnostics) the beam was captured, recorded and the transverse intensity profile was displayed using the second moment ($D4\sigma$) technique. The beam diameter was measured at the laser output, post beam expansion and at the beam focus.

2.4 Assembly of the photo-translocation setup

Following laser characterisation, the optical setup that was used for the translocation of ARV drugs into HIV-1 permissive cells was assembled. A schematic illustration of the dual objective photo-translocation setup that was assembled is shown in Figure 2.3. A NIR, pulsed Gaussian beam was emitted by

a Fianium FemtoPower laser. The diameter of the input laser beam was expanded to overfill the back aperture of a 60 X air objective (Nikon) lens with a numerical aperture (NA) of 0.8. To expand the beam, a two-plano convex lens telescope was positioned in the path of the beam as it propagated. The laser beam was expanded by a predetermined magnification factor, M , defined by the following expression:

$$M = \frac{f_2}{f_1} \quad (2.1)$$

Where f_2 is the focal length of L_2 and f_1 is the focal length of L_1 . The lenses that were used, L_1 and L_2 , have focal lengths of $f_1 = 50$ mm and $f_2 = 200$ mm respectively.

An electronic shutter (Newport, SA) was placed before the telescope on the path of the beam to regulate the time that the beam was exposed to the cell membrane at the sample plane situated on a XYZ translation stage. After expansion the beam was reflected by mirror M_1 and then by a periscope composed of mirrors M_2 and M_3 . The beam was reflected by a dichroic mirror, DM, which also transmitted white light from the Koehler illumination system. The Koehler illumination system was composed of a series of apertures and lenses (L_3 , L_4 , and L_5) and served to facilitate the uniform illumination and imaging of the sample being viewed. The white light and laser light bounced off mirror M_4 and subsequently focused by a tube lens (TL, $f=175$ mm) and directed onto the sensor of a CCD camera.

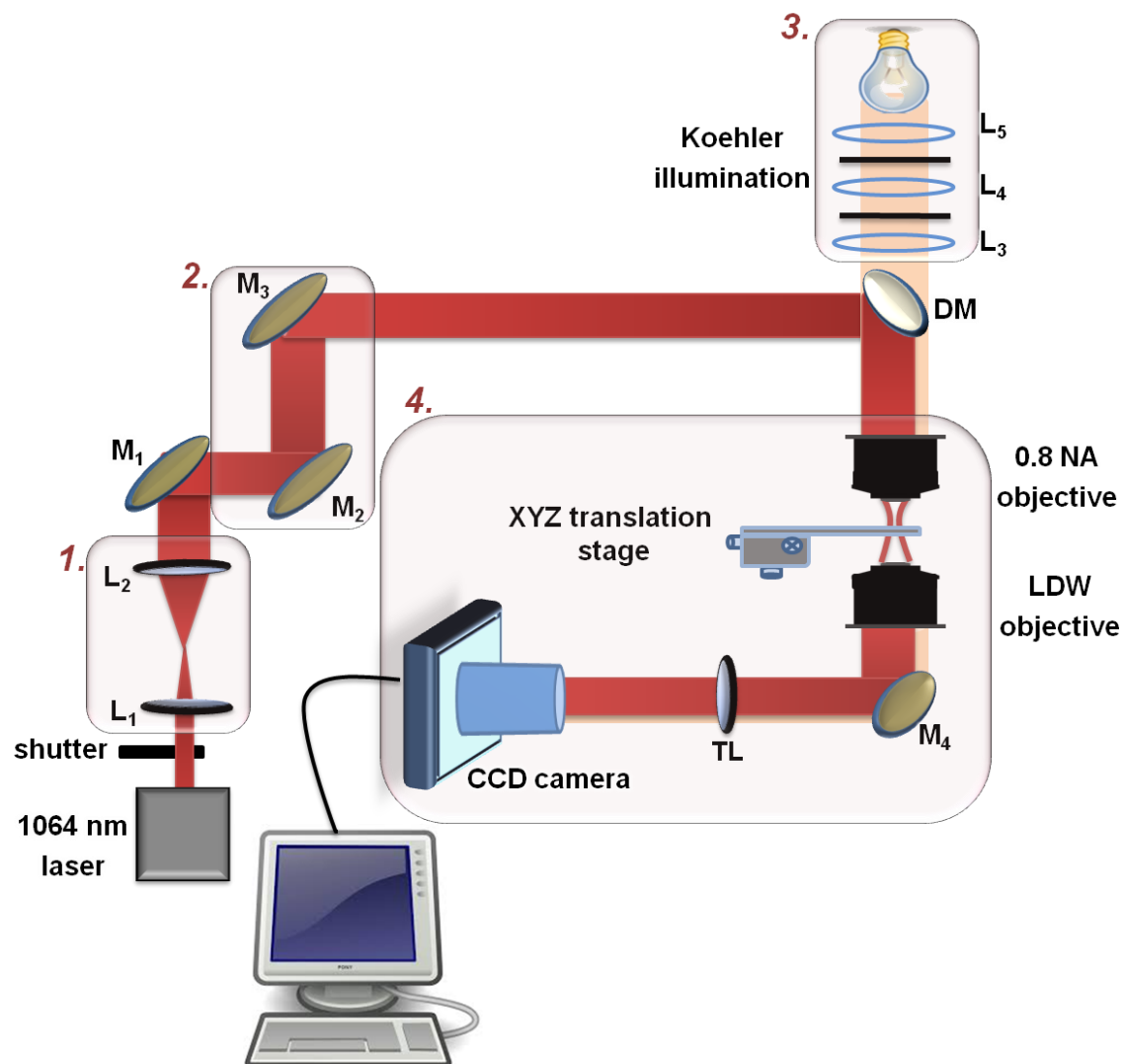


Figure 2.3: Arrangement of the photo-translocation set up.

Division 1, beam expansion; division 2, elevation of the laser beam; division 3, illumination system; division 4, sample magnification and imaging system. The NIR Gaussian beam was emitted by a Fianium FemtoPower laser where the beam travelled through an electronic shutter before being expanded by a two lens telescope to fit into the back aperture of a 60X objective lens. L₁₋₅, lenses; M₁₋₄, mirrors; DM, dichroic mirror; NA, numerical aperture; LDW, long distance working; TL, tube lens; CCD, charge coupled device.

2.5 Evaluation of the photo-translocation system

2.5.1 Trypan blue photo-translocation into TZM-bl cells

In early studies of photoporation Stevenson *et al.*, (2006) made use of a viability dye which is normally impermeable to the cell membrane, trypan blue, in order to confirm that photoporation of cells resulted in the perforation of the cell membrane without compromising the integrity of the cell. In this study, trypan blue was used not only to confirm translocation of exogenous materials into the cell's cytoplasm but more importantly, it was used to indicate which laser-to-cell exposure time and laser power levels would be optimal for drug delivery while retaining the integrity of the cell. An area of the cells to be treated was clearly marked using a permanent marker and the same field was viewed under the microscope before, during and after the cells were treated with the laser. TZM-bl cells that were photoporated successfully were expected to internalize the viability dye and retain the blue colour of the dye while cells not treated with the laser would remain intact and not internalise the trypan blue molecules. The laser-to-cell exposure time and power level that achieved such results was considered optimal for the delivery of drugs. The properties of dead cells in the demarcated area to be treated were noted.

In these experiments, TZM-bl cells (3×10^3 cells) were seeded in 200 μ l of GM in a 35 mm diameter glass bottom tissue culture treated petri dish with a 10 mm diameter working area (Wirsam Scientific, SA). The cell cultures were incubated overnight in normal growth conditions. The monolayer was washed in 1 \times PBS and submerged in 20 μ l of 0.4% trypan blue exclusion dye and the sample diameter was covered with a 8 mm diameter type-1 sterile coverslip (Labotech, SA). The targeted photo-translocation was administered to individual cells in 3

doses within the selected area where different power levels (40 mW to 100 mW increasing each time with increments of 10 mW) and different laser-to-cell exposure times (30 ms to 1 second increasing each time by 10 ms). Following laser irradiation, the monolayer was washed with PBS to remove residual trypan blue. Thereafter, the treated cells were viewed using a CCD camera connected to an Olympus microscope (Wirsam Scientific, SA). The cell cultures were viewed using the bright field microscope setting where images of the cells were captured.

2.5.2 Photo-translocation of ARV drugs into TZM-bl cells

The photo-translocation of ARV drugs like that of trypan blue consists of two steps. The first step involved the photoporation of the cell and the second step involved the actual translocation of these exogenous agents into the cell cytoplasm. A sample of TZM-bl cells (2×10^3) was seeded and prepared as described in section 2.5.1. The cell monolayer was submerged in 20 μ l of neat GM (without FBS and PEST) which contained a final concentration of 20 μ g/ml of tenofovir, efavirenz or nevirapine. In order to differentiate between laser assisted drug delivery and the spontaneous uptake of the drugs by the cells, control sample dishes were also prepared. Each laser treated experimental dish was accompanied by a control dish which is referred to as a drug control (DC). The DC contained cells submerged in either one of the three ARV used in the study, but in these controls the delivery of drugs was not facilitated by laser irradiation. Following three doses of laser irradiation using 60 mW as the optimal power level and 50 ms as the laser-to-cell exposure time, the monolayer was washed with 1 \times PBS. The cell monolayer was supplemented with 200 μ l of GM and incubated overnight.

2.5.3 HIV-1 inhibition assay

To detect the successful photo-translocation of ARV drugs into TZM-bl cells, the Bright Glo luciferase assay kit was used. Alongside the preparation of the photo-translocation experimental and DC dishes, additional controls were prepared in a 96-well, flat bottom, transparent, Corning microtiter plate (The Scientific group). These controls were the cell control (CC), the virus control (VC) and the positive control (PC). The PC contained cells infected with *Env*-pseudotyped virus and exposed to the drugs for the full duration of incubation (48 hours). The 96-well plate that contained the additional controls was incubated alongside the glass bottom dishes which contained the laser irradiated cells and the DC. This was done to ensure that all the wells of the 96-well plate and the glass bottom dishes were treated under the same conditions in an identical manner.

GM (60 μ l) was added to each well and an additional 25 μ l was added to the CC to compensate for the volume of the *Env*-pseudotyped virus. The appropriate drug was added to the PC to a final concentration of 20 μ g/ml which resulted in a 5 times dilution of the drug. *Env*-pseudotyped virus (25 μ l with a dosage of 100 TCID₅₀) was added to all wells except those of the CC. An additional 50 μ l of GM which contained DEAE dextran to a final concentration of 20 μ g/ml was added to each well. DEAE dextran was added in order to increase HIV-1 binding to cells in turn enhancing the infectivity of the *Env*-pseudotyped viruses. After an incubation period of 48 hours in normal cell growth conditions, the RLUs were measured using a multiplate reader. In this assay, viral Tat protein induces the expression of the reporter genes within TZM-bl cells. Luciferase activity is directly proportional

to the number of infectious virus particles that were present in the initial inoculum that were capable of cell entry and viral genome integration.

2.5.4 Cytotoxicity assay

There exist a variety of assays for the investigation of metabolic and physical conditions of cells. In this study we showed the effects of irradiating TZM-bl cells with a laser in the presence of various ARV drugs using the Cell Titer 96 Non-Radioactive cell Proliferation assay (Anatech Instruments). The assay is a colorimetric method used to estimate the number of viable cells in culture post laser irradiation. The assay contains MTT tetrazolium salts [3-(4,5-dimethylthiazol-2-yl)-2,5-diphenyltetrazolium bromide] which readily penetrates viable eukaryotic cells. Viable cells with an active metabolism are able to convert MTT into a purple coloured formazan product. Dead cells have an inability to convert MTT to formazan rendering formazan formation a useful marker for the detection of viable cells.

In the MTT assay, 2×10^3 TZM-bl cells were seeded per well, and prepared as described in section 2.5.1. To evaluate the effects of laser irradiation, the cell monolayer was washed with $1 \times$ PBS following a 24 hour incubation period. The monolayer was submerged in 20 μ l of GM not containing FBS or PEST. To differentiate between the metabolic and physical conditions of TZM-bl cells that were exposed to the laser, control cell cultures were prepared. Each laser treated experimental dish was therefore accompanied by a control dish which is referred to here as the LC. The LC contained cells submerged in GM without FBS and PEST. To evaluate if the combination of the laser with the respective drugs did

not cause cytotoxic effects on the cells, experimental (EXP) and DC dishes were prepared for each of the three drugs as described in section 2.5.2. Additional controls namely; a CC, PC and Triton X-100 (TC, Sigma Aldrich, SA) were prepared in a 96-well multiwell plate and incubated alongside the glass bottom dishes. Triton X-100 is a non-ionic surfactant which is used to lyse cells where the agent leads to the disruption of the cell membrane for protein purification. When used in large amounts or exposed to cells for prolonged periods of time, the cells die. In such cases triton X-100 leads to the disruption of the compartments and integrity of the lipid membrane due to the disruptive action of the triton X-100 molecule's polar head group on the hydrogen bonding present within the cells membrane (Koley *et al.*, 2010).

Following three doses of laser irradiation using 60 mW as an optimal power level and 50 mW as the laser-to-cell exposure time the monolayer was washed with 1 × PBS. The cell monolayer was supplemented with 200 µl of GM and incubated overnight. GM (50 µl) was added to all wells except for PC and TC wells where GM was added with respective drugs used in the study accordingly to the appropriate final concentration. An additional 50 µl of GM was added to all wells of the 96-well plate, EXP and LC dishes were incubated for 48 hours in normal cell growth environmental conditions. MTT dye solution (15 µl) was added to each well followed by a 4 hour incubation period in appropriate growth conditions. After incubation, 100 µl of the solubilisation solution or stop mix was added to all wells and incubated at room temperature for an hour. Without causing any bubble formation, the solutions within the wells were mixed by pipetting and solutions of

the glass bottom dishes were transferred to the 96-well plate. Using a multi-plate reader, absorbance profiles were recorded at a wavelength of 570 nm.

2.6 Statistical analyses

The data in this study was analysed using Mathematica version 9 for windows 7, Matlab, Excel and Origin. Non-parametric one-way analysis of variance was used to investigate the statistical significance of data. Statistical difference is shown in the results by an asterisk. Statistical methods performed are discussed accordingly with reported results in chapter 3.

3. Results

3.1 Laser beam characterisation

This study aimed to evaluate the ability of a home-built photo-translocation DDS setup to more efficiently deliver ARV drugs tenofovir, efavirenz and nevirapine into TZM-bl cells compared to the absence of a DDS. In order for the setup to be built, the laser device was characterised to assess adequate functionality. Following full characterisation and assembly of the setup, the ARV drugs were translocated into the mammalian cells by diffusion through a pore generated by the precise alignment of a tightly focused laser onto the cell membrane.

3.1.1 Validation of laser pulse trains and determination of pulse repetition rate

The monitoring of pulse trains using an oscilloscope allowed us to determine whether the laser master source is a passively mode-locked fiber laser at a repetition rate in the MHz range. The spectrums displaying the pulse-to-pulse stability of the Fianium laser master source is shown in Figure 3.1. Irrespective of the set time and amplitude on the oscilloscope, the pulses showed temporal stability in real time. The oscillator repetition rate obtained from the oscilloscope was 76.5 MHz. This repetition rate is comparable to that of 76.6 MHz reported by the manufacturer.

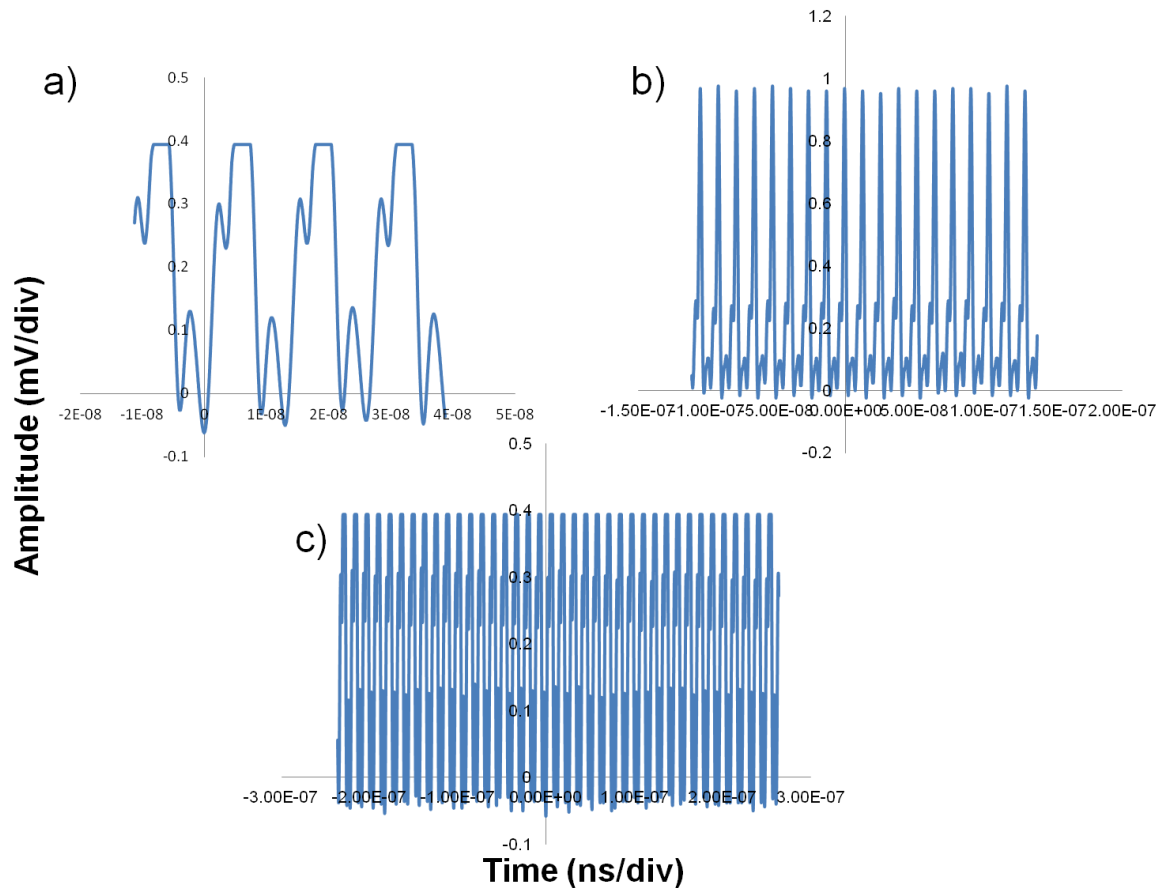


Figure 3.1: Validation of laser pulse trains.

Pulse trains were validated at varying time scales and amplitudes; a) 5 ns/div, 50 mV/div; b) 20 ns/div, 200 mV/div and c) 50 ns/div, 50 mV/div respectively. Conversion factors $2e^{-9}$, $2.5e^{-9}$ and $2e^{-9}$ were used for the scaling of the time for graphs a, b and c respectively. Conversion factors 0.002, 0.001 and 0.002 were used for the scaling of the amplitude for graphs a, b and c respectively.

3.1.2 Central wavelength and spectral bandwidth measurements

The central wavelength refers to the central operating wavelength of a laser. This wavelength is defined by a peak mode measurement and is where the optical power of the laser resides. Figure 3.2 shows that the central wavelength of the laser was 1063.8 nm. The obtained central wavelength is within the acceptable range of 1063 to 1065 nm given by the manufacturer. The central wavelength is indicated on the spectrum in Figure 3.2 by the red vertical line.

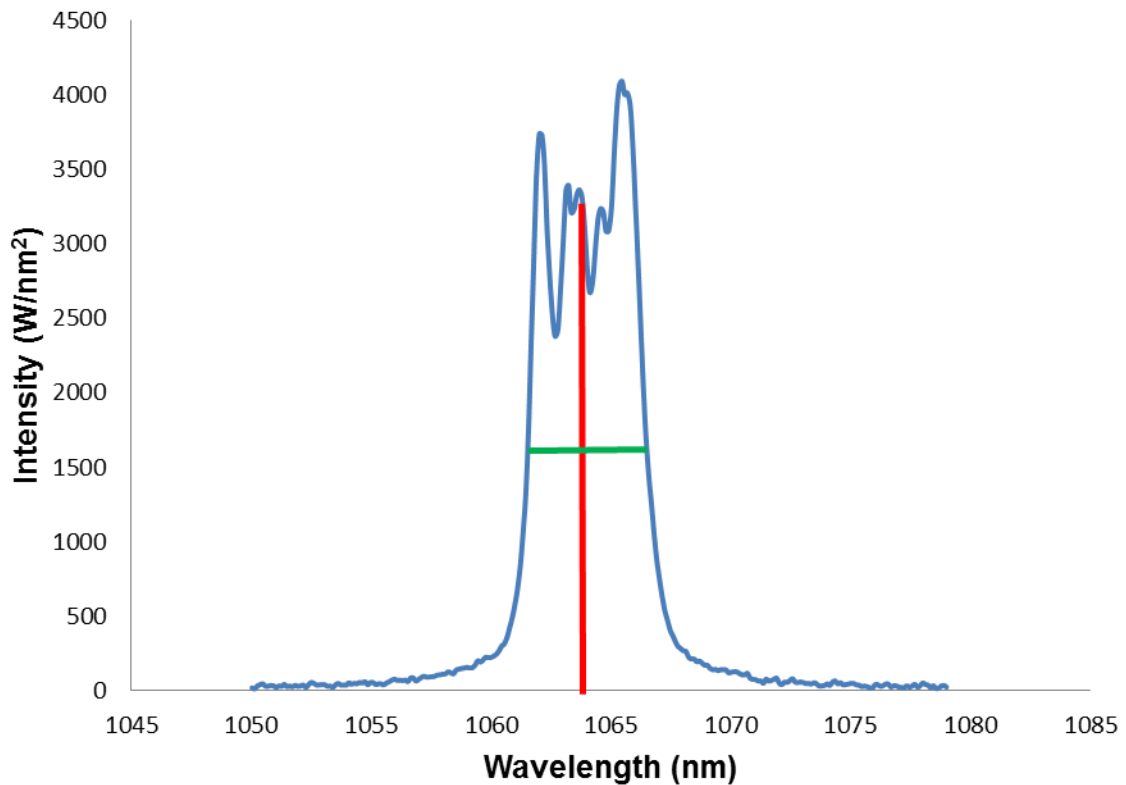


Figure 3.2: Spectrum showing the measured central wavelength and bandwidth of the Fianium laser.

The central wavelength is indicated by the red line while the calculation of the bandwidth at full width half maximum (FWHM) is indicated by the green line.

The bandwidth of the laser was calculated using the spectrum at FWHM. The calculated bandwidth of 5.2 nm is acceptable for the Fianium laser as it falls within the range of 5.0 to 15.0 nm stipulated by the manufacturer.

3.1.3 Pulse duration measurement

The temporal profile of the Fianium FemtoPower laser was measured at the laser output. This measurement is important for this study as it makes it possible to account for the time that a single pulse is exposed to each cell. In turn the efficiency of drug delivery and the integrity of the cell can be accounted for with respect to time (Amat-Roldan *et al.*, 2004, Trebino *et al.*, 1997).

Following the acquisition of a FROG signal, a spectrum of the signal was acquired (Figure 3.3) by using a spectrometer.

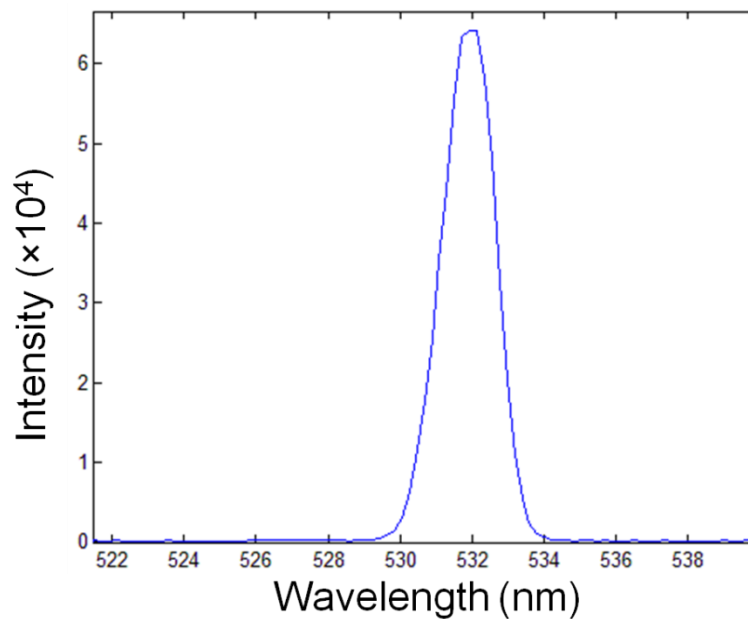


Figure 3.3: Spectrum of the measured FROG signal where intensity was plotted against wavelength.

The central wavelength of the obtained FROG signal was 532 nm as anticipated. The signal was generated when the two incident pulses overlapped in the crystal.

FROG measurements involve the recording of tens or thousands of spectra for different arrival time differences between the two pulses. The resultant measurement is displayed in a spectrogram with a colour scale of the intensity as a function of time delay and optical frequency or wavelength. Two sets of measurements were taken in this study first using a BBO nonlinear crystal which was cut to function optimally at a wavelength of 800 nm. Secondly, the measurements were taken using a potassium titanyl phosphate (KTP) crystal cut to function optimally at a wavelength of 1064 nm. The time that it took to measure

each pulse using both nonlinear crystals is shown in the spectrograms in Figure 3.4.

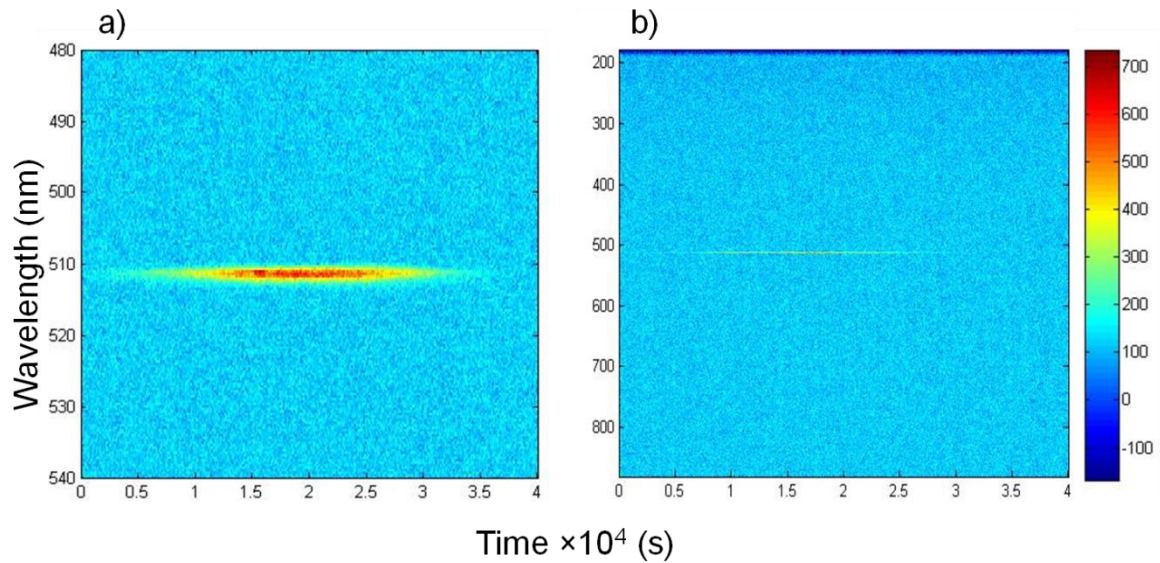


Figure 3.4: Spectrograms showing the time it took to measure each pulse.

a) shows results obtained when a BBO crystal was used and b) when a KTP crystal was used in the FROG optical setup. In the intensity indicator bar shown on the right of the spectrograms, red is indicative of a high intensity while blue is indicative of a low intensity.

The time taken to measure a single pulse was converted to the actual length of the pulse using the following equation:

$$\text{Pulse duration} = t \times \text{scanning velocity} \times 2 \times 3.33667 \times 10^{-12} \times 0.707 \quad (3.1)$$

where t is time, scanning velocity is the velocity of the translation stage, 2 represents that the pulse that was reflected by mirror M_3 travelled the same distance twice, 3.33667×10^{-12} is the speed of light converted to mm/s and finally 0.707 is the deconvolution factor of a Gaussian beam. By substituting x values into the equation, the pulse duration at FWHM was measured to be 10 ps. This pulse length did not compare with that obtained by the manufacturer of 210 fs.

The spectrograms obtained for the pulse duration measurements are depicted in Figure 3.5.

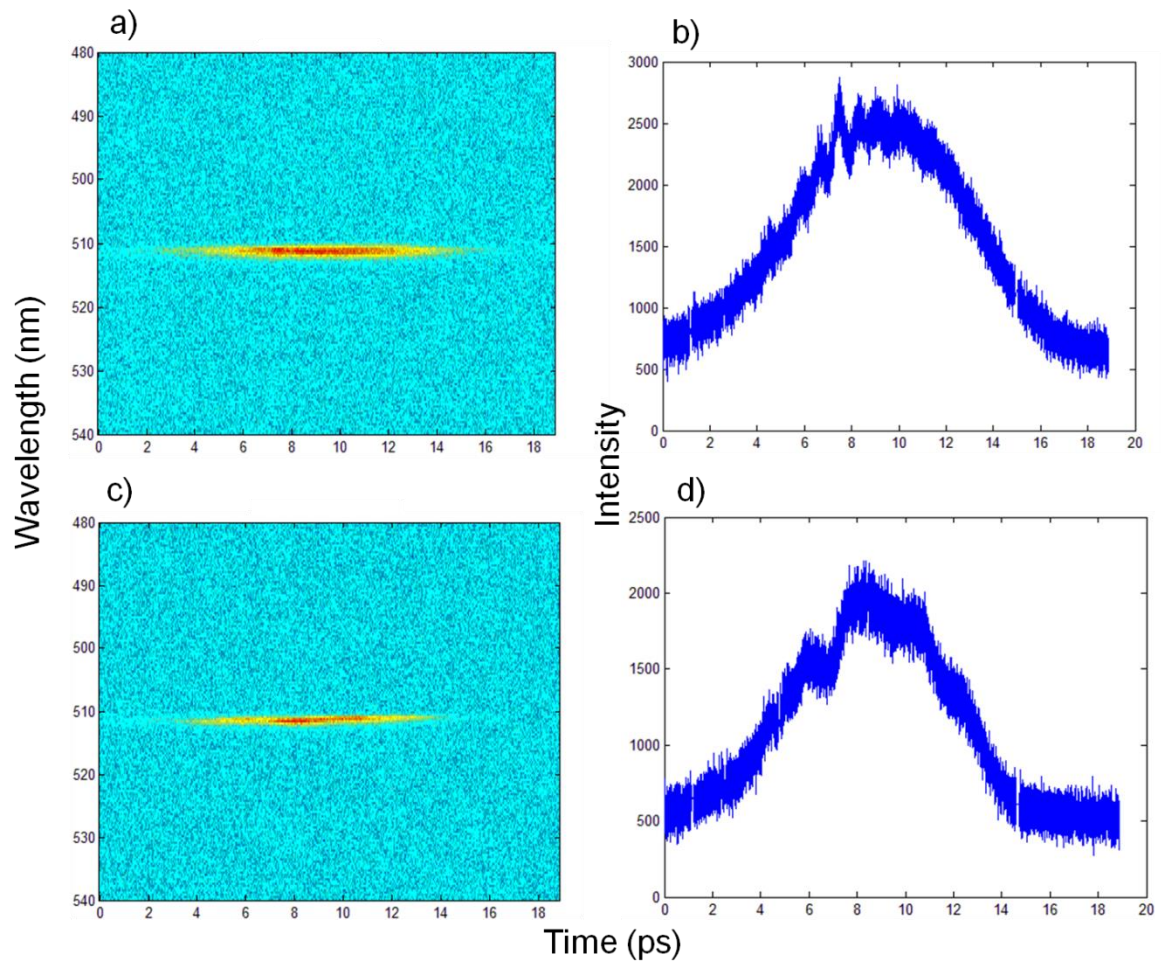


Figure 3.5: FROG traces of the pulse duration measurement.

A BBO crystal was used in a) and b) while a KTP crystal was used for measurements of c) and d). In a) and c) FROG traces of wavelength versus time are shown and in b) and d) the temporal distribution of the Gaussian pulse where the FROG traces were summed over various wavelengths is shown. The intensity was plotted against time.

3.1.4 Determination of the beam quality

The measurement of M^2 is an integral part of characterising a laser. The beam quality of a TEM₀₀ Gaussian beam is $M^2=1$ however, this beam quality is impossible to achieve with real life lasers. The quality of real life lasers is ideal when $M^2>1$, but as close to 1 as possible. The lower the value of the quality factor

the greater the quality of the beam (Siegman, 1993). Essentially, M^2 describes how close to a perfect Gaussian a real life laser is.

As Gaussian beams propagate through space, the beam radius varies with distance by,

$$\omega(z) = \omega_0 \sqrt{1 + \left(\frac{M^2 \lambda (z - z_0)}{\pi \omega_0^2} \right)^2} \quad (3.2)$$

where z is the distance propagated by the beam from where the wavefront is flat, λ is the wavelength of laser light, $\omega(z)$ is the beam width and ω_0 is the width at the beam waist (Saleh *et al.*, 1991). To calculate the beam quality factor equation 3.2 can be expanded to the following quadratic equation:

$$\omega^2(z) = \left(\frac{M^2 \lambda}{\pi \omega_0} \right)^2 z^2 - 2z_0 \left(\frac{M^2 \lambda}{\pi \omega_0} \right)^2 z + \left(\frac{M^2 \lambda}{\pi \omega_0} \right)^2 z_0^2 + \omega_0^2 \quad (3.3)$$

The derivation of equation 3.3 from equation 3.2 is shown in appendix A-1.

The data obtained from the beam quality measurements were fitted to a two order polynomial where the square of the beam radius was plotted against the distance along the propagation axis. The two order polynomial therefore takes the form,

$$Y = Az^2 + Bz + C \quad (3.4)$$

where Y is the square of the beam waist and A , B and C are the coefficients of the polynomial fit. Comparing the terms of equation 3.3 to those of equation 3.4 we obtained that

$$A = \left(\frac{M^2 \lambda}{\pi \omega_0} \right)^2 \quad (3.5a)$$

$$B = -2z_0 \left(\frac{M^2 \lambda}{\pi \omega_0} \right)^2 \quad (3.5b)$$

$$C = \left(\frac{M^2 \lambda}{\pi \omega_0} \right)^2 z_0^2 + \omega_0^2 \quad (3.5c).$$

Equation 3.3 can then be compared to the fitted equation to determine the beam quality, beam waist and the z position as follows:

$$M^2 = \frac{\pi}{\lambda} \sqrt{AC - \frac{B^2}{4}}, \quad (3.6a)$$

$$\omega_0 = \sqrt{C - \frac{B^2}{4A}}, \quad (3.6b)$$

$$z_0 = -\frac{B}{2A}. \quad (3.6c)$$

The parameters that were measured from the quadratic fit are shown in Table 3.1 and the accompanying graph showing the square of the measured beam radii as the laser propagated is shown in Figure 3.6.

Table 3.1: Measured beam parameters for the Fianium FemtoPower laser

Parameter	Measured
M^2	1.15
ω_0 (mm)	0.24
z_0 (mm)	307

M^2 ; Beam quality factor

ω_0 ; Beam radius

z_0 ; z position where the diffraction limited spot is situated

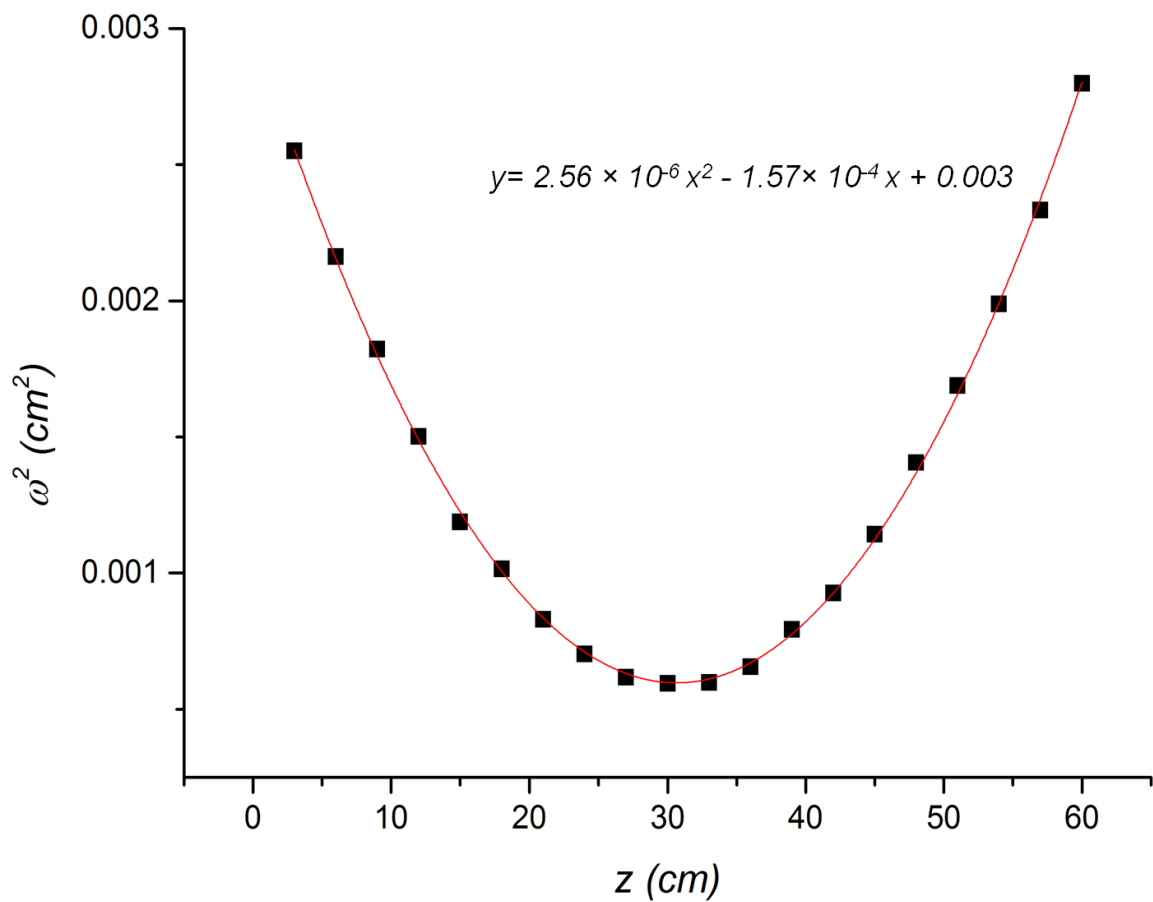


Figure 3.6: Graph showing the calculation of the beam quality.

The black squares are of the values representing the square of the measured beam widths at various distances from the lens. The red trendline represents a fitting of the data points and is based on the quadratic equation shown in the graph. ω , beam radius and z , distance away from the lens.

These results demonstrate that the Fianium FemtoPower laser produces a good quality beam. The obtained quality factor $M^2 = 1.15$ compares with that of $M^2 = 1.1$ which was specified by the manufacturer. Also, the manufacturer stated that an acceptable range for the beam quality factor is $1.0 \leq M^2 \leq 1.3$ where M^2 cannot be smaller than 1.0 and cannot be greater than 1.3.

Figure 3.7 illustrates how the diameter of the beam changes as it propagates along the z axis. The z position is that where a diffraction limited spot is attained. The diameter of the beam decreases as the beam approaches the focus of $f = 300$ mm and increases as the beam propagates away from the focus. The z position calculated as shown above and displayed in Table 3.1 of $z_0 = 307$ mm compares with the focal length of the lens that was used for this measurement.

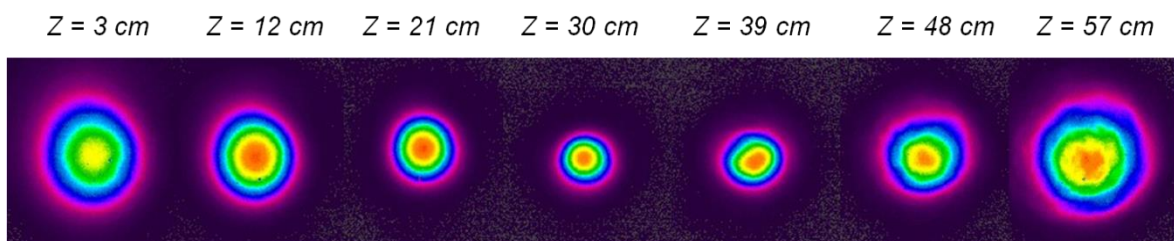


Figure 3.7: Images of the laser beam as it propagated along the z axis.

The images shown were captured at various distances from the lens indicated by $z = 3$ cm to $z = 57$ cm in intervals of 9 cm.

3.1.5 Beam diameter measurements

The discussion and specifications of beam propagation characteristics necessitate that the beam diameter is defined. The beam diameter is most often defined as the diameter where the intensity of the beam has fallen to $1/e^2$ (13.5%) of its peak value (Andrews *et al.*, 2005). In this study the beam diameter was measured at

various points of the photo-translocation setup to ensure that the desired effects of the optical setup were met. Eighty six percent of the beam is carried within a circle with a radius $\omega(z)$ and is regarded as the beam width along the propagation direction of the beam. The beam diameter, $2\omega_0$, is also referred to as the spot size. Firstly, the spot size was measured at the laser output and yielded the results shown in Figure 3.8.

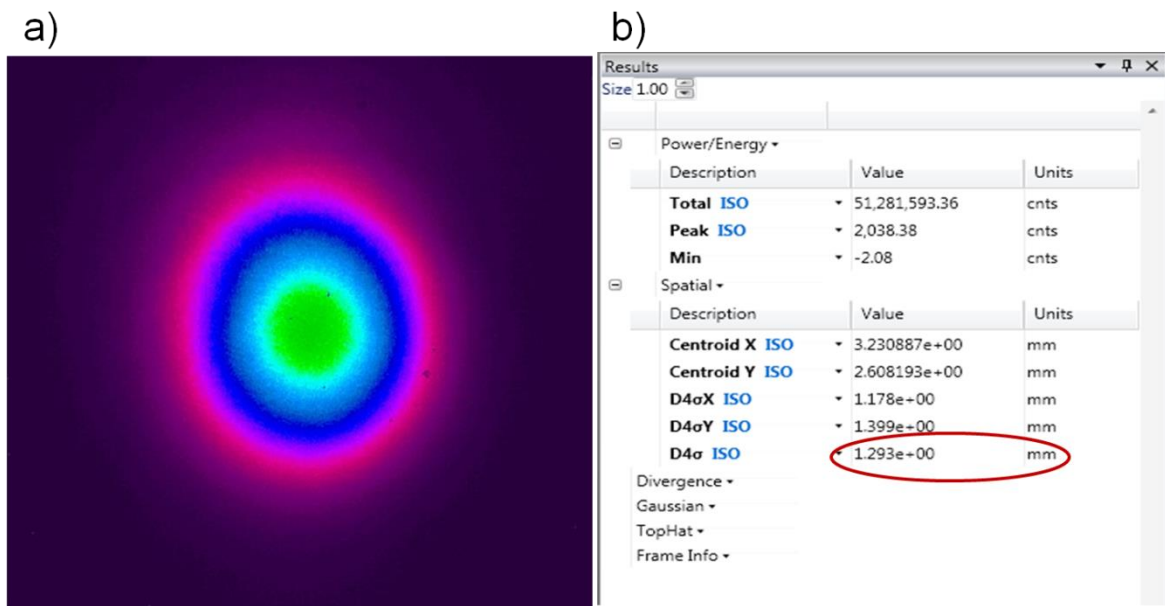


Figure 3.8: Beam diameter measurement at the laser output.

a) Image of the cross section of the laser beam. This is the image to which the statistical data in b) was based. The obtained spot size from the statistical data is highlighted by the red oval.

A theoretical model of the beam waist measurement was carried out and the following Gaussian exponential function was plotted:

$$I(z) = \exp\left(-\frac{2z^2}{\omega_0^2}\right) \quad (3.7)$$

where $I(z)$ is intensity as a function of propagation distance z . The resultant intensity distribution plot is depicted in Figure 3.9.

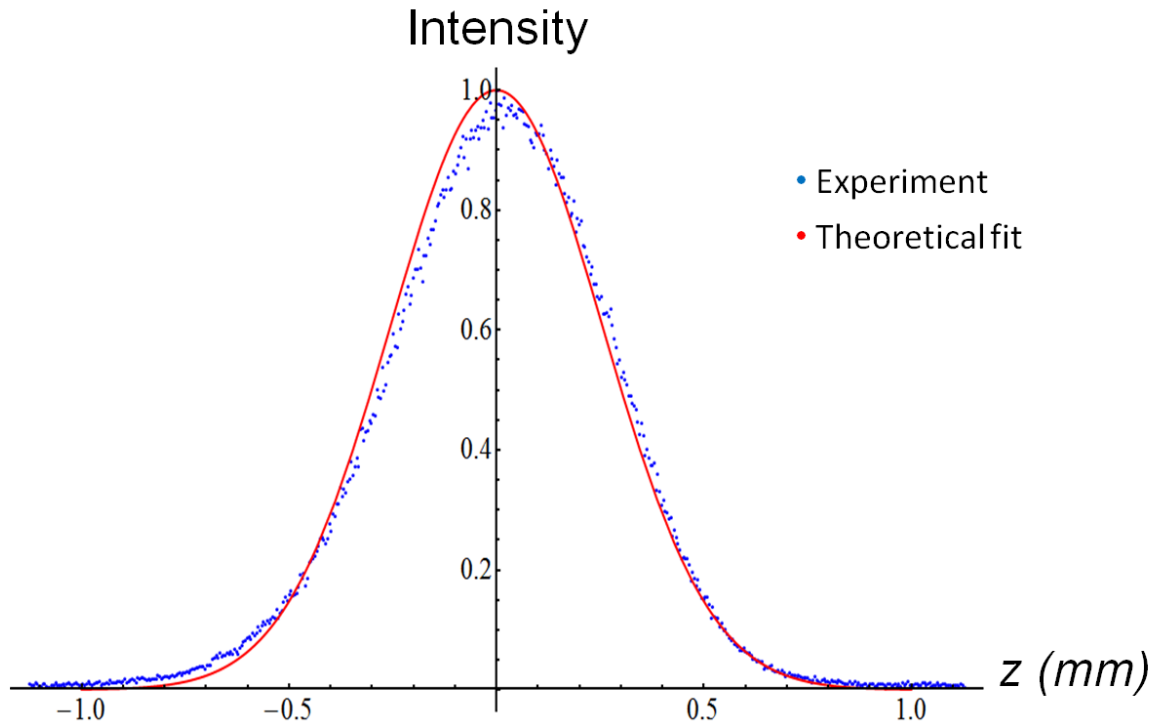


Figure 3.9: Intensity distribution of the laser beam as a function of z , propagation distance (in mm).

The data was captured at the laser output. The red trendline is representative of a fitting of the data points acquired using a beam profiler and is based on the Gaussian exponential equation.

Table 3.2: Measured spot size and beam radius of the Fianium FemtoPower laser against the theoretical estimate of the beam radius.

Measured $2\omega_0$ (mm)	Measured ω_0 (mm)	Estimated ω_0 (mm)	Estimated ω_0 standard error
1.3	0.65	0.51	0.0016

$2\omega_0$; Beam diameter

ω_0 ; Beam radius

The difference between the measured and estimated beam waist was not significant (Table 3.2). The obtained beam diameter of 1.3 mm compares well with that of 1.2 mm which was given by the manufacturer. The measurement was also within the acceptable range of 1 – 2.5 mm given by the manufacturer. This result was optimal and allowed us to continue with the assembly of the photo-

translocation setup. Using the measured beam diameter, the size of the beam was expanded to overfill the back aperture of the objective lens that was used to focus the beam to a diffraction limited spot. The laser beam was expanded by a predetermined magnification value, M (equation 2.1). The resultant beam after expansion is shown in Figure 3.10. Table 3.3 describes the magnification factor used for the expansion of the beam diameter using a two lens telescope. The table also shows the expected beam diameter and the measured beam diameter after magnification of the spot size was done.

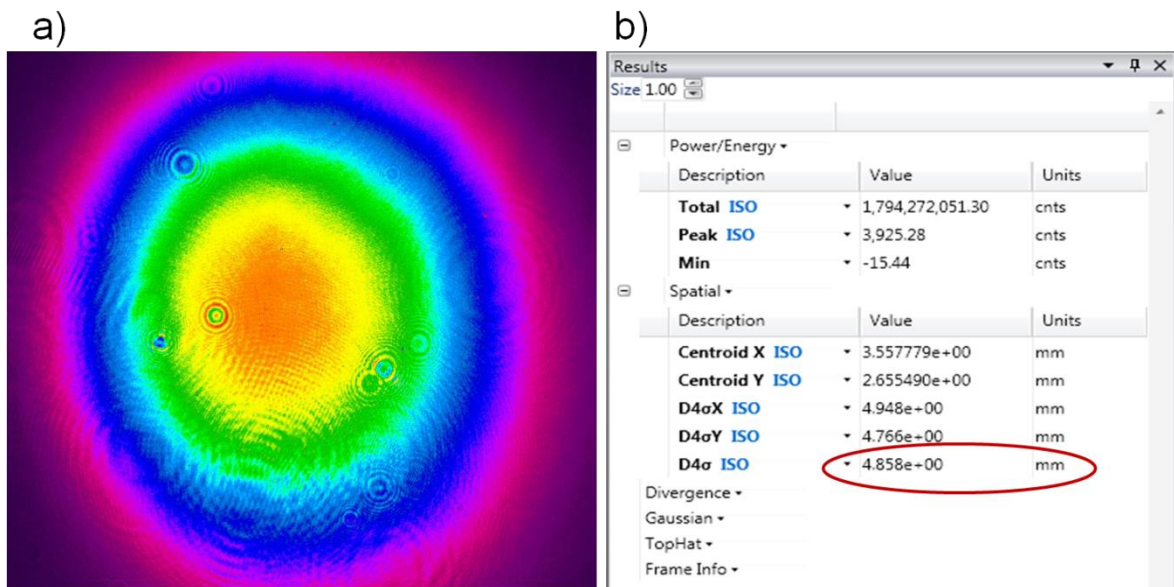


Figure 3.10: Beam diameter measurement after the beam was expanded.

a) shows an image of the cross section of the expanded laser beam. This is the image to which the statistical data in b) was based. The obtained spot size from the statistical data is highlighted by the red oval.

Table 3.3: Measurement of the magnification factor for the expansion of the beam spot size, as well as the measured and expected spot sizes following beam expansion.

Measured $2\omega_0$ (mm) at laser output	Magnification factor (M)	Measured $2\omega_0$ (mm) after expansion	Expected $2\omega_0$ (mm)
1.3	$M = 200 / 50 = 4$	4.9	$1.3 \times 4 = 5.2$

$2\omega_0$; Beam diameter

M ; Magnification factor

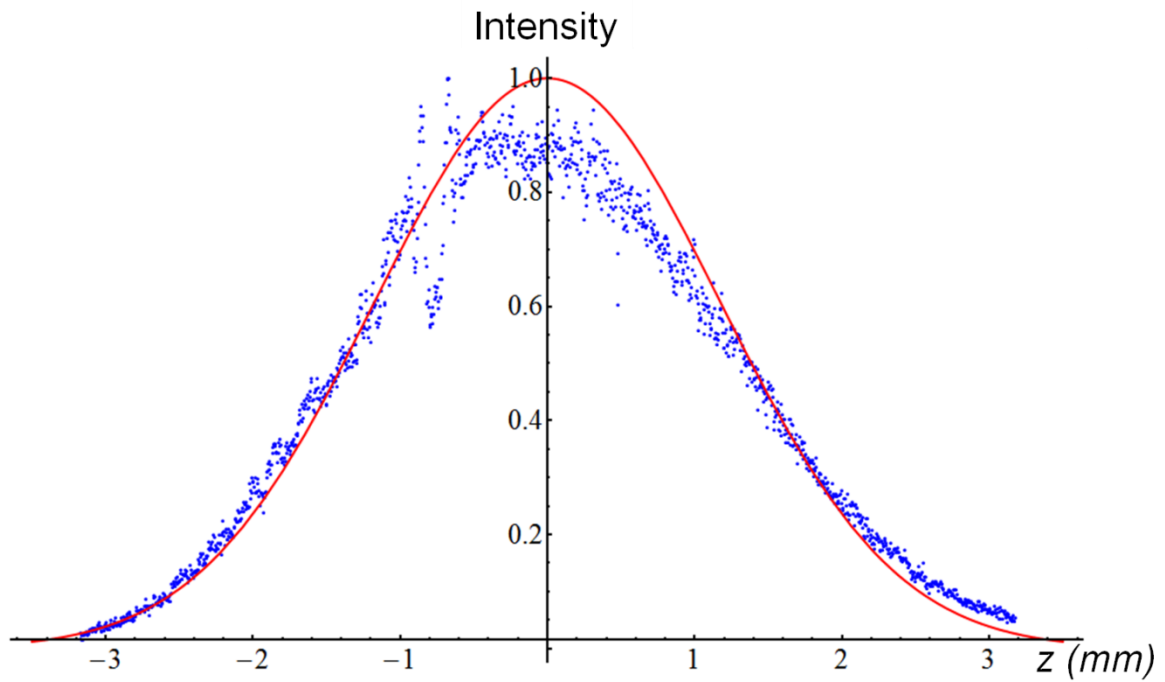


Figure 3.11: Intensity distribution of the laser beam as a function of z , propagation distance (in mm).

The data was captured after the beam diameter was expanded. The red trendline is representative of a fitting of the data points acquired using a beam profiler and is based on the Gaussian exponential equation.

After the laser beam was focused with the objective lens, the beam diameter was measured once again. The obtained spot size is depicted in Figure 3.12.

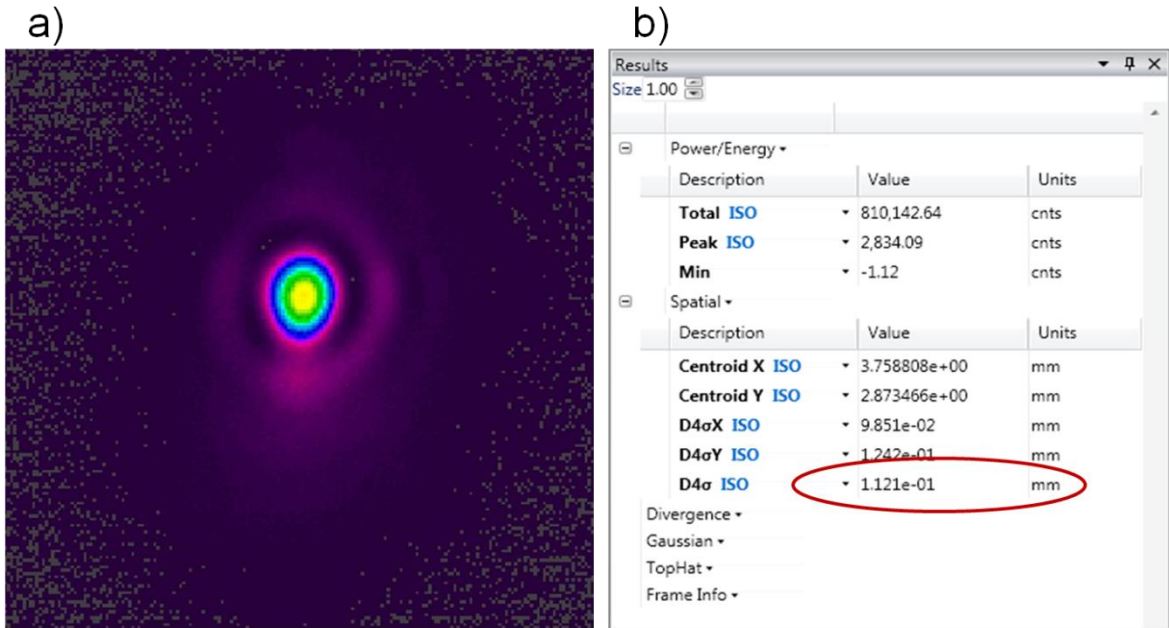


Figure 3.12: Beam diameter measurement after the beam was focused through the objective lens.

a) Shows an image of the cross section of the focused laser beam. This is the image to which the statistical data in b) was based. The obtained spot size from the statistical data is highlighted by the red oval.

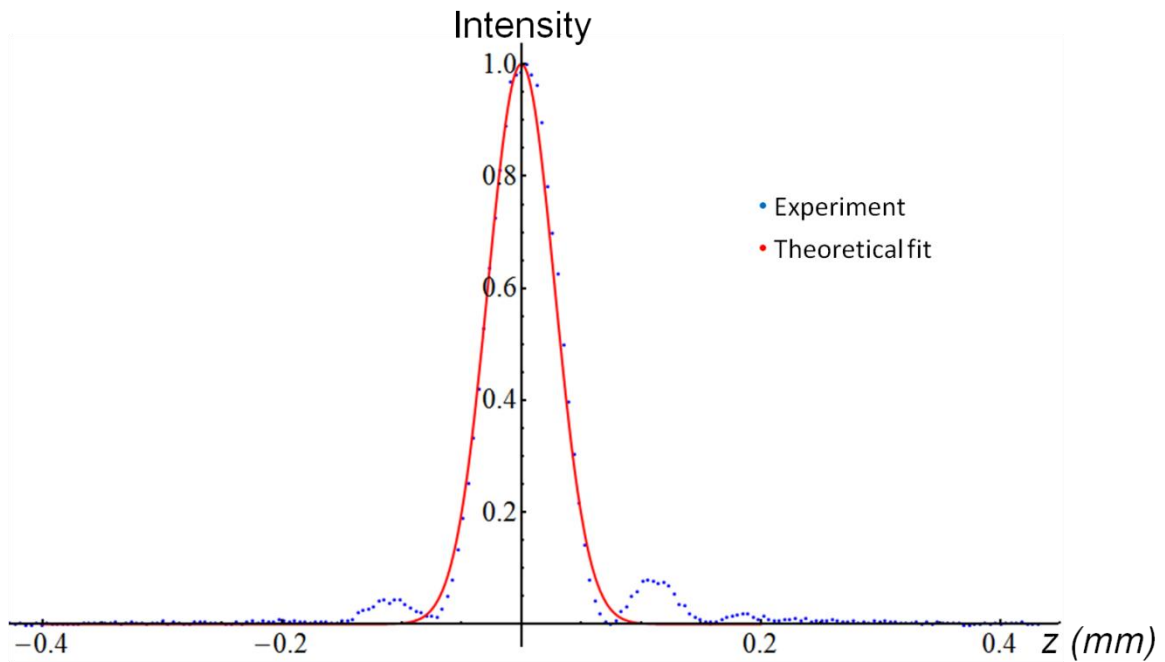


Figure 3.13: Intensity distribution of the laser beam as a function of propagation distance.

The data was captured at the laser focus. The red trendline is representative of a fitting of the data points acquired using a beam profiler and is based on the Gaussian exponential equation.

Table 3.4: Measured spot size and beam radius of the focused Fianium FemtoPower laser against the theoretical estimate of the beam radius.

Measured $2\omega_0$ (mm)	Measured ω_0 (mm)	Estimated ω_0 (mm)	Estimated ω_0 standard error
0.11	0.055	0.05	0.002

$2\omega_0$; Beam diameter

ω_0 ; Beam radius

3.2 Assembly of photo-translocation set up

Following full characterisation of the Fianium laser, the photo-translocation setup was assembled according to the schematic provided in chapter 2. An image of the completed setup used in the study is depicted in Figure 3.14.

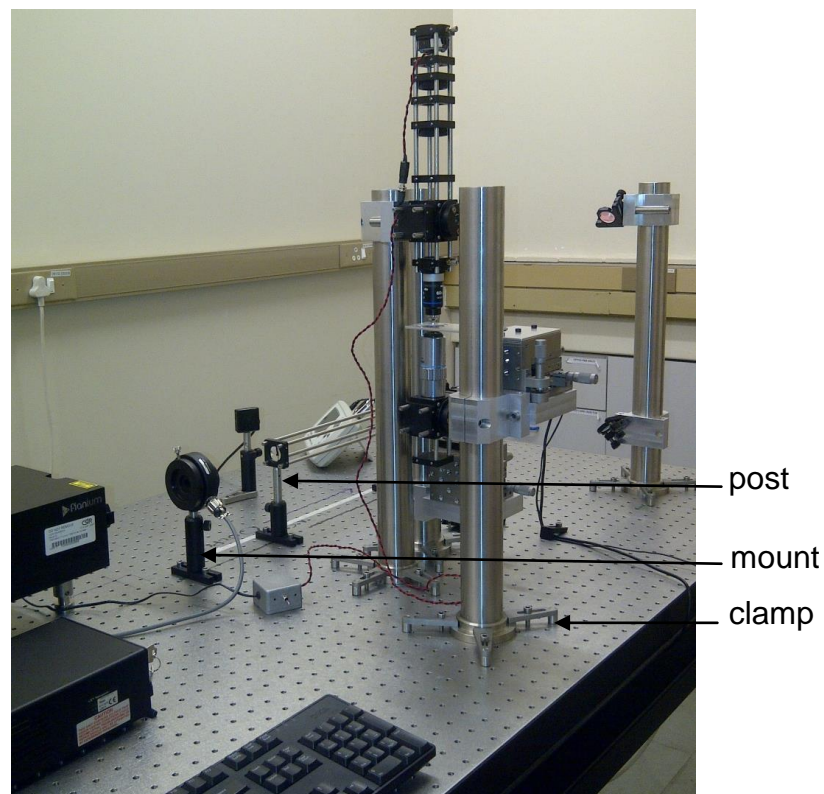


Figure 3.14: Image of the completed home-built photo-translocation setup.

The optical components of the set up were mounted and firmly screwed into a vibration damped (floated) table with optical supports such as clamps, posts and mounts and depicted if Figure 3.14. The alignment of a laser through the microscope objective is crucial to allowing a diffraction limited spot. This is critical for the production of a high quality three dimensional single-beam for the poration of the cell membrane. The expanding and collapsing of the airy disc formed as a result of the circular back aperture of the microscope objective is best illustrated by a video. Here, we however show a sequence of images displaying the focusing of the airy disc (Figure 3.15).

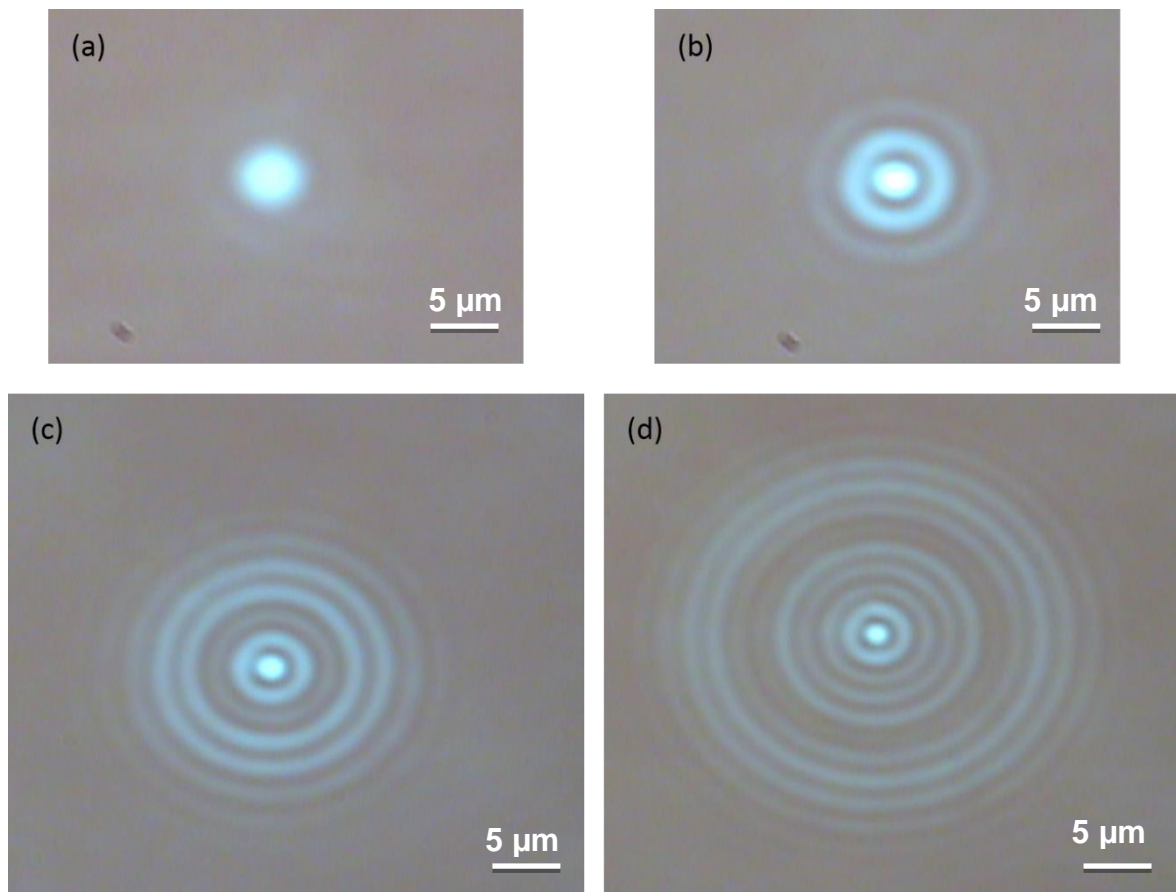


Figure 3.15 (a) to (d): Images illustrating the expansion and collapsing of an airy disc during focusing. These images were taken using a 60X objective lens.

The obtained airy disc was optimal for the photo-translocation studies as it was free of spherical aberrations, coma and astigmatism. To ensure that the laser beam was not clipped as it propagated through the microscope objective and that it was aligned accordingly, the airy disc was evaluated in greater detail. From Figure 3.15 it is clear that the airy disc is not clipped as perfect rings are observed. The obtained airy disc was compared to that shown in literature by (Ming Lee *et al.*, 2007). Figure 3.16 shows a sequence of images resembling those obtained in this study for the collapsing and expanding of the airy disc (Lee *et al.*, 2007).

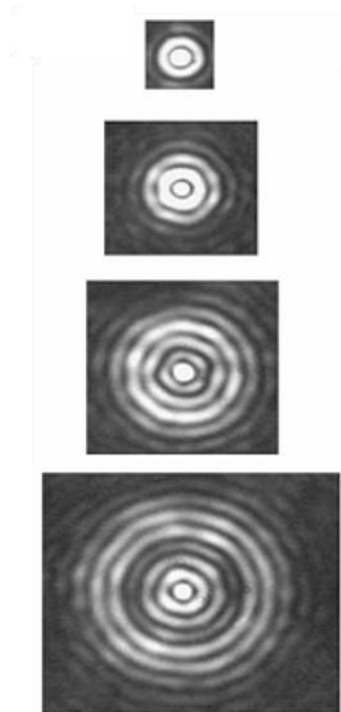


Figure 3.16: Image showing the focusing of an airy disc through collapsing and expanding.

Copied from (Ming Lee *et al.*, 2007).

Figure 3.17(a) depicts an example of a focused laser which is optimal for optical manipulation setups such as photo-translocation systems. The Figure also shows airy discs with unwanted aberrations (Figure 3.17(b) – (d)) during assembly of a functional optical system.

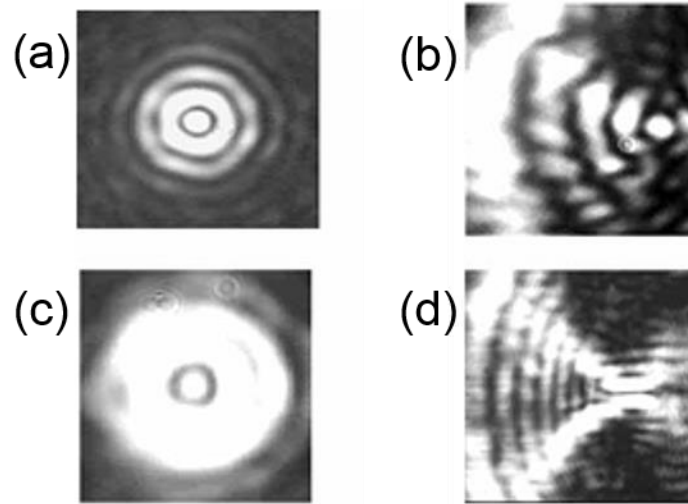


Figure 3.17: (a) Example of a focused, well aligned airy disc while (b) to (d) show examples of unwanted spherical aberrations.

Copied from (Lee *et al.*, 2007).

These images assert that the photo-translocation setup assembled in this study was optimally aligned and suited for the photo-translocation studies due to the absence of spherical aberrations on the resultant airy disc.

3.3 Photo-translocation of trypan blue viability dye

Trypan blue, a membrane impermeable viability dye was photo-translocated into TZM-bl cells under varying experimental parameters. Different exposure times of the laser to the cells and varying power levels were used in order to determine which parameters would not compromise the integrity of the cells. The marked area containing the cells that were treated was checked before and after laser treatment. The experiments were also carried out to demonstrate that the delivery of exogenous materials into cells can be achieved using a laser source. Subsequent to trypan blue photo-translocation, the optimal experimental parameters were used for the delivery of the selected ARV drugs into the HIV-1

permissive cell line. The bright-field microscope images in Figure 3.18 show the effects of photo-translocating trypan blue at a constant exposure time of 50 ms and varying power levels of 100, 80 and 60 mW.

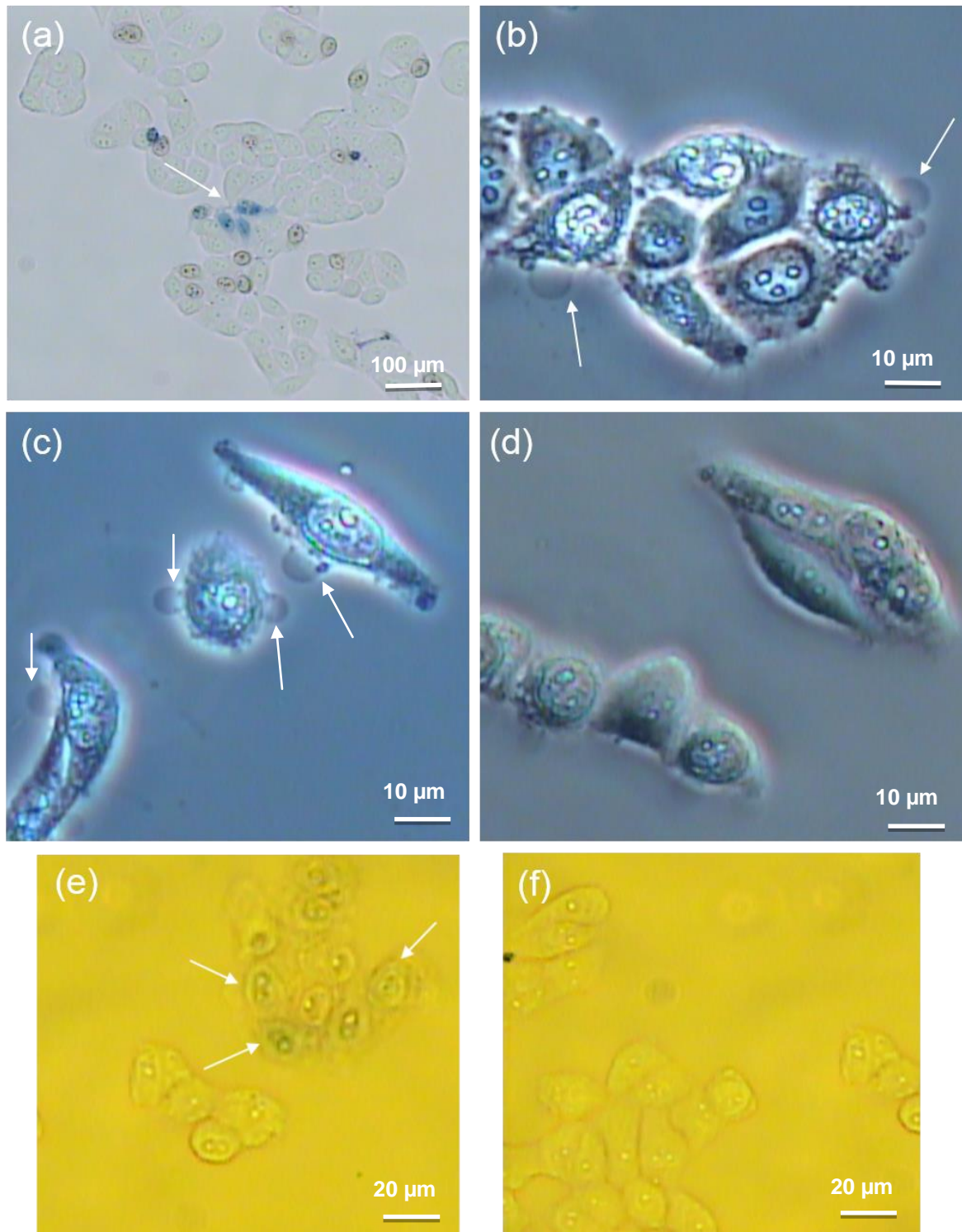


Figure 3.18: Bright field images of TZM-bl cells photo-porated in the presence of a membrane impermeable viability dye, trypan blue.

Photo-translocation was carried out at 1064 nm, 76 MHz, 10 ps and 50 ms. In a) and b) laser irradiation was done at a power level of 100 mW. More specifically a) shows photo-translocated cells where the white arrow indicates the treated cells. These images were taken using a 4X microscope objective. In b) irradiated cells are shown using a 40X microscope objective and arrows indicate cell blebbing. In c) and d) photo-translocation of the dye was done at 80 mW and the images were taken at a 40X magnification. In c) cell damage in the form of cell blebbing is shown and indicated by white arrows while d) shows cells that were not irradiated by the laser. In e) and f) laser assisted delivery of trypan blue was done at 60 mW. In e) irradiated cells which internalized the dye 5 minutes after photoporation are indicated by white arrows while f) shows untreated cells which did not internalize the dye. These images were taken using a 20X microscope objective.

In all three instances it was evident to the user that outside of the treated cells trypan blue was not internalized by the adjacent non-irradiated cells as these cells retained their natural transparent appearance. These, and all laser based experiments in this study, were done live and visualised in the computer as they took place. As such, these experiments would have been better reported as a video rather than in images as done in this report (outside the scope of this dissertation). At first glance 100 mW did not appear to exhibit negative effects on the integrity of the cells when the images were captured using a 4X magnification (Figure 3.18 (a)). Upon magnifying the images 10 times by using a 40X magnification (Figure 3.18 (b)), cell blebbing where a cytoplasmic spillage occurred was observed. Cell blebbing is seen in the images as circular extensions of the cells. Image 3.18 (b) appears to be darker than 3.18 (a) because residual trypan blue which remained after washing the cell monolayer with 1X PBS was more apparent when higher magnifications were used for imaging. At higher magnifications more detail on the cells was also observed.

When 80 mW was used as the photoporation power level, cell blebbing was observed amongst irradiated cells (Figure 3.18 (c)). This is contrary to when the cells were not treated by the laser in Figure 3.18 (d) where no cell blebbing was observed. Due to the residual trypan blue in the cell sample it is not clear which

cells retained the blue colour as a result of photo-translocation but it is clear that there is cell blebbing as a result of laser irradiation. Upon lowering the laser power to 60 mW no cell blebbing was observed amongst laser treated cells. Irradiated cells took up the blue dye which appears to be situated in the nucleus of the cells (Figure 3.18 (e)). The colour intensity of the internalised dye seems to be lower when the power level used is 60 mW compared to when laser treatment was done at higher powers. A higher amount of the dye appears to have been taken up at higher laser powers.

From these results we concluded that the optimal parameters to use for the photo-translocation of ARV drugs were to treat the cells with 3 doses of laser treatment at 60 mW with the shutter exposure time of 50 ms per shot.

3.4 Photo-translocation of ARV drugs into TZM-bl cells

Since the use of impermeable dyes is a gold standard for optimizing parameters such as laser power, exposure time and location of irradiation (Stevenson *et al.*, 2006, Pravan *et al.*, 2011), the parameters for trypan blue were extrapolated to drug delivery for the purposes of this study (where parameters are unknown). The ability of the newly assembled photo-translocation setup to assist in enhancing the intracellular delivery of ARV drugs was evaluated by monitoring the inhibitory effect on viral integration of a subtype C *env*-pseudotyped virus (ZM53), using a TZM-bl cell based assay. In this study 150 cells in a population of 2000 TZM-bl cells (7.5%) were treated with the laser.

The ability of DDS-assisted tenofovir, nevirapine and efavirenz delivered by photo-translocation to inhibit ZM53 replication in TZM-bl cells was quantified by measuring luciferase activity in RLUs. As shown in Figures 3.19 and 3.20 below, the photo-translocation of both tenofovir and nevirapine into TZM-bl cells respectively contributed to a higher inhibition of ZM53 compared to when drug delivery was not facilitated by the laser during the time where the cells were exposed to the drugs for 30 minutes. For both tenofovir and nevirapine delivery into TZM-bl cells the PCs showed the highest percentage of drug inhibition (refer to Table 3.5). The formula for the calculation of % inhibition is shown in Appendix B-1. The VCs for both tenofovir and nevirapine inhibition studies showed the highest level of infectivity. Viral activity and viral inhibition is assessed with reference to RLU values where a high RLU value is indicative of low pseudoviral inhibition while a low RLU value is indicative of a high pseudoviral by the ARV drugs. Differences in RLU values between the three independent experiments shown are attributed to different pseudovirus stocks.

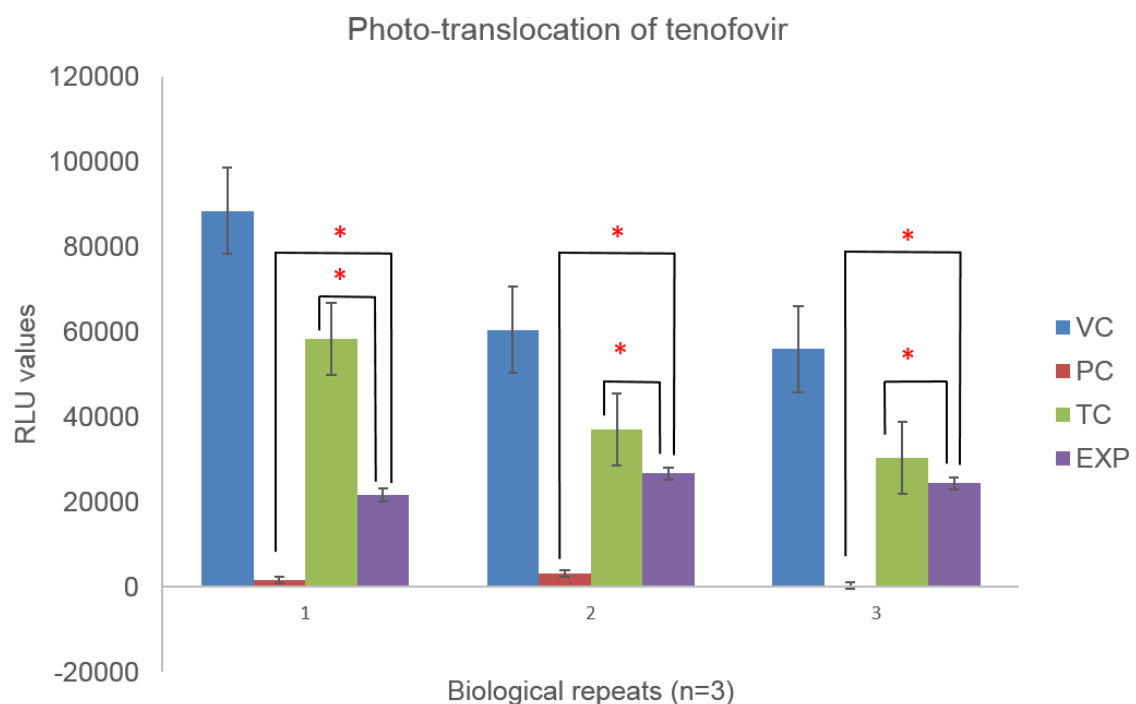


Figure 3.19: Bar graph showing the RLU values of the laser assisted delivery of tenofovir.

For tenofovir (EXP, purple) the cells were exposed to the drug for a period of 30 minutes while being irradiated. Data is shown against cells that were exposed to tenofovir for 30 minutes without laser treatment (TC, green), a positive control where the cells were exposed to tenofovir for 48 hours (complete duration of HIV-1 inhibition assay, PC, red) and against a negative control (VC, blue) where cells were infected with ZM53 *env*-pseudotyped virus in the absence of tenofovir. EXP, TC and PC were all challenged with ZM53. In all presented instances a higher inhibition of ZM53 was observed when the delivery of the drug was photo-translocated into the TZM-bl cells as represented by lower RLU values compared to TC. RLU values represent the means \pm standard error of the mean (SEM) for three independent experiments done in triplicate where error bars represent the SEM (n=3). The asterisk is a representation of significant difference amongst data sets where the standard t-test was used ($p < 0.05$).

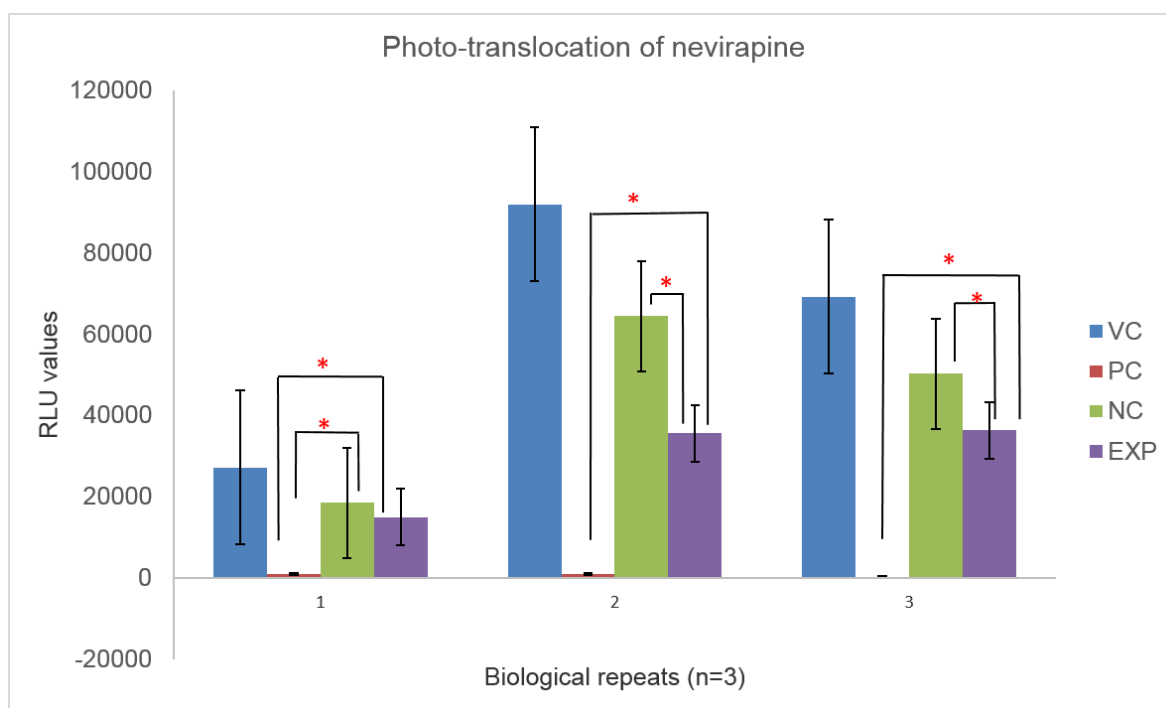


Figure 3.20: Bar graph showing the RLU values of the laser assisted delivery of nevirapine.

For nevirapine (EXP, purple) the cells were exposed to the drug for a period of 30 minutes. Data is shown against cells that were exposed to nevirapine for 30 minutes without laser treatment (NC, green), a positive control where the cells were exposed to nevirapine for 48 hours (complete duration of HIV-1 inhibition assay, PC, red) and against a negative control (VC, blue) where cells were infected with ZM53 *env*-pseudotyped virus in the absence of nevirapine. EXP, NC and PC were all challenged with ZM53. In all presented instances a higher inhibition of ZM53 was observed when drug delivery was facilitated by a laser as represented by lower RLU values compared to NC. RLU values represent the means \pm standard error of the mean (SEM) for three independent experiments done in triplicate where error bars represent the SEM (n=3). The asterisk is a representation of significant difference amongst data sets where the standard t-test was used ($p < 0.05$).

The RLU values obtained following the treatment of TZM-bl cells with efavirenz was significantly lower than the virus control in all instances at the utilized drug concentration (Figure 3.21). Both laser treated and untreated cells achieved 99%

inhibition of ZM53. Further, a prolonged exposure of the cell population to efavirenz (from 30 minutes compared to 48 hours) resulted in an inhibition percentage of 98% (Table 3.5).

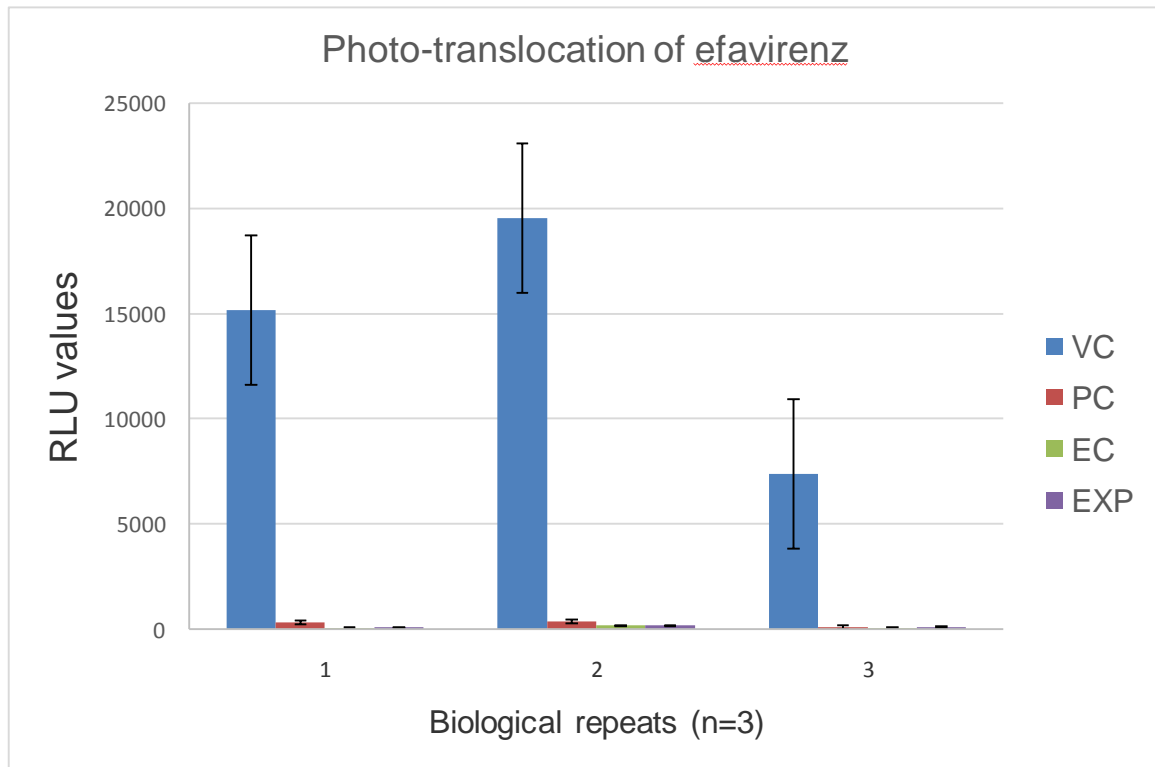


Figure 3.21: Bar graph showing the RLU values of the laser assisted delivery of efavirenz.

For efavirenz (EXP, purple) the cells were exposed to the drug for 30 minutes. Data is shown against cells that were exposed to efavirenz for 30 minutes without laser treatment (EC, green), a positive control where the cells were exposed to efavirenz for 48 hours (complete duration of HIV-1 inhibition assay, PC, red) and against a negative control (VC, blue) where cells were infected with ZM53 *env*-pseudotyped virus in the absence of efavirenz. EXP, EC and PC were all challenged with ZM53. In all presented cases efavirenz was able to successfully inhibit infection by ZM53 with no superiority to laser assisted drug delivery or drug to cell exposure time. RLU values represent the means \pm SEM for three independent experiments done in triplicate where the SEM is represented by error bars. No significant difference amongst data sets was observed when the standard t-test was used ($p < 0.05$).

Table 3.5: The percentage inhibition values of photo-translocated ARV drugs against drug taken up naturally by the cells with drug to cell exposure times of 30 minutes and 48 hours by measuring luciferase activity in HIV-1 infected TZM-bl cells.

% INHIBITION			
Sample	Tenofovir	Nevirapine	Efavirenz
PC	97 ± 26	99 ± 11	98 ± 22
TC/NC/EC	39 ± 14	29 ± 9	99 ± 36
EXP	64 ± 5	54 ± 6	99 ± 16

PC: Drug control where the cells were exposed to the drugs for 48 hours.

TC: Tenofovir control where the cells were exposed to tenofovir for 30 minutes.

NC: Nevirapine control where the cells were exposed to nevirapine for 30 minutes.

EC: Efavirenz control where the cells were exposed to efavirenz for 30 minutes.

EXP: Experiment where the laser was used to porate the cell membrane to allow diffusion of tenofovir, nevirapine and efavirenz.

3.5 Cytotoxicity assay

ARV drugs were delivered into TZM-bl cells through a laser induced pore on the cell membrane. The resultant percentage viability was measured relative to a drug control where the cells were exposed to the respective drug for 48 hours and against cells exposed to the drug for 30 minutes. In addition, a cell control (CC) with cells that were not treated with the laser or with drugs was kept under optimal growth conditions for the duration of the entire experiment. Cells which were treated with 1% Triton X-100 were included as a positive control. As shown in Figures 3.22 to 3.25 the viability of irradiated cells in all instances is greater than 70%. When the cells were exposed to the drugs for 30 minutes the percentage viabilities ranged from 53% to 100%. Further, in all instances the positive control showed low levels of viability ranging from 1% to 3%. Cells that were not treated with the laser or the drug (laser control (LC), Figure 3.22) showed a percentage viability of 100%. A percentage viability of 86% was observed in the tenofovir drug

control (Figure 3.23) while both nevirapine and efavirenz controls (Figure 3.24 and 3.25 respectively) showed significant differences ($p < 0.05$) to when drugs were exposed to the cell population for 30 minutes both in the presence and absence of laser irradiation. Table 3.6 shows the percentage viability for each reported instance (the formula used to calculate % viability is shown in Appendix B-1).

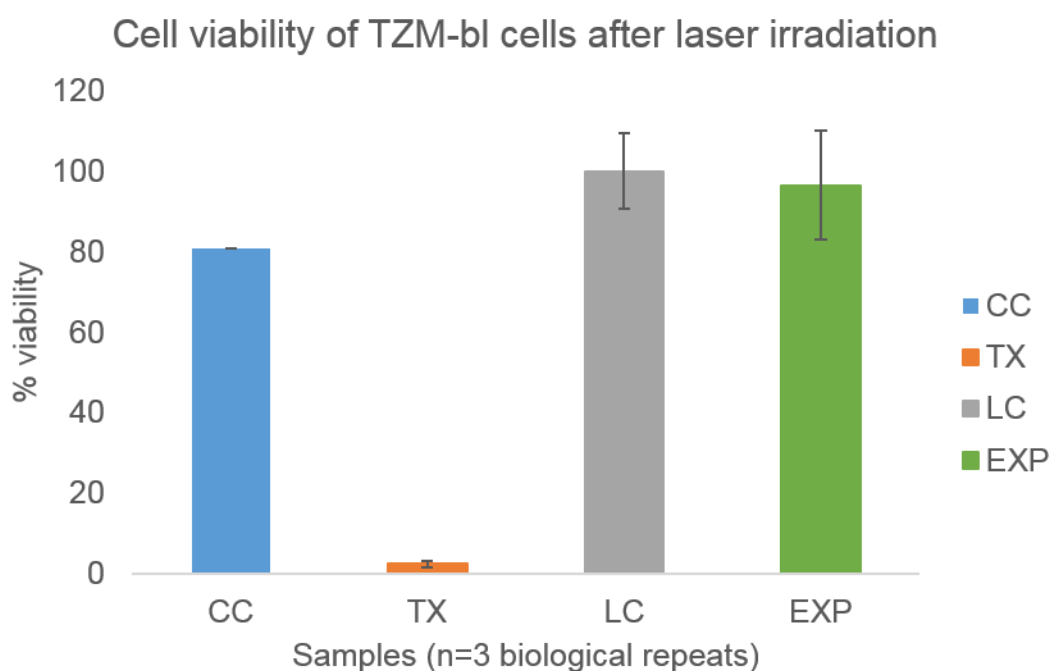


Figure 3.22: MTT assay for laser irradiated cells.

TZM-bl cells were irradiated with a laser at 1064 nm, 60 mW for a 50 ms exposure time per dose of a total of three doses per cell. Untreated cells (CC, blue), were kept under optimal growth conditions for the duration of the experiment, cells were treated with 1% Triton X-100 (TX, orange) as a positive control and laser treated cells (EXP, green) compared to cells that were not irradiated by the laser (LC, grey). Both laser treated and untreated cells showed % viabilities of 96.5 and 100% respectively. Error bars represent the SEM (n=3). No significant difference amongst data sets was observed when the standard t-test was used.

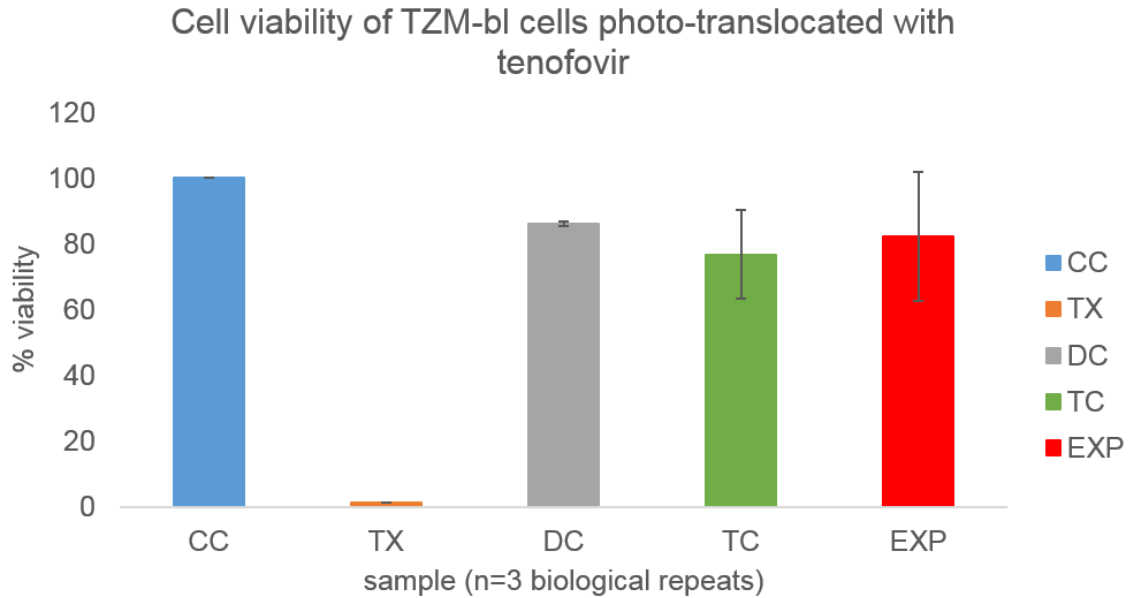


Figure 3.23: MTT assay for the photo-translocation of tenofovir into TZM-bl cells.

Tenofovir was photo-translocated into TZM-bl cells (EXP, red) and compared to the tenofovir control (TC, green) where the delivery of tenofovir was not assisted by the laser and tenofovir was exposed to the cells for 30 minutes. Additional controls where TZM-bl cells were exposed to the drug (DC, grey), 1% Triton X-100 (TX, orange) for 48 hours and a cell control (CC, blue) where the cells were not treated with the laser or ARV drugs while kept under optimal growth conditions for the duration of the experiment were included. In all instances either than TX, % viabilities of above 75% were achieved after treatment. Error bars are a representation of the SEM (n=3). No significant difference amongst data sets was observed when the standard t-test was used.

Cell viability of TZM-bl cells photo-translocated with nevirapine

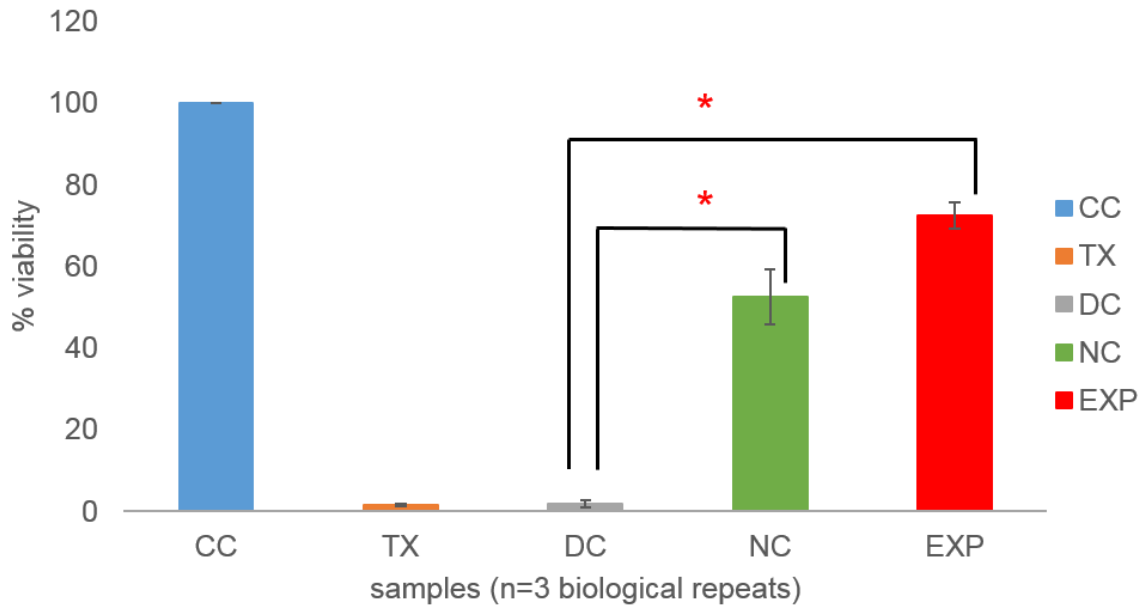


Figure 3.24: MTT assay for the photo-translocation of nevirapine into TZM-bl cells.

Nevirapine was photo-translocated into TZM-bl cells (EXP, red) and compared to the nevirapine control (NC, green) where the delivery of the drug was not assisted by a laser and the cell-to-drug exposure time was limited to 30 minutes. Additional controls where TZM-bl cells were exposed to 1% Triton X-100 (TX, orange) and a drug control (DC, grey) for 48 hours, and a cell control (CC, blue) where the cells were not treated with the laser or ARV drugs while kept under optimal growth conditions for the duration of the experiment were included. In all instances where the cells were treated with the laser and/or exposed to the drug for 30 minutes, % viabilities of above 50% were achieved with laser treated cells showing greater levels of viability than those not treated with the laser. When cells were treated with nevirapine for 48 hours (DC, grey) the viability of the cell population was severely compromised. A positive control where cells were treated with 1% Triton X-100 (TX, orange) was also included. Error bars are a representation of the SEM (n=3). Using the standard t-test an asterisk is a representation of significant difference.

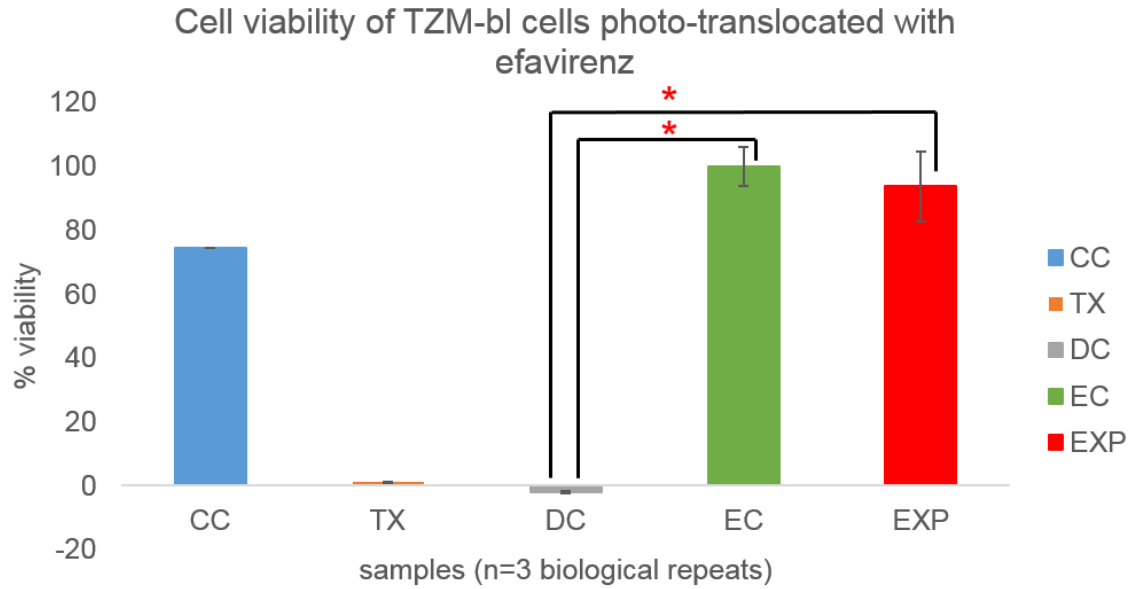


Figure 3.25: MTT assay for the photo-translocation of efavirenz into TZM-bl cells.

Efavirenz was photo-translocated into TZM-bl cells (EXP, red) and compared to the efavirenz control (EC, green) where the delivery of the drug was not assisted by a laser and the cell-to-drug exposure time was limited to 30 minutes. Additional controls where TZM-bl cells were exposed to 1% Triton X-100 (TX, orange), a drug control (DC, grey) and a cell control (CC, blue) where the cells were not treated with the laser or ARV drugs while kept under optimal growth conditions for the duration of the experiment were included. In all instances where the cells were treated with the laser and/or exposed to the drug for 30 minutes, % viabilities of above 50% were achieved with laser treated cells showing greater levels of viability than those not treated with the laser. When cells were treated with efavirenz for 48 hours (DC, grey) the viability of the cell population was severely compromised. A positive control where cells were treated with 1% Triton X-100 (TX, orange) was also included. Error bars are a representation of the SEM (n=3). Using the standard t-test an asterisk is a representation of significant difference between data sets.

Table 3.6: Percentage viabilities of laser irradiated cells and ARV photo-translocated cells assessed using the MTT assay.

% VIABILITY				
Sample	Laser alone	Tenofovir	Nevirapine	Efavirenz
CC	81.8 ± 0.0	100 ± 0.0	100 ± 0.0	74.6 ± 0.0
TX	2.4 ± 0.7	1.0 ± 0.1	1.0 ± 0.2	1.1 ± 0.2
DC	-	86 ± 1.3	2.0 ± 0.8	-2.1 ± 0.4
LC/TC/NC/EC	100 ± 9.2	77 ± 13	53 ± 6.7	100 ± 6.1
EXP	96.5 ± 12.4	82 ± 20	73 ± 3.3	93.8 ± 10.9

TX: Triton-x 100 - positive control where the cells were exposed to Triton-X 100 for 48 hours.

DC: Drug control where the cells were exposed to the drugs for 48 hours.

LC: Laser control where the cells were not treated with a laser and placed in the same environment as the cells treated by a laser for 30 minutes.

TC: Tenofovir control where the cells were exposed to tenofovir for 30 minutes.

NC: Nevirapine control where the cells were exposed to nevirapine for 30 minutes.

EC: Efavirenz control where the cells were exposed to efavirenz for 30 minutes.

EXP: Experiment where the laser was used to porate the cell membrane to allow diffusion of tenofovir, nevirapine and efavirenz.

CC: Cell control where the cell were not treated with the laser and the drugs. These cells were kept under optimal growth conditions throughout the duration of the experiments.

4. Discussions

The applicability of photo-translocation as a DDS to successfully deliver therapeutic agents to target cells was demonstrated by the ability of a home built fs laser to enhance the uptake of selected ARV drugs into HIV-1 permissive cells.

4.1 Characterisation of the laser towards the assembly of a functional photo-translocation setup

The more effective translocation of ARV drugs into TZM-bl cells relies on the efficiency of the assembled photo-translocation set up as well as accurate functioning of the laser beam. The functionality of the laser can be assessed by characterization which takes into account some laser parameters. These parameters include beam shape, beam quality and how the beam may be altered as it propagates in free space and through the optical system. In this study a pulsed laser was used and features such as pulse duration, central wavelength and spectral wavelength had to be taken into consideration during characterisation. It is possible to determine these characteristics experimentally which is important because it gives us information that is necessary during the assembly of the optical system and when preparing for the drug delivery experiments in the study. These characteristics are often predetermined by the manufacturer and given to the customer together with the laser system's manual. Acquiring more accurate values for these parameters experimentally is important to verify the standard specifications provided by the manufacturer as well as to ensure that the optical setup is assembled using precise measurements. The experimental setup has to be assembled to encourage the optimal operation of the laser especially where it interacts with the cell membrane.

4.1.1 Mode-locking nature of the Fianium FemtoPower laser

Lasers are able to oscillate on various longitudinal modes with frequencies that are spaced equally by intermodal spacing. These modes usually oscillate independently but external means can be adopted to couple the modes and lock their phases together. When the phases are locked together a periodic pulse train is formed (Bahaa *et al.*, 1991). A mode locked laser ensures that there is stability amongst the emitted pulses. According to the consistency of the pulses as they propagate along the z axis it was observed that the laser is passively mode locked (Figure 3.1). A repetition rate of 76.6 MHz was obtained for the pulses of the laser used in this study. High repetition rates such as this are recommended for photoporation as they can yield up to several millions of pulses at a single laser exposed spot on the cell membrane (Vogel *et al.*, 2005).

4.1.2 Laser pulse durations

The measurement of the pulse duration was acquired and carried out using FROG as stipulated in section 2.3.3. A FROG measurement provides information about time, wavelength as well as intensity. As the two pulses generated by the BS propagate towards the nonlinear crystal, one of the pulses is delayed in time by increasing or decreasing the path length compared to the other. By overlapping the two pulses in space and time within the nonlinear crystal, light with twice the frequency of the input laser was produced. This light is mostly referred to in this study as the FROG signal. In the case where the two laser pulses do not overlap in time within the nonlinear crystal no autocorrelation signal would be obtained (Trebino *et al.*, 1997).

The pulse duration of 10 ps obtained from the FROG measurements is not ideal for photoporation experiments as ps pulses have been reported to yield low poration efficiencies and can result in negative mechanical effects on the cell (Schinkel *et al.*, 2008). Due to financial constraints we were not able to purchase an alternative fs laser source and due to time constraints we were not able to return the laser to the manufacturer for further investigation. We however continued to use the Fianium laser to perform the drug delivery experiments that were intended for this study as we believed that the findings of this study can contribute to the advancement of the fields of biophotonics and drug delivery. The effects of using a fs laser against a ps laser are discussed further in section 4.5.

4.1.3 Beam quality contribution to the efficiency of photo-translocation

In this study an optimal quality of the beam was essential because it influences the success of the photo-translocation of the ARV drugs. A high quality laser has a smooth wavefront which means that focusing the laser with an objective lens will result in a plane wavefront which is desirable for this study. In a case where the quality of the beam is low, the wavefront would be scrambled resulting in difficulty when focusing the beam (Siegman, 1990). The ability to acquire a diffraction limited spot is the essence of photo-translocation as it is with a tightly focused laser that a pore can be efficiently generated on the cell membrane. Further, it is through the generated pore that the drugs are able to diffuse into the cell. A scrambled wavefront at the beam focus would therefore interfere with the photo-translocation of the drugs.

According to the obtained M^2 result of 1.15, the Fianium laser is approximately 1.15 times diffraction limited as compared to a true Gaussian beam profile (Siegman, 1993). The quality of the Fianium laser (based on the obtained M^2 value) is of a good standard as it is close to 1.0 which is the M^2 value of a true Gaussian beam.

4.1.4 Functionality of assembled photo-translocation setup

During assembly where optics were placed accordingly following the schematic depicted in chapter 2, the alignment of the laser was critical to ensure functionality of the complete set up. As the beam propagated through the optical elements of the setup, care was taken to ensure that the laser landed on the centre of all the optics. This ensured that the laser was not clipped and remained circular and propagated straight and levelled. To achieve this, pin holes were strategically placed along the setup where passage through all the pin holes confirmed that the laser beam was at the centre of the optics and that it was levelled in terms of height as it propagated. In the setup, cages were also employed to hold some of the optical components making it easier to align the laser (as shown in Figure 3.14).

4.2 Establishment of an HIV-1 inhibition assay

Laser assisted delivery of exogenous materials into cells has been explored in various sectors of biomedicine and biotechnology. As mentioned in earlier sections, the efficiency of the technology has previously been quantified by the delivery of dyes and fluorescent DNA plasmids (Stevenson *et al.*, 2006, Tirlapur *et al.*, 2002). In this study, our focus was not only to evaluate the efficiency of the

technology but was primarily to prove and show for the first time that the technology can be applied to enhance the therapeutic effects of ARV drugs that have been photo-translocated into HIV-1 permissive cells. This proof-of-principle study therefore made use of a HIV-1 *env*-pseudotyped inhibition assay to show the technology is applicable to enhancing drug delivery *in vitro*.

This primarily quantitative assay is widely utilized to measure the effect of various inhibitors such as antibodies (Montefiori, 2005), aptamers (Mufhandu *et al.*, 2012) and other lead compounds (ARV drugs) on viral replication. The assay is standardised and reproducible making it an ideal tool for the primary screening of the effects of photo-translocation also taking into account its reported levels of accuracy (Polonis *et al.*, 2008). The assay can be performed using peripheral blood mononuclear cells (PBMCs) and replication competent virus derived from PBMCs. These viruses make use of an error prone RT in order to replicate thus representing a heterogeneous viral population. For reproducibility purposes and ease of comparison we used a homogeneous viral population of an *env*-pseudotyped viral strain, ZM53 (Polonis *et al.*, 2008). The advantage presented by using a pseudovirus includes the exclusion of variables such as growth kinetics which could influence the results and compromise the primary purpose of this study.

Here we chose to use ZM53 as the *env*-pseudotyped virus to assist in evaluating that the ARV drugs were indeed internalised by the TZM-bl cells during photo-translocation. The pseudovirus is clinically relevant as it is a subtype C viral strain and as such dominant in Sub-Saharan Africa. ZM53 is categorised by Seaman *et*

al., (2010) as a tier 2 *env* pseudovirus when they assessed the stringency of a panel of 109 molecularly cloned HIV-1 *env* pseudoviruses. Compared to tier 1 viruses which are easily neutralised, ZM53 is a more resistant pseudovirus to neutralisation (Seaman *et al.*, 2010). It is therefore considered clinically relevant and ideal for screening purposes in this study.

The ARV drugs that were chosen in the study namely; tenofovir, nevirapine and efavirenz are FDA approved drugs for the treatment of HIV-1. At the time the study was conducted, these drugs were highly recommended as a regimen for the first line defence against HIV-1 infection in South Africa. As such, these selected drugs were locally relevant for the purposes of this study.

4.2.1 Fate of the ARV drugs used in the study

The ARV drugs used in this study are orally administered, immediate release tablets. These drugs therefore disintegrate rapidly and are dissolved to facilitate the release of the medicament (Jaimini, 2013). They are absorbed in the GIT which is also a major barrier to the bioavailability of drugs. The GIT contains metabolising enzymes, efflux proteins and physiochemical properties which contribute to the hindrance to the absorption of the drugs (Pang, 2003).

The primary site for the metabolism of both nevirapine and efavirenz is the liver. The liver contains cytochromes (CYP) P450 which are proteins characterised by possessing an absorption maximum at 450 nm after carbon monoxide (CO) binding. These proteins which comprise of a superfamily of specific gene products

that contain different specificities catalyse the oxidative metabolism of endogenous and exogenous substances. Molecular isoforms of CYP are induced when exposed to chemical stimuli (Khatsenko *et al.*, 1993).

Nevirapine and efavirenz are such chemical stimuli as they are moderate inducers of CYP (Riska *et al.*, 1999, Cristofolletti *et al.*, 2013). Both drugs are metabolised through biotransformation by the isoenzymes CYP3A4 and CYP2B6 (Cristofolletti *et al.*, 2013, Erickson *et al.*, 1999, Riska *et al.*, 1999, Adkins *et al.*, 1998). By virtue of being inducers, these drugs are able to increase the rate of hepatic metabolism of other drugs by increasing the transcription of CYP messenger tRNA (Back *et al.*, 2003). Consequently, the production of more enzymes occurs and a decrease in the plasma concentration of the drug being metabolised by the induced pathway takes place (Wood *et al.*, 2001). Both nevirapine and efavirenz are eliminated in the urine after glucoronidation to water soluble conjugates for rapid elimination from the body (Cammett *et al.*, 2009).

Unlike nevirapine and efavirenz that are metabolised by CYP, tenofovir disoproxil fumarate (TDF) is not metabolised by these enzymes but rather undergoes several intracellular processes. TDF is a prodrug of tenofovir which goes through esterase hydrolysis for the removal of the ester group in the compound after being administered orally. Tenofovir requires intracellular phosphorylation to the active moiety (Cristofolletti *et al.*, 2013). It is taken up by the cells where it is phosphorylated by cellular nucleoside diphosphate kinases to the active diphosphate form. The activation of tenofovir takes place in both active and resting cells.

4.3 Effects of ARV photo-translocation on the inhibition of ZM53 env-pseudotyped virus replication

The primary objective of this study was to show that a laser can be used as an effective DDS. This was done by assisting the uptake of ARV drugs by an HIV-1 permissive cell line. Subsequently, a ps laser source was employed to create a pore on the cell membrane through which higher amounts of drugs were expected to enter the cell compared to natural drug uptake by cells by active diffusion (Gerber, 2000). As mentioned, TZM-bl cells are able to take up ARV drugs naturally so the superiority in laser assisted drug delivery was demonstrated through the resultant inhibition percentage of ZM53 when the drug-to-cell exposure time is limited to 30 minutes. During this 30 minute period \pm 150 cells in a total of 2000 pre-seeded cells per sample were photo-porated.

The photo-translocation of tenofovir and nevirapine resulted in enhanced viral inhibition. In both cases the percentage of viral inhibition was 25% greater than when TZM-bl cells took up the drug naturally without the assistance of a laser in the same time period. Future studies of the work should investigate mechanisms either than photo-translocation and active diffusion which could be contributing to the significant difference observed between irradiated and non-irradiated cells after treatment of only 7.5% of the cell population. The same result was however not obtained when efavirenz was photo-translocated into the cells. Instead, TZM-bl cells were able to rapidly take up efavirenz irrespective of laser facilitation. The percentage viral inhibition of ZM53 in both comparable instances of 30 minute drug-to-cell exposure periods was 99%.

The mode of action of tenofovir is such that the analogue competes with endogenous DNA-triphosphate to hinder RT activity. Nevirapine and tenofovir on the other hand involves non-competitively binding to the RT enzyme. In all three of the drug cases, the result of their interference prevents RT from converting viral RNA to viral DNA (Sosnik *et al.*, 2009). The manner in which drugs interact with the body is referred to as pharmacokinetics. The behaviour of efavirenz in this study may be explained by this concept which speaks to the absorption, transport, distribution, metabolism or the manner in which a drug is excreted from the cell (Wood *et al.*, 2001).

With a long half-life of 40-45 hours and a wide distribution among various body compartments, efavirenz has found wide application in the treatment of HIV-1. However, one of the challenges of efavirenz is its association with variable responses amongst different individuals and even failure to therapy in some patients (Ward *et al.*, 2003). Efavirenz has also been reported to possess low stability in turn compromising its administration, absorption and biodistribution (Sosnik *et al.*, 2009). In this study TZM-bl cells were able to efficiently take up efavirenz. The susceptibility of individuals to diseases as well as how individuals respond to drugs varies. Due to the activity and expression of CYPs displaying individual differences, the pharmacokinetics of efavirenz show inter-individual variability (Adkins *et al.*, 1998).

The inter-individual variability of efavirenz is seen mostly in the CYP2B6 which is the main isoenzyme responsible for the metabolism of efavirenz. The variability is a result of the polymorphic variants of CYP2B6 which leads to different

functionality of the isoenzyme between different patients. The variability can also be accounted for by population variables such as age and gender (Marzolini *et al.*, 2001). To explain the possible reason for the ability of TZM-bl cells to metabolise efavirenz with such efficiency may be attributed to the genetic properties of HeLa cells as such, genotyping the HeLa cells in the future may account for the obtained result.

Efavirenz is metabolised through hydroxylation by CYP2B6 (Bienvenu *et al.*, 2014) whose presence has been reported to be more prevalent in African Americans than in Caucasians (Cholewinska, 2007). Through this observation it becomes clear that the photo-translocation of drugs as a DDS may be selective in functionality depending on the pharmacokinetics of the delivered drug and the host genetics in the treated individual. This highlights that in developing a DDS, the effects of pharmacogenetics and pharmacokinetics should be taken into consideration. Due to the genetic background of the TZM-bl cells, the DDS demonstrated in this study was able to contribute to an elevated viral inhibition of tenofovir and nevirapine but did not have an effect when efavirenz was photo-translocated. It is therefore unclear if other cells will respond in a similar manner to the laser facilitated delivery of ARV drugs. This requires further investigation where other cell lines, different donors and different cell types such as CD4⁺ T cells which are major HIV-1 target cells should be treated using a laser as a DDS.

4.4 Effects of laser irradiation and ARV photo-translocation on TZM-bl cell viability

The final aim of this study was to confirm that no toxicity resulted from the laser treatment of the cells when the laser was used on its own and in conjunction with ARV drugs selected for the study. The standard and classical method for assessing viability within a cell population is trypan blue exclusion. This visual method (making use of light microscopy) assesses the late apoptotic and necrotic stages of viability detection where viable cells have an intact cell membrane and can therefore exclude the entry of trypan blue (Strober, 2001). The MTT assay used in this study is an analytical biochemical procedure where mitochondrial activity is measured as reflected by the conversion of the tetrazolium salt, MTT, into formazan crystals (van Meerloo *et al.*, 2011). The MTT assay is advantageous compared to the trypan blue exclusion test because it operates at a metabolic level. As such, cells that present with intact cellular membranes with a slow or malfunctioning metabolism can be detected by the MTT assay as cells that are not viable (St-Louis Lalonde *et al.*, 2013).

The laser was used to porate cells in the absence of drugs and the resultant measured cell viability was $96.5 \pm 12.4\%$. This means that when used on its own at an output power of 60 mW and a laser-to-cell exposure time of 50 ms per shot, treated cells did not show negative reactions to photoporation. This result is similar to that of St-Louis Lalonde *et al.*, (2013) where they tested the viability of melanoma cells in Roswell Park Memorial Institute (RPMI) 1640 medium following irradiating them with a 1064 nm, 5 ns pulsed laser source at 1 J/cm^2 . St-Louis Lalonde *et al.*, (2013) also used the MTT assay to evaluate the viability of the cell

populations treated in their study where they obtained constant viabilities of above 95%. In the absence of laser treatment slightly higher viabilities were observed amongst the TZM-bl cell population although not significantly different.

The viability of the cells was again evaluated post photo-translocation of the respective ARV drugs. In all instances cell viabilities were greater than 70% at the photo-translocated ARV drug concentrations utilised. The ARV drug concentrations used were based on 50% inhibitory concentrations (IC_{50} s) of the drugs as reported in literature (Cheeseman *et al.*, 1993, McRae *et al.*, 2006); as such we did not expect to observe cytotoxic effects in any of the photo-translocated drugs compared to when drugs were allowed to diffuse into the cells on their own. This was indeed the case for the tenofovir DC ($86 \pm 1.3\%$) but not for nevirapine ($2 \pm 0.8\%$) and efavirenz ($-2 \pm 0.4\%$) DC's. Here, a significant difference in cell viabilities was observed compared to when the nevirapine ($73 \pm 3.3\%$) and efavirenz ($94 \pm 10.9\%$) was photo-translocated and exposed to the cell population for 30 minutes. This unexpected result may be because the IC_{50} s adapted from the literature were based on *in vivo* rather than *in vitro* studies taking into consideration that clinical drug dosages are significantly higher than those administered *in vitro*. Clinically, this is necessary to ensure that target sites receive an adequate amount of drug to be able to result in the desired therapeutic effect as majority of the drug is expected to interfere with areas of the body that are not intended thus not requiring exposure to the drugs.

The percentage viabilities observed for the laser control (LC) and when the cells were porated in the absence of ARV drugs were greater than the % viabilities of CC (see Table 3.6). This was also the case when efavirenz was administered to the cells and the drug-to-cell exposure time was 30 minutes both in the absence and presence of laser treatment (see Table 3.6). These results are common when the MTT viability assay is used (Soares *et al.*, 2013, Golden *et al.*, 2009, Melo *et al.*, 2012, Barahuie *et al.*, 2014, Kehoe *et al.*, 2013).

These results highlight the potential advantages of using a DDS for the delivery of therapeutic drugs. Here, nevirapine and efavirenz were highly toxic when exposed to the cell population for prolonged periods of time (48 hours). This is contrary to when the exposure time was decreased to 30 minutes. In the case of nevirapine, after targeting only ± 150 cells in a population of 2000 cells in a 30 minute period, an enhanced level of viral inhibition was observed. On the contrary, efavirenz showed no preference to laser irradiation or exposure time where inhibition of viral replication was concerned. In light of the percentage viability results, it is apparent that the cells exposed to the drugs for 48 hours may have not been viable after photo-translocation of the drugs which means that the observed percentage inhibitions were due to the fact that the cells were not metabolically viable after the incubation period and may have also been dead, and incapable of supporting viral replication. This observation is true for both nevirapine and efavirenz.

From this we can deduce that a decrease in drug-to-cell exposure periods and photo-translocation of drugs during this period contributes to enhanced cellular

percentage viabilities while still contributing to enhanced viral inhibition in the case of nevirapine.

4.5 ps versus fs laser sources

The technology of photo-translocating extracellular material has been shown to yield the best result when a fs laser source is used (Mthunzi *et al.*, 2010, Tirlapur *et al.*, 2002, Uchugonova *et al.*, 2008, Zeira *et al.*, 2003). In this study the laser used was reported by the manufacturer to have a path length of 210 fs. In our hands the laser pulse length was measured to be 10 ps which is contrary to the manufacturer's measurement of 210 fs. We therefore used a ps laser source for this study. The efficiency of fs laser sources was confirmed by Tirlapur *et al.*, (2002) where they observed high precision microsurgery of CHO cells where vital cellular function remained intact.

In our experiment, the use of ps laser pulses was appropriate in the facilitation of photo-translocation of the extracellular materials with minimal damage exerted on the treated cell population. Similarly, Schinkel *et al.*, (2008) used a ps laser source in their study where the obtained results were satisfactory. The low energy levels of the laser (60 mW) during experiments was below the threshold for dielectric break-down in water which means that shock waves may have been the cause of the openings on the cell membrane (Noack *et al.*, 1998). The mechanism of photoporation with a ps laser source is plasma formation resulting from linear absorption while the mechanism of fs laser sources is multiphoton plasma formation (Vogel *et al.*, 2005). The main disadvantage of ps laser sources besides the possible mechanical effects when high laser energies are used is the

complexity that is experienced in generating high repetition rate ps laser sources (Omatsu *et al.*, 2007). The laser used in this study is commercially available so difficulties in generating the high repetition rates of the laser source were not an issue for our purposes.

4.6 Limitations of the study

Photo-translocation of drugs in this study was carried out one cell at a time. In a time period of 30 minutes \pm 150 cells were porated. The single cell treatment nature of the technology is a limitation as it does not allow for the treatment of large cell populations. In this study the ability to treat the entire cell population in each sample would have led to a more accurate comparison of the positive control and the cells where the laser was used to assist ARV drug delivery. In future, an additional control experiment comparing drug concentrations before and after the uptake of drugs in both the populations treated with the laser and those not exposed to the laser should be carried out. Such an experiment would serve to prove that there is indeed a difference between photo-translocation of drugs as opposed to when photo-translocation is not administered. We believe that the ability to treat entire cell population would have led to percentage inhibitions similar to the positive control in a short drug-to-cell exposure time.

This limitation was also observed by Marchington *et al.*, (2010) where they suggested and demonstrated that an automated system in the form of a microfluidic device which they used to deliver cells to the focus of a laser could lead to a higher throughput of cell treatment. Although such a technology would increase the throughput of photo-translocation it would not be applicable in this

study because TZM-bl cells are an adherent cell line. Such a technology would be more suited for the poration of suspension cells such as PBMCs and lymph node explants as this study progresses to other cell types.

Antkowiak *et al.*, (2013) has recently demonstrated the use of a computer based interface for the targeting and poration of the cell membrane. The platform combines a fast steering mirror and LabView software to create a touch screen based interface for the control of photoporation. The automated system allows the experimenter to point-and-transfect target cells by simply touching the cell on the screen. Such a technology would be applicable to this study as it allows for photoporation of adherent cells.

Another limitation of the current study is that for successful photoporation to take place, accurate alignment of the focused Gaussian beam spot and the focused cell membrane must occur. A slight misalignment leads to a decrease in the efficiency of photoporation. This careful alignment is however time consuming thus contributing to the fact that the technology is not high throughput. To mitigate this limitation, Tsampoula *et al.*, (2007) used a non-diffracting light beam known as the Bessel beam (BB) in their optical transfection studies.

Section 1.5 outlined the propagation properties of Gaussian beams. Due to the diffractive nature of Gaussian beams they have a short axial distance to which the cell membrane is aligned during photoporation (McGloin *et al.*, 2005). BBs on the other hand can be referred to as 'pseudo non-diffracting' beams as these beams

have a narrow rod-like core which is not prone to diffraction over extended distances (Dholakia *et al.*, 2008). Due to this property of the BB, it is possible to place the focused cell membrane along any point of the beam thus allowing for the treatment of more cells in the sample. Tsampoula *et al.*, (2007) showed in their study that BBs offer photo-transfection at axial distances 20 times greater than that of Gaussian beams. As such, the use of BBs would contribute to the photo-translocation of ARV drugs into an increased number of cells in turn strengthening the accuracy of the study outcomes.

The current proof-of-principle study included a variety of control tests with the aim to show that using a DDS has the potential to enhance the treatment of target cells. However, in the study there is no control eliminating the possible effects of laser treatment in the absence of the ARV drugs on ZM53 replication, as such, a control of this nature should be included in future studies.

5. Conclusions and Future perspectives

5.1 Conclusions

In this study we assembled and characterised a fully functional photo-translocation system to facilitate the delivery of ARV drugs into an HIV-1 permissive cell line, TZM-bl cells. Following photo-translocation the cells were then infected with a subtype C *Env*-pseudotyped virus. The selective nature of the technology was demonstrated by the photo-translocation of trypan blue into targeted TZM-bl cells. This proof-of-principle study has demonstrated that a ps laser source can be employed to more efficiently deliver ARV drugs into TZM-bl cells and contribute to an enhanced level of viral inhibition with little to no compromise to the viability of the treated cells. The delivery of drugs into cells using this technology was demonstrated through the amalgamation of a molecular biology assay rather than light microscopy. The study provides preliminary data showing that by employing a DDS for the delivery of drugs in a targeted manner, the drug-to-cell exposure time can be significantly decreased in turn decreasing the toxic effects of drugs especially when drugs are administered in high and otherwise toxic concentrations.

5.2 Future perspectives

As this was a proof-of-principle study to primarily demonstrate the application of a pulsed, high repetition laser source for the enhanced delivery of ARV drugs into target cells, there is still a lot of work to be done to further optimize the technology at an *in vitro* level with intentions to ultimately progress to *in vivo* studies possibly in mouse models. The DDS should be tested in the future in different cell lines and against varying drug concentrations (including dose-dependent response

studies) as well as in varying drug-to-cell exposure periods, with the appropriate controls.

To increase the throughput of the technology, the technology should in future be automated to enable treatment of the entire cell population at a quicker period of time. This study made use of a Gaussian beam for all experiments, in future the photo-translocation of drugs could be done using a BB where the results can be compared to those attained using a Gaussian beam.

The results of this study highlighted the importance of taking into consideration the pharmacokinetics of a drug and the pharmacogenetics of the patient in drug administration. Although demonstrated in TZM-bl cells, the study should progress to deliver more ARV drugs with different modes of action as well as those used in the current study in other cell lines and other cell types from blood donors. For example the cell types that could be treated in future include PBMCs, lymph node extracts and CD4⁺ T cells which are a major target cell for HIV. The ability of the technology to contribute to enhanced levels of ZM53 inhibition must be interrogated against a panel of *env*-pseudotyped viruses from different HIV-1 subtypes in so doing assessing the broad applicability of the technology. Lastly, ZM53 is only capable of one round of infection, as such the technology should in future be investigated for its ability to facilitate enhanced viral inhibition against replication competent viruses.

References

- ADKINS, J. C. & NOBLE, S. (1998) Efavirenz. *Drugs*, 56, 1055-1064.
- AL-JAMAL, W. T. & KOSTARELOS, K. (2011) Liposomes: from a clinically established drug delivery system to a nanoparticle platform for theranostic nanomedicine. *Accounts of chemical research*, 44, 1094-1104.
- AL-WATBAN, F. A. H. & ZHANG, X. Y. (2004) The comparison of effects between pulsed and CW lasers on wound healing. *Journal of clinical laser medicine & surgery*, 22, 15-18.
- ALEXAKI, A., LIU, Y. & WIGDAHL, B. (2008) Cellular Reservoirs of HIV-1 and their role in viral persistence. *Current HIV Research*, 6(5), 388-400.
- ALKHATIB, G., COMBADIÈRE, C., BRODER, C. C., FENG, Y., KENNEDY, P. E., MURPHY, P. M. & BERGER, E. A. (1996) CC CKR5: a RANTES, MIP-1 α , MIP-1 β receptor as a fusion cofactor for macrophage-tropic HIV-1. *Science*, 272, 1955-1958.
- ALLEN, T. M. & CULLIS, P. R. (2004) Drug delivery systems: entering the mainstream. *Science*, 303, 1818-1822.
- AMAT-ROLDAN, I., CORMACK, I., LOZA-ALVAREZ, P., GUALDA, E. & ARTIGAS, D. (2004) Ultrashort pulse characterisation with SHG collinear-FROG. *Optics express*, 12, 1169-1178.
- AN, D. S., XIE, Y., MAO, S. H., MORIZONO, K., KUNG, S. K. P. & CHEN, I. S. Y. (2003) Efficient lentiviral vectors for short hairpin RNA delivery into human cells. *Human gene therapy*, 14, 1207-1212.
- ANDREWS, L. C. & PHILLIPS, R. L. (2005) *Laser beam propagation through random media*, SPIE press Bellingham.
- ANISHETTY, S., PULIMI, M. & PENNATHUR, G. (2005) Potential drug targets in *Mycobacterium tuberculosis* through metabolic pathway analysis. *Computational biology and chemistry*, 29, 368-378.
- ANTKOWIAK, M., TORRES-MAPA, M. L., WITTS, E. C., MILES, G. B., DHOLAKIA, K. & GUNN-MOORE, F. J. (2013) Fast targeted gene transfection and optogenetic modification of single neurons using femtosecond laser irradiation. *Scientific reports*, 3.
- ARTS, E. J. & HAZUDA, D. J. (2012) HIV-1 Antiretroviral drug therapy. *Cold Spring Harbor Perspectives in Medicine*, doi: 10.1101/cshperspect.9007161
- BACK, D., GIBBONS, S. & KHOO, S. (2003) Pharmacokinetic drug interactions with nevirapine. *JAIDS Journal of Acquired Immune Deficiency Syndromes*, 34, S8-S14.
- BAHAA, E. A. S. & MALVIN, C. T. (1991) Fundamentals of photonics. *New York/A WILEY-INTERSCIENCE PUBLICATION*.
- BALLY, M. B., HARVIE, P., WONG, F. M. P., KONG, S., WASAN, E. K. & REIMER, D. L. (1999) Biological barriers to cellular delivery of lipid-based DNA carriers. *Advanced drug delivery reviews*, 38, 291-315.
- BARAHUÏE, F., HUSSEIN, M. Z., FAKURAZI, S. & ZAINAL, Z. (2014) Development of Drug Delivery Systems Based on Layered Hydroxides for Nanomedicine. *International journal of molecular sciences*, 15, 7750-7786.
- BARRE-SINOUSSE, F. O., CHERMANN, J.-C., REY, F., NUGEYRE, M. T., CHAMARET, S., GRUEST, J., DAUGUET, C., AXLER-BLIN, C., VEZINET-BRUN, F. O. & ROUZIOUX, C. (1983) Isolation of a T-lymphotropic retrovirus from a patient at risk for acquired immune deficiency syndrome (AIDS). *Science*, 220, 868-871.

- BARRETT, L. E., SUL, J. Y., TAKANO, H., VAN BOCKSTAELE, E. J., HAYDON, P. G. & EBERWINE, J. H. (2006) Region-directed phototransfection reveals the functional significance of a dendritically synthesized transcription factor. *Nat Methods*, 3, 455-60.
- BATTEY, N. H., JAMES, N. C., GREENLAND, A. J. & BROWNLEE, C. (1999) Exocytosis and endocytosis. *The Plant Cell Online*, 11, 643-659.
- BELTING, M., SANDGREN, S. & WITTRUP, A. (2005) Nuclear delivery of macromolecules: barriers and carriers. *Advanced drug delivery reviews*, 57, 505-527.
- BIENVENU, E., SWART, M., DANDARA, C. & ASHTON, M. (2014) The role of genetic polymorphisms in cytochrome P450 and effects of tuberculosis co-treatment on the predictive value of CYP2B6 SNPs and on efavirenz plasma levels in adult HIV patients. *Antiviral research*, 102, 44-53.
- BLANKSON, J. N., PERSAUD, D. & SILICIANO, R. F. (2002) The challenge of viral reservoirs in HIV-1 infection. *Annual review of medicine*, 53, 557-593.
- BOLHASSANI, A., SAFAIYAN, S. & RAFATI, S. (2011) Improvement of different vaccine delivery systems for cancer therapy. *Mol Cancer*, 10, 1-20.
- BOWERMAN, B., BROWN, P. O., BISHOP, J. M. & VARMUS, H. E. (1989) A nucleoprotein complex mediates the integration of retroviral DNA. *Genes & development*, 3, 469-478.
- BRASS, A. L., DYKXHOORN, D. M., BENITA, Y., YAN, N., ENGELMAN, A., XAVIER, R. J., LIEBERMAN, J. & ELLEDGE, S. J. (2008) Identification of host proteins required for HIV infection through a functional genomic screen. *science*, 319, 921-926.
- BRENCHLEY, J. M., SCHACKER, T. W., RUFF, L. E., PRICE, D. A., TAYLOR, J. H., BEILMAN, G. J., NGUYEN, P. L., KHORUTS, A., LARSON, M. & HAASE, A. T. (2004) CD4+ T cell depletion during all stages of HIV disease occurs predominantly in the gastrointestinal tract. *The Journal of experimental medicine*, 200, 749-759.
- BRETSCHER, M. S. (1984) Endocytosis: relation to capping and cell locomotion. *Science*, 224, 681-686.
- BRIONES, E., COLINO, C. I. & LANA O, J. M. (2008) Delivery systems to increase the selectivity of antibiotics in phagocytic cells. *J Control Release*, 125, 210-27.
- BROOKS, J. T., KAPLAN, J. E. & MASUR, H. (2009) What's new in the 2009 US guidelines for prevention and treatment of opportunistic infections among adults and adolescents with HIV. *Top HIV Med*, 17, 109-114.
- BUKRINSKY, M. I., SHAROVA, N., MCDONALD, T. L., PUSHKARSKAYA, T., TARPLEY, W. G. & STEVENSON, M. (1993) Association of integrase, matrix, and reverse transcriptase antigens of human immunodeficiency virus type 1 with viral nucleic acids following acute infection. *Proceedings of the National Academy of Sciences*, 90, 6125-6129.
- CAMMETT, A. M., MACGREGOR, T. R., WRUCK, J. M., FELIZARTA, F., MIAILHES, P., MALLOLAS, J. & PILIERO, P. J. (2009) Pharmacokinetic assessment of nevirapine and metabolites in human immunodeficiency virus type 1-infected patients with hepatic fibrosis. *Antimicrobial agents and chemotherapy*, 53, 4147-4152.
- CHAN, L., LOWES, S. & HIRST, B. H. (2004) The ABCs of drug transport in intestine and liver: efflux proteins limiting drug absorption and bioavailability. *European journal of pharmaceutical sciences*, 21, 25-51.

- CHEESEMAN, S. H., HATTOX, S. E., MCLAUGHLIN, M. M., KOUP, R. A., ANDREWS, C., BOVA, C. A., PAV, J. W., ROY, T., SULLIVAN, J. L. & KEIRNS, J. J. (1993) Pharmacokinetics of nevirapine: initial single-rising-dose study in humans. *Antimicrobial agents and chemotherapy*, 37, 178-182.
- CHEN, X., SHAH, D., KOSITRATNA, G., MANSTEIN, D., ANDERSON, R. R. & WU, M. X. (2012) Facilitation of transcutaneous drug delivery and vaccine immunization by a safe laser technology. *J Control Release*, 159, 43-51.
- CHEN, Y., ZHU, X., ZHANG, X., LIU, B. & HUANG, L. (2010) Nanoparticles modified with tumor-targeting scFv deliver siRNA and miRNA for cancer therapy. *Molecular Therapy*, 18, 1650-1656.
- CHILLISTONE, S. & HARDMAN, J.G. (2014) Factors affecting drug absorption and distribution. *Anaesthesia & Intestine Care Medicine*, 15(7), 309-313.
- CHO, K., WANG, X., NIE, S. & SHIN, D. M. (2008) Therapeutic nanoparticles for drug delivery in cancer. *Clinical cancer research*, 14, 1310-1316.
- CHOI, S., KIM, Y., LEE, J.W., PARK, J., PRAUSNITS, M.R. & ALLEN, M.G. (2012) Intracellular protein delivery and gene transfection by electroporation using a microneedle electrode array. *Small*, 8, 1081-1091.
- CHOLEWINSKA, G. Y. (2007) Pharmacogenetics in HIV Clinical Practice. *HIV & AIDS Review*, 6, 9-14.
- CLARK, S. J., SAAG, M. S., DECKER, W. D., CAMPBELL-HILL, S., ROBERSON, J. L., VELDKAMP, P. J., KAPPES, J. C., HAHN, B. H. & SHAW, G. M. (1991) High titers of cytopathic virus in plasma of patients with symptomatic primary HIV-1 infection. *New England Journal of Medicine*, 324, 954-960.
- COHEN, M. S., GAY, C. L., BUSCH, M. P. & HECHT, F. M. (2010) The detection of acute HIV infection. *Journal of Infectious Diseases*, 202, S270-S277.
- CRISTOFOLETTI, R., NAIR, A., ABRAHAMSSON, B., GROOT, D. W., KOPP, S., LANGGUTH, P., POLLI, J. E., SHAH, V. P. & DRESSMAN, J. B. (2013) Biowaiver monographs for immediate release solid oral dosage forms: Efavirenz. *Journal of pharmaceutical sciences*, 102, 318-329.
- DAHL, V., JOSEFSSON, L. & PALMER, S. (2010) HIV reservoirs, latency, and reactivation: prospects for eradication. *Antiviral research*, 85, 286-294.
- DANIEL, S. A., HARMAN, S. D., LATHROP III, R. L., MUELLER, R. L., MURPHY-CHUTORIAN, D., RICHARDSON, B. & WITHAM, L. (1999) Laser assisted drug delivery. Google Patents.
- DAVIS, R. E., PARRA, A., LOVERDE, P. T., RIBEIRO, E., GLORIOSO, G. & HODGSON, S. (1999) Transient expression of DNA and RNA in parasitic helminths by using particle bombardment. *Proceedings of the National Academy of Sciences*, 96, 8687-8692.
- DERDEYN, C. A., DECKER, J. M., BIBOLLET-RUCHE, F., MOKILI, J. L., MULDOON, M., DENHAM, S. A., HEIL, M. L., KASOLO, F., MUSONDA, R. & HAHN, B. H. (2004) Envelope-constrained neutralization-sensitive HIV-1 after heterosexual transmission. *Science*, 303, 2019-2022.
- DHOLAKIA, K., REECE, P. & GU, M. (2008) Optical micromanipulation. *Chemical Society Reviews*, 37, 42-55.
- DING, X., MA, D., ZHANG, Q., PENG, W., FAN, M. & SUO, W.S. (2014) Progress of *in-vivo* electroporation in the rodent brain. *Current Gene Therapy*, 14, 211-217.

- DOCCHIO, F. & SACCHI, C. A. (1988) Shielding properties of laser-induced plasmas in ocular media irradiated by single Nd: YAG pulses of different durations. *Investigative ophthalmology & visual science*, 29, 437-443.
- DOCCHIO, F., SACCHI, C. A. & MARSHALL, J. (1986) Experimental investigation of optical breakdown thresholds in ocular media under single pulse irradiation with different pulse durations. *Lasers Ophthalmol*, 1, 83-93.
- ECKERT, D. M. & KIM, P. S. (2001) Mechanisms of viral membrane fusion and its inhibition. *Annual review of biochemistry*, 70, 777-810.
- EICHELBAUM, M., INGELMAN-SUNDBERG, M. & EVANS, W. E. (2006) Pharmacogenomics and individualized drug therapy. *Annu. Rev. Med.*, 57, 119-137.
- ENSIGN, L. M., CONE, R. & HANES, J. (2012) Oral drug delivery with polymeric nanoparticles: the gastrointestinal mucus barriers. *Advanced drug delivery reviews*, 64, 557-570.
- ERICKSON, D. A., MATHER, G., TRAGER, W. F., LEVY, R. H. & KEIRNS, J. J. (1999) Characterization of the in vitro biotransformation of the HIV-1 reverse transcriptase inhibitor nevirapine by human hepatic cytochromes P-450. *Drug metabolism and disposition*, 27, 1488-1495.
- ESTE, J. A. & CIHLAR, T. (2010) Current status and challenges of antiretroviral research and therapy. *Antiviral Res*, 85, 25-33.
- ESTE, J. A. & TELENTI, A. (2007) HIV entry inhibitors. *Lancet*, 370, 81-8.
- EVANS, W. E. & RELLING, M. V. (1999) Pharmacogenomics: translating functional genomics into rational therapeutics. *science*, 286, 487-491.
- FARQUHAR, M. G. (1983) Multiple pathways of exocytosis, endocytosis, and membrane recycling: validation of a Golgi route. *Federation proceedings*.
- FAUCI, A. S. (1993) HIV infection is active and progressive in lymphoid tissue during the clinically latent stage of disease. *Nature*, 362, 25.
- FURMAN, P. A. & BARRY, D. W. (1988) Spectrum of antiviral activity and mechanism of action of zidovudine. An overview. *The American journal of medicine*, 85, 176-181.
- FURTADO, M. R., CALLAWAY, D. S., PHAIR, J. P., KUNSTMAN, K. J., STANTON, J. L., MACKEN, C. A., PERELSON, A. S. & WOLINSKY, S. M. (1999) Persistence of HIV-1 transcription in peripheral-blood mononuclear cells in patients receiving potent antiretroviral therapy. *N Engl J Med*, 340, 1614-22.
- GANSER, B. K., LI, S., KLISHKO, V. Y., FINCH, J. T. & SUNDQUIST, W. I. (1999) Assembly and analysis of conical models for the HIV-1 core. *Science*, 283, 80-83.
- GEHL, J., SÄ, RENSEN, T. H., NIELSEN, K., RASKMARK, P., NIELSEN, S. L., SKOVSGAARD, T. & MIR, L. M. (1999) In vivo electroporation of skeletal muscle: threshold, efficacy and relation to electric field distribution. *Biochimica et Biophysica Acta (BBA)-General Subjects*, 1428, 233-240.
- GERBER, J. G. (2000) Using pharmacokinetics to optimize antiretroviral drug-drug interactions in the treatment of human immunodeficiency virus infection. *Clinical infectious diseases*, 30, S123-S129.
- GLAUSER, T., ASTAFIEVA, I. & HOSSAINY, S. F. A. (2014) Coatings for implantable medical devices for controlled release of a hydrophilic drug and a hydrophobic drug. Google Patents.
- GOFF, S. P. (1992) Genetics of retroviral integration. *Annual review of genetics*, 26, 527-544.

- GOLDEN, E. B., LAM, P. Y., KARDOSH, A., GAFFNEY, K. J., CADENAS, E., LOUIE, S. G., PETASIS, N. A., CHEN, T. C. & SCHONTHAL, A. H. (2009) Green tea polyphenols block the anticancer effects of bortezomib and other boronic acid-based proteasome inhibitors. *Blood*, 113, 5927-5937.
- GOMES, C. P., FERREIRA LOPES, C. T. D., DUARTE MORENO, P. M., VARELA-MOREIRA, A., ALONSO, M. J. & PEGO, A. P. (2014) Translating chitosan to clinical delivery of nucleic acid-based drugs. *MRS bulletin*, 39, 60-70.
- GOVENDER, T., OJEWOLE, E., NAIDOO, P. & MACKRAJ, I. (2008) Polymeric nanoparticles for enhancing antiretroviral drug therapy. *Drug delivery*, 15, 493-501.
- GUO, G., HUSS, M., TONG, G. Q., WANG, C., LI SUN, L., CLARKE, N. D. & ROBSON, P. (2010) Resolution of cell fate decisions revealed by single-cell gene expression analysis from zygote to blastocyst. *Developmental cell*, 18, 675-685.
- GUPTA, B., LEVCHENKO, T. S. & TORCHILIN, V. P. (2005) Intracellular delivery of large molecules and small particles by cell-penetrating proteins and peptides. *Advanced drug delivery reviews*, 57, 637-651.
- HE, P., DAVIS, S. S. & ILLUM, L. (1998) In vitro evaluation of the mucoadhesive properties of chitosan microspheres. *International Journal of Pharmaceutics*, 166, 75-88.
- HEISTERKAMP, A., MAXWELL, I. Z., MAZUR, E., UNDERWOOD, J. M., NICKERSON, J. A., KUMAR, S. & INGBER, D. E. (2005) Pulse energy dependence of subcellular dissection by femtosecond laser pulses. *Optics Express*, 13, 3690-3696.
- HU, J., LIU, H. & WANG, L. (2000) Enhanced delivery of AZT to macrophages via acetylated LDL. *J Control Release*, 69, 327-35.
- ILLUM, L. (2003) Nasal drug delivery - possibilities, problems and solutions. *Journal of Controlled Release*, 87, 187-198.
- ILLUM, L., FARRAJ, N. F. & DAVIS, S. S. (1994) Chitosan as a novel nasal delivery system for peptide drugs. *Pharmaceutical research*, 11, 1186-1189.
- IWAMI, S., NAKAOKA, S. & TAKEUCHI, Y. (2008) Viral diversity limits immune diversity in asymptomatic phase of HIV infection. *Theoretical population biology*, 73, 332-341.
- JAIMINI, M. (2013) A review on immediate release drug delivery system by using design of experiment. *Journal of drug discovery and therapeutics*, 1.
- JORDAN, M., SCHALLHORN, A. & WURM, F. M. (1996) Transfecting mammalian cells: optimization of critical parameters affecting calcium-phosphate precipitate formation. *Nucleic acids research*, 24, 596-601.
- JORDAN, M. & WURM, F. (2004) Transfection of adherent and suspended cells by calcium phosphate. *Methods*, 33, 136-143.
- KAKKAR, V., SINGH, S., SINGLA, D. & KAUR, I. P. (2011) Exploring solid lipid nanoparticles to enhance the oral bioavailability of curcumin. *Molecular nutrition & food research*, 55, 495-503.
- KASPER, L. H. & BUZONI-GATEL, D. (1998) Some opportunistic parasitic infections in AIDS: candidiasis, pneumocystosis, cryptosporidiosis, toxoplasmosis. *Parasitology Today*, 14, 150-156.
- KATLAMA, C., DEEKS, S. G., AUTRAN, B., MARTINEZ-PICADO, J., VAN LUNZEN, J., ROUZIQUX, C., MILLER, M., VELLA, S., SCHMITZ, J. E. &

- AHLERS, J. (2013) Barriers to a cure for HIV: new ways to target and eradicate HIV-1 reservoirs. *The Lancet*.
- KEHOE, S., TREMBLAY, M.-L., COUGHLAN, A., TOWLER, M. R., RAINEY, J. K., ABRAHAM, R. J. & BOYD, D. (2013) Preliminary investigation of the dissolution behavior, cytocompatibility, effects of fibrinogen conformation and platelet adhesion for radiopaque embolic particles. *Journal of Functional Biomaterials*, 4, 89-113.
- KESHARWANI, P., JAIN, K. & JAIN, N. K. (2014) Dendrimer as nanocarrier for drug delivery. *Progress in Polymer Science*, 39, 268-307.
- KHATSENKO, O. G., GROSS, S. S., RIFKIND, A. B. & VANE, J. R. (1993) Nitric oxide is a mediator of the decrease in cytochrome P450-dependent metabolism caused by immunostimulants. *Proceedings of the National Academy of Sciences*, 90, 11147-11151.
- KIM, G. C., KIM, G. J., PARK, S. R., JEON, S. M., SEO, H. J., IZA, F. & LEE, J. K. (2009) Air plasma coupled with antibody-conjugated nanoparticles: a new weapon against cancer. *J. Phys. D: Appl. Phys*, 42, 032005.
- KLATZMANN, D., CHAMPAGNE, E., CHAMARET, S., GRUEST, J., GUETARD, D., HERCEND, T., GLUCKMAN, J.-C. & MONTAGNIER, L. (1984) T-lymphocyte T4 molecule behaves as the receptor for human retrovirus LAV.
- KLEIN, T. M., WOLF, E. D., WU, R. & SANFORD, J. C. (1987) High-velocity microprojectiles for delivering nucleic acids into living cells. *Nature*, 327, 70-73.
- KNIPE, J. M., PETERS, J. T. & PEPPAS, N. A. (2013) Theranostic agents for intracellular gene delivery with spatiotemporal imaging. *Nano today*, 8, 21-38.
- KOENIG, K., KRAUSS, O. & RIEMANN, I. (2002) Intratissue surgery with 80 MHz nanojoule femtosecond laser pulses in the near infrared. *Optics Express*, 10, 171-176.
- KOLEY, D. & BARD, A. J. (2010) Triton X-100 concentration effects on membrane permeability of a single HeLa cell by scanning electrochemical microscopy (SECM). *Proceedings of the National Academy of Sciences*, 107, 16783-16787.
- KOO, O. M., RUBINSTEIN, I. & ONYUKSEL, H. (2005) Role of nanotechnology in targeted drug delivery and imaging: a concise review. *Nanomedicine: Nanotechnology, Biology and Medicine*, 1, 193-212.
- KOWALSKI, M., POTZ, J., BASIRIPOUR, L., DORFMAN, T., GOH, W. C., TERWILLIGER, E., DAYTON, A., ROSEN, C., HASELTINE, W. & SODROSKI, J. (1987) Functional regions of the envelope glycoprotein of human immunodeficiency virus type 1. *Science*, 237, 1351-1355.
- KULKOSKY, J. & POMERANTZ, R. J. (2002) Approaching eradication of highly active antiretroviral therapy-persistent human immunodeficiency virus type 1 reservoirs with immune activation therapy. *Clinical infectious diseases*, 35, 1520-1526.
- KUMAR, C. S. S. R. & MOHAMMAD, F. (2011) Magnetic nanomaterials for hyperthermia-based therapy and controlled drug delivery. *Advanced drug delivery reviews*, 63, 789-808.
- KUMAR, R. & PHILIP, A. (2007) Modified transdermal technologies: Breaking the barriers of drug permeation via the skin. *Tropical journal of pharmaceutical research*, 6, 633-644.
- LACKNER, M. (2008) *Lasers in chemistry*, Wiley-VCH.

- LAPPE-SIEFKE, C., MAAS, C. & KNEUSSEL, M. (2008) Microinjection into cultured hippocampal neurons: A straightforward approach for controlled cellular delivery of nucleic acids, peptides and antibodies. *Journal of neuroscience methods*, 175, 88-95.
- LEE, H., LYTTON-JEAN, A. K. R., CHEN, Y., LOVE, K. T., PARK, A. I., KARAGIANNIS, E. D., SEHGAL, A., QUERBES, W., ZURENKO, C. S. & JAYARAMAN, M. (2012) Molecularly self-assembled nucleic acid nanoparticles for targeted in vivo siRNA delivery. *Nature nanotechnology*, 7, 389-393.
- LEE, W. M., REECE, P. J., MARCHINGTON, R. F., METZGER, N. K. & DHOLAKIA, K. (2007) Construction and calibration of an optical trap on a fluorescence optical microscope. *Nature protocols*, 2, 3226-3238.
- LENNERNAS, H., PALM, K., FAGERHOLM, U. & ARTURSSON, P. (1996) Comparison between active and passive drug transport in human intestinal epithelial (Caco-2) cells in vitro and human jejunum in vivo. *International journal of pharmaceuticals*, 127, 103-107.
- LEVINE, R. R. (1970) Factors affecting gastrointestinal absorption of drugs. *The American journal of digestive diseases*, 15, 171-188.
- LEWIN, S. R. & ROUZIOUX, C. (2011) HIV cure and eradication: how will we get from the laboratory to effective clinical trials? *Aids*, 25, 885-897.
- LI, J., FENG, L., FAN, L., ZHA, Y., GUO, L., ZHANG, Q., CHEN, J., PANG, Z., WANG, Y. & JIANG, X. (2011) Targeting the brain with PEG - PLGA nanoparticles modified with phage-displayed peptides. *Biomaterials*, 32, 4943-4950.
- LIFSON, J. D., FEINBERG, M. B., REYES, G. R., RABIN, L., BANAPOUR, B., CHAKRABARTI, S., MOSS, B., WONG-STAAAL, F., STEIMER, K. S. & ENGLEMAN, E. G. (1986) Induction of CD4-dependent cell fusion by the HTLV-III/LAV envelope glycoprotein. *Nature*, 323, 725-728.
- LIU, H.-L., HUA, M.-Y., YANG, H.-W., HUANG, C.-Y., CHU, P.-C., WU, J.-S., TSENG, I. C., WANG, J.-J., YEN, T.-C. & CHEN, P.-Y. (2010) Magnetic resonance monitoring of focused ultrasound/magnetic nanoparticle targeting delivery of therapeutic agents to the brain. *Proceedings of the National Academy of Sciences*, 107, 15205-15210.
- LU, A. Y. H. (1998) Drug-Metabolism research challenges in the new millennium individual variability in drug therapy and drug safety. *Drug metabolism and disposition*, 26, 1217-1222.
- LU, Y. & LOW, P. S. (2012) Folate-mediated delivery of macromolecular anticancer therapeutic agents. *Advanced drug delivery reviews*, 64, 342-352.
- LUCAS, S. B. (1990) Missing infections in AIDS. *Transactions of the Royal Society of Tropical Medicine and Hygiene*, 84, 34-38.
- LUNDKVIST, A.-J. S., ALDRIDGE, E. J., BHAT, V. D. & SLATER, R. C. (2003) Method and apparatus for intracellular delivery of an agent. Google Patents.
- LUO, D. & SALTZMAN, W. M. (2000) Enhancement of transfection by physical concentration of DNA at the cell surface. *Nature biotechnology*, 18, 893-895.
- LYLES, R. H., MUNOZ, A., YAMASHITA, T. E., BAZMI, H., DETELS, R., RINALDO, C. R., MARGOLICK, J. B., PHAIR, J. P. & MELLORS, J. W. (2000) Natural history of human immunodeficiency virus type 1 viremia after

- seroconversion and proximal to AIDS in a large cohort of homosexual men. *Journal of Infectious Diseases*, 181, 872-880.
- MACK, K. D., WEI, R., ELBAGARRI, A., ABBEY, N. & MCGRATH, M. S. (1998) A novel method for DEAE-dextran mediated transfection of adherent primary cultured human macrophages. *Journal of immunological methods*, 211, 79-86.
- MADDON, P. J., DALGLEISH, A. G., MCDOUGAL, J. S., CLAPHAM, P. R., WEISS, R. A. & AXEL, R. (1986) The T4 gene encodes the AIDS virus receptor and is expressed in the immune system and the brain. *Cell*, 47, 333-348.
- MALLIPEDDI, R. & ROHAN, L. C. (2010) Progress in antiretroviral drug delivery using nanotechnology. *Int J Nanomedicine*, 5, 533-47.
- MANNO, C. S., PIERCE, G. F., ARRUDA, V. R., GLADER, B., RAGNI, M., RASKO, J. J. E., OZELO, M. C., HOOTS, K., BLATT, P. & KONKLE, B. (2006) Successful transduction of liver in hemophilia by AAV-Factor IX and limitations imposed by the host immune response. *Nature medicine*, 12, 342-347.
- MARCHINGTON, R. F., ARITA, Y., TSAMPOULA, X., GUNN-MOORE, F. J. & DHOLAKIA, K. (2010) Optical injection of mammalian cells using a microfluidic platform. *Biomedical optics express*, 1, 527-536.
- MARIVIN, E., MOUROT, B., LOYER, P., RIME, H., BOBE, J. & FOSTIER, A. (2015) Transfection of isolated rainbow trout, *Oncorhynchus mykiss*, granulosa cells through chemical transfection and electroporation at 12°C. *General and Comparative Endocrinology*.
- MARTINEZ, M. A., CLOTET, B. & ESTE, J. A. (2002a) RNA interference of HIV replication. *TRENDS in immunology*, 23, 559-561.
- MARTINEZ, M. N. & AMIDON, G. L. (2002b) A mechanistic approach to understanding the factors affecting drug absorption: a review of fundamentals. *The Journal of Clinical Pharmacology*, 42, 620-643.
- MARZOLINI, C., TELENTI, A., DECOSTERD, L. A., GREUB, G., BIOLLAZ, J. R. M. & BUCLIN, T. (2001) Efavirenz plasma levels can predict treatment failure and central nervous system side effects in HIV-1-infected patients. *Aids*, 15, 71-75.
- MAXWELL, I., CHUNG, S. & MAZUR, E. (2005) Nanoprocessing of subcellular targets using femtosecond laser pulses. *Medical laser application*, 20, 193-200.
- MCALLISTER, D. V., WANG, P. M., DAVIS, S. P., PARK, J.-H., CANATELLA, P. J., ALLEN, M. G. & PRAUSNITZ, M. R. (2003) Microfabricated needles for transdermal delivery of macromolecules and nanoparticles: fabrication methods and transport studies. *Proceedings of the National Academy of Sciences*, 100, 13755-13760.
- MCCUNE, J. M. (2001) The dynamics of CD4+ T-cell depletion in HIV disease. *Nature*, 410, 974-979.
- MCGLOIN, D. & DHOLAKIA, K. (2005) Bessel beams: diffraction in a new light. *Contemporary Physics*, 46, 15-28.
- MCRAE, M. P., LOWE, C. M., TIAN, X., BOURDET, D. L., HO, R. H., LEAKE, B. F., KIM, R. B., BROUWER, K. L. R. & KASHUBA, A. D. M. (2006) Ritonavir, saquinavir, and efavirenz, but not nevirapine, inhibit bile acid transport in human and rat hepatocytes. *Journal of Pharmacology and Experimental Therapeutics*, 318, 1068-1075.

- MEHANDRU, S., POLES, M. A., TENNER-RACZ, K., HOROWITZ, A., HURLEY, A., HOGAN, C., BODEN, D., RACZ, P. & MARKOWITZ, M. (2004) Primary HIV-1 infection is associated with preferential depletion of CD4+ T lymphocytes from effector sites in the gastrointestinal tract. *The Journal of experimental medicine*, 200, 761-770.
- MEHIER-HUMBERT, S. & GUY, R. H. (2005) Physical methods for gene transfer: improving the kinetics of gene delivery into cells. *Adv Drug Deliv Rev*, 57, 733-53.
- MELO, C. D. S., PEREIRA, B. G., SILVA-CUNHA, A. & FIALHO, S. L. (2012) Poly- ϵ -caprolactone microspheres containing interferon alpha as alternative formulations for the treatment of chronic hepatitis C. *Brazilian Journal of Pharmaceutical Sciences*, 48, 51-59.
- MENEZES, V., MATHEW, Y., TAKAYAMA, K., KANNO, A. & HOSSEINI, H. (2012) Laser plasma jet driven microparticles for DNA/drug delivery. *PLoS One*, 7, e50823.
- MILONNI, P. W. & EBERLY, J. H. (2010) Introduction to Laser Operation. *Laser Physics*. John Wiley & Sons, Inc.
- MINGOZZI, F., MAUS, M. V., HUI, D. J., SABATINO, D. E., MURPHY, S. L., RASKO, J. E. J., RAGNI, M. V., MANNO, C. S., SOMMER, J. & JIANG, H. (2007) CD8+ T-cell responses to adeno-associated virus capsid in humans. *Nature medicine*, 13, 419-422.
- MONTEFIORI, D. C. (2005) Evaluating neutralizing antibodies against HIV, SIV, and SHIV in luciferase reporter gene assays. *Current protocols in immunology*, 12.11. 1-12.11. 17.
- MONTEFIORI, D. C. (2009) Measuring HIV neutralization in a luciferase reporter gene assay. *HIV protocols*. Springer.
- MTHUNZI, P., DHOLAKIA, K. & GUNN-MOORE, F. (2010) Phototransfection of mammalian cells using femtosecond laser pulses: optimization and applicability to stem cell differentiation. *Journal of Biomedical optics*, 15, 041507-041507-7.
- MUFHANDU, H. T., GRAY, E. S., MADIGA, M. C., TUMBA, N., ALEXANDRE, K. B., KHOZA, T., WIBMER, C. K., MOORE, P. L., MORRIS, L. & KHATI, M. (2012) UCLA1, a Synthetic Derivative of a gp120 RNA Aptamer, Inhibits Entry of Human Immunodeficiency Virus Type-1 Subtype C. *Journal of virology*, JVI. 06893-11.
- MULLER, R. H. & KECK, C. M. (2004) Challenges and solutions for the delivery of biotech drugs: a review of drug nanocrystal technology and lipid nanoparticles. *Journal of biotechnology*, 113, 151-170.
- NAIK, A., KALIA, Y. N. & GUY, R. H. (2000a) Transdermal drug delivery: overcoming the skin's barrier function. *Pharmaceutical science & technology today*, 3, 318-326.
- NAIK, A., KALIA, Y. N. & GUY, R. H. (2000b) Transdermal drug delivery: overcoming the skin's barrier function. *Pharmaceutical science & technology today*, 3, 318-326.
- NATHWANI, A. C., TUDDENHAM, E. G. D., RANGARAJAN, S., ROSALES, C., MCINTOSH, J., LINCH, D. C., CHOWDARY, P., RIDDELL, A., PIE, A. J. & HARRINGTON, C. (2011) Adenovirus-associated virus vector-mediated gene transfer in hemophilia B. *New England Journal of Medicine*, 365, 2357-2365.

- NELSON, P. R. & KENT, K. C. (2002) Microinjection of DNA into the nuclei of human vascular smooth muscle cells. *Journal of Surgical Research*, 106, 202-208.
- NIIOKA, H., SMITH, N. I., FUJITA, K., INOUE, Y. & KAWATA, S. (2008) Femtosecond laser nano-ablation in fixed and non-fixed cultured cells. *Opt Express*, 16, 14476-95.
- NOACK, J., HAMMER, D. X., NOOJIN, G. D., ROCKWELL, B. A. & VOGEL, A. (1998) Influence of pulse duration on mechanical effects after laser-induced breakdown in water. *Journal of Applied Physics*, 83, 7488-7495.
- OGG, G. S., JIN, X., BONHOEFFER, S., DUNBAR, P. R., NOWAK, M. A., MONARD, S., SEGAL, J. P., CAO, Y., ROWLAND-JONES, S. L. & CERUNDOLO, V. (1998) Quantitation of HIV-1-specific cytotoxic T lymphocytes and plasma load of viral RNA. *Science*, 279, 2103-2106.
- OMATSU, T., NAWATA, K., OKIDA, M. & FURUKI, K. (2007) MW ps pulse generation at sub-MHz repetition rates from a phase conjugate Nd: YVO₄ bounce amplifier. *Optics express*, 15, 9123-9128.
- OVERALL, C. M. & KLEIFELD, O. (2006) Validating matrix metalloproteinases as drug targets and anti-targets for cancer therapy. *Nature Reviews Cancer*, 6, 227-239.
- PALUMBO, G., CARUSO, M., CRESCENZI, E., TECCE, M. F., ROBERTI, G. & COLASANTI, A. (1996) Targeted gene transfer in eucaryotic cells by dye-assisted laser optoporation. *Journal of Photochemistry and Photobiology B: Biology*, 36, 41-46.
- PANG, K. S. (2003) Modeling of intestinal drug absorption: roles of transporters and metabolic enzymes (for the Gillette Review Series). *Drug metabolism and disposition*, 31, 1507-1519.
- PANYAM, J. & LABHASEWAR, V. (2003) Biodegradable nanoparticles for drug and gene delivery to cells and tissue. *Advanced drug delivery reviews*, 55, 329-347.
- PATEL, M. V. & CHEN, F.-J. (2001) Triglyceride-free compositions and methods for enhanced absorption of hydrophilic therapeutic agents. Google Patents.
- PATERSON, L., AGATE, B., COMRIE, M., FERGUSON, R., LAKE, T. K., MORRIS, J. E., CARRUTHERS, A. E., BROWN, C. T. A., SIBBETT, W. & BRYANT, P. E. (2005) Photoporation and cell transfection using a violet diode laser. *Quantum Electronics and Laser Science Conference, 2005. QELS'05*. IEEE.
- PIERSON, T., MCARTHUR, J. & SILICIANO, R. F. (2000) Reservoirs for HIV-1: mechanisms for viral persistence in the presence of antiviral immune responses and antiretroviral therapy. *Annual review of immunology*, 18, 665-708.
- PLAPIED, L., DUHEM, N., DES RIEUX, A. & PREAT, V. (2011) Fate of polymeric nanocarriers for oral drug delivery. *Current opinion in colloid & interface science*, 16, 228-237.
- POLONIS, V. R., BROWN, B. K., BORGES, A. R., ZOLLA-PAZNER, S., DIMITROV, D. S., ZHANG, M.-Y., BARNETT, S. W., RUPRECHT, R. M., SCARLATTI, G. & FENYO, E.-M. (2008) Recent advances in the characterization of HIV-1 neutralization assays for standardized evaluation of the antibody response to infection and vaccination. *Virology*, 375, 315-320.

- PRAUSNITZ, M. R. & LANGER, R. (2008) Transdermal drug delivery. *Nature biotechnology*, 26, 1261-1268.
- PRICE, J., TURNER, D. & CEPKO, C. (1987) Lineage analysis in the vertebrate nervous system by retrovirus-mediated gene transfer. *Proceedings of the National Academy of Sciences*, 84, 156-160.
- PUCIHAR, G., KOTNIK, T., MIKLAVCIC, D. & TEISSIE, J. (2008) Kinetics of transmembrane transport of small molecules into electropermeabilized cells. *Biophysical journal*, 95, 2837-2848.
- RASMUSSEN, J. W., MARTINEZ, E., LOUKA, P. & WINGETT, D. G. (2010) Zinc oxide nanoparticles for selective destruction of tumor cells and potential for drug delivery applications. *Expert opinion on drug delivery*, 7, 1063-1077.
- RATNER, L., HASELTINE, W., PATARCA, R., LIVAK, K. J., STARCICH, B., JOSEPHS, S. F., DORAN, E. R., RAFALSKI, J. A., WHITEHORN, E. A. & BAUMEISTER, K. (1985) Complete nucleotide sequence of the AIDS virus, HTLV-III.
- REED, L.J. & MUENCH, H. (1938). A simple method of estimating fifty percent endpoints. *American Journal of Hygiene*, 27, 493-497.
- REVICKI, D. A., BROWN, R. E., FEENY, D. H., HENRY, D., TEEHAN, B. P., RUDNICK, M. R. & BENZ, R. L. (1995) Health-related quality of life associated with recombinant human erythropoietin therapy for predialysis chronic renal disease patients. *American Journal of Kidney Diseases*, 25, 548-554.
- RISKA, P., LAMSON, M., MACGREGOR, T., SABO, J., HATTOX, S., PAV, J. & KEIRNS, J. (1999) Disposition and biotransformation of the antiretroviral drug nevirapine in humans. *Drug Metabolism and Disposition*, 27, 895-901.
- RUDD, M. E., KIM, Y. K., MADISON, D. H. & GAY, T. J. (1992) Electron production in proton collisions with atoms and molecules: energy distributions. *Reviews of modern physics*, 64, 441.
- SALEH, B. E. A. & TEICH, M. C. (1991) Fundamentals of photonics. *NASA STI/Recon Technical Report A*, 92, 35987.
- SCHINKEL, H., JACOBS, P., SCHILLBERG, S. & WEHNER, M. (2008) Infrared picosecond laser for perforation of single plant cells. *Biotechnology and bioengineering*, 99, 244-248.
- SCHLESSINGER, L. & WRIGHT, J. (1979) Inverse-bremsstrahlung absorption rate in an intense laser field. *Physical Review A*, 20, 1934.
- SCHNECKENBURGER, H., HENDINGER, A., SAILER, R., STRAUSS, W. S. L. & SCHMITT, M. (2002) Laser-assisted optoporation of single cells. *Journal of biomedical optics*, 7, 410-416.
- SEAMAN, M. S., JANES, H., HAWKINS, N., GRANDPRE, L. E., DEVOY, C., GIRI, A., COFFEY, R. T., HARRIS, L., WOOD, B. & DANIELS, M. G. (2010) Tiered categorization of a diverse panel of HIV-1 Env pseudoviruses for assessment of neutralizing antibodies. *Journal of virology*, 84, 1439-1452.
- SHAN, L., DENG, K., SHROFF, N. S., DURAND, C. M., RABI, S. A., YANG, H.-C., ZHANG, H., MARGOLICK, J. B., BLANKSON, J. N. & SILICIANO, R. F. (2012) Stimulation of HIV-1-specific cytolytic T lymphocytes facilitates elimination of latent viral reservoir after virus reactivation. *Immunity*, 36, 491-501.
- SHARMA, P. & GARG, S. (2010) Pure drug and polymer based nanotechnologies for the improved solubility, stability, bioavailability and targeting of anti-HIV drugs. *Adv Drug Deliv Rev*, 62, 491-502.

- SHASTRY, B. S. (2005) Pharmacogenetics and the concept of individualized medicine. *The Pharmacogenomics Journal*, 6, 16-21.
- SHEFI, O., SIMONNET, C., BAKER, M. W., GLASS, J. R., MACAGNO, E. R. & GROISMAN, A. (2006) Microtargeted gene silencing and ectopic expression in live embryos using biolistic delivery with a pneumatic capillary gun. *The Journal of neuroscience*, 26, 6119-6123.
- SHEN, H., SUN, T. & FERRARI, M. (2012) Nanovector delivery of siRNA for cancer therapy. *Cancer gene therapy*, 19, 367-373.
- SHEN, L. & SILICIANO, R. F. (2008) Viral reservoirs, residual viremia, and the potential of highly active antiretroviral therapy to eradicate HIV infection. *Journal of Allergy and Clinical Immunology*, 122, 22-28.
- SHIRAIISHI, T. & NIELSEN, P. E. (2012) Nanomolar cellular antisense activity of peptide nucleic acid (PNA) cholic acid ("Umbrella") and cholesterol conjugates delivered by cationic lipids. *Bioconjugate chemistry*, 23, 196-202.
- SIEGMAN, A. E. (1990) New developments in laser resonators. *OE/LASE'90*, 14-19 Jan., Los Angeles, CA. International Society for Optics and Photonics.
- SIEGMAN, A. E. (1993) Defining, measuring, and optimizing laser beam quality. *OE/LASE'93: Optics, Electro-Optics, & Laser Applications in Science & Engineering*. International Society for Optics and Photonics.
- SILICIANO, J. D. & SILICIANO, R. F. (2004) A long-term latent reservoir for HIV-1: discovery and clinical implications. *Journal of Antimicrobial Chemotherapy*, 54, 6-9.
- SINGH, B. N. & KIM, K. H. (2000) Floating drug delivery systems: an approach to oral controlled drug delivery via gastric retention. *Journal of Controlled Release*, 63, 235-259.
- SOARES, P. B., JEREMIAS, T. S., ALVAREZ-SILVA, M., LICINIO, M. A., SANTOS-SILVA, M. C. & VITURI, C. L. (2013) In vitro inhibitory effects of imatinib mesylate on stromal cells and hematopoietic progenitors from bone marrow. *Brazilian Journal of Medical and Biological Research*, 46, 39-51.
- SODROSKI, J., GOH, W. C., ROSEN, C., CAMPBELL, K. & HASELTINE, W. A. (1986) Role of the HTLV-III/LAV envelope in syncytium formation and cytopathicity.
- SOMAN, P., ZHANG, W., UMEDA, A., ZHANG, Z.J. & CHEN, S. (2011) Femtosecond laser-assisted optoporation for drug and gene delivery into single mammalian cells. *Journal of Biomedical Nanotechnology*, 7, 334-341.
- SOSNIK, A., CHIAPPETTA, D. A. & CARCABOSO, Ñ. N. M. (2009) Drug delivery systems in HIV pharmacotherapy: what has been done and the challenges standing ahead. *Journal of Controlled release*, 138, 2-15.
- ST-LOUIS LALONDE, B., BOULAIS, Ñ. T., LEBRUN, J.-J. & MEUNIER, M. (2013) Visible and near infrared resonance plasmonic enhanced nanosecond laser optoporation of cancer cells. *Biomedical optics express*, 4, 490-499.
- STAMATATOS, L., MORRIS, L., BURTON, D. R. & MASCOLA, J. R. (2009) Neutralizing antibodies generated during natural HIV-1 infection: good news for an HIV-1 vaccine? *Nature medicine*, 15, 866-870.
- STEVENSON, D., AGATE, B., TSAMPOULA, X., FISCHER, P., BROWN, C. T. A., SIBBETT, W., RICHES, A., GUNN-MOORE, F. & DHOLAKIA, K. (2006) Femtosecond optical transfection of cells: viability and efficiency. *Opt. Express*, 14, 7125-7133.

- STEVENSON, D. J., GUNN-MOORE, F. J., CAMPBELL, P. & DHOLAKIA, K. (2010) Single cell optical transfection. *J R Soc Interface*, 7, 863-71.
- STROBER, W. (2001) Trypan blue exclusion test of cell viability. *Current protocols in immunology*, A. 3B. 1-A. 3B. 2.
- STUART, B. C., FEIT, M. D., HERMAN, S., RUBENCHIK, A. M., SHORE, B. W. & PERRY, M. D. (1996) Nanosecond-to-femtosecond laser-induced breakdown in dielectrics. *Physical Review B*, 53, 1749.
- SUGIYAMA, O., AN, D. S., KUNG, S. P. K., FEELEY, B. T., GAMRADT, S., LIU, N. Q., CHEN, I. S. Y. & LIEBERMAN, J. R. (2005) Lentivirus-mediated gene transfer induces long-term transgene expression of BMP-2 in vitro and new bone formation in vivo. *Molecular Therapy*, 11, 390-398.
- SZEBENI, J., MUGGIA, F., GABIZON, A. & BARENHOLZ, Y. (2011) Activation of complement by therapeutic liposomes and other lipid excipient-based therapeutic products: prediction and prevention. *Advanced drug delivery reviews*, 63, 1020-1030.
- TANNER, F. C., CARR, D. P., NABEL, G. J. & NABEL, E. G. (1997) Transfection of human endothelial cells. *Cardiovascular research*, 35, 522-528.
- THANOU, M., VERHOEF, J. C. & JUNGINGER, H. E. (2001) Oral drug absorption enhancement by chitosan and its derivatives. *Advanced drug delivery reviews*, 52, 117-126.
- TIRLAPUR, U. K. & KONIG, K. (2002) Targeted transfection by femtosecond laser. *Nature*, 418, 290-1.
- TJELLE, T.E., SALTE, R., MATHIESEN, I. & KJEKEN, R. (2006) A novel electroporation device for gene delivery in large animals and humans. *Vaccine*, 24, 4667-4670)
- TORCHILIN, V. P. (2000) Drug targeting. *European Journal of Pharmaceutical Sciences*, 11, S81-S91.
- TREBINO, R., DELONG, K. W., FITTINGHOFF, D. N., SWEETSER, J. N., KRUMBUGEL, M. A., RICHMAN, B. A. & KANE, D. J. (1997) Measuring ultrashort laser pulses in the time-frequency domain using frequency-resolved optical gating. *Review of Scientific Instruments*, 68, 3277-3295.
- TSAMPOULA, X., GARCES-CHAVEZ, V., COMRIE, M., STEVENSON, D. J., AGATE, B., BROWN, C. T. A., GUNN-MOORE, F. & DHOLAKIA, K. (2007) Femtosecond cellular transfection using a nondiffracting light beam. *Applied Physics Letters*, 91, 053902.
- TSUKAKOSHI, M., KURATA, S., NOMIYA, Y., IKAWA, Y. & KASUYA, T. (1984) A novel method of DNA transfection by laser microbeam cell surgery. *Applied Physics B*, 35, 135-140.
- UCHUGONOVA, A., KONIG, K., BUECKLE, R., ISEMANN, A. & TEMPEA, G. (2008) Targeted transfection of stem cells with sub-20 femtosecond laser pulses. *Opt Express*, 16, 9357-64.
- UNAIDS (2014) 2014 UNAIDS Report on the Global AIDS Epidemic.
- VAN DEN BERG, A. & DOWDY, S. F. (2011) Protein transduction domain delivery of therapeutic macromolecules. *Current opinion in biotechnology*, 22, 888-893.
- VAN MEERLOO, J., KASPERS, G. J. L. & CLOOS, J. (2011) Cell sensitivity assays: the MTT assay. *Cancer Cell Culture*. Springer.
- VASIR, J. K., REDDY, M. K. & LABHASETWAR, V. D. (2005) Nanosystems in drug targeting: opportunities and challenges. *Current Nanoscience*, 1, 47-64.

- VENUGOPALAN, V., GUERRA III, A., NAHEN, K. & VOGEL, A. (2002) Role of laser-induced plasma formation in pulsed cellular microsurgery and micromanipulation. *Physical review letters*, 88, 078103.
- VIOLA, A. & LUSTER, A. D. (2008) Chemokines and their receptors: drug targets in immunity and inflammation. *Annu. Rev. Pharmacol. Toxicol.*, 48, 171-197.
- VOGEL, A., NOACK, J., HATTMAN, G. & PALTAUF, G. (2005) Mechanisms of femtosecond laser nanosurgery of cells and tissues. *Applied Physics B*, 81, 1015-1047.
- VON BRIESEN, H., RAMGE, P. & KREUTER, J. R. (2000) Controlled release of antiretroviral drugs. *AIDS Rev*, 2, 31-38.
- WANG, H. & MATISE, M.P. (2013) In vivo electroporation chick spinal cords. *Methods in Molecular Biology*, 1018, 133-140.
- WARD, B. A., GORSKI, J. C., JONES, D. R., HALL, S. D., FLOCKHART, D. A. & DESTA, Z. (2003) The cytochrome P450 2B6 (CYP2B6) is the main catalyst of efavirenz primary and secondary metabolism: implication for HIV/AIDS therapy and utility of efavirenz as a substrate marker of CYP2B6 catalytic activity. *Journal of Pharmacology and Experimental Therapeutics*, 306, 287-300.
- WARNKE, D., BARRETO, J. & TEMESGEN, Z. (2007) Antiretroviral drugs. *J Clin Pharmacol*, 47, 1570-9.
- WEFERS, B., MEYER, M., ORTIZ, O., DE ANGELIS, M. H., HANSEN, J., WURST, W. & KAHN, R. (2013) Direct production of mouse disease models by embryo microinjection of TALENs and oligodeoxynucleotides. *Proceedings of the National Academy of Sciences*, 110, 3782-3787.
- WONG, F. K., HAFFNER, C., HUTTNER, W. B. & TAVERNA, E. (2014) Microinjection of membrane-impermeable molecules into single neural stem cells in brain tissue. *Nature protocols*, 9, 1170-1182.
- WOOD, A. J. J., PISCITELLI, S. C. & GALLICANO, K. D. (2001) Interactions among drugs for HIV and opportunistic infections. *New England Journal of Medicine*, 344, 984-996.
- YAO, S., BECKLEY, M.L. & LIN, D. (2014) Delivery of plasmid DNA into dental tissues of developing rat teeth by electroporation. *Methods in Molecular Biology*, 1121, 179-188.
- ZACK, J. A., CANN, A. J., LUGO, J. P. & CHEN, I. S. (1988) HIV-1 production from infected peripheral blood T cells after HTLV-I induced mitogenic stimulation. *Science*, 240, 1026-1029.
- ZEIGLER, M. B. & CHIU, D. T. (2009) Laser Selection Significantly Affects Cell Viability Following Single-Cell Nanosurgery. *Photochemistry and photobiology*, 85, 1218-1224.
- ZEIRA, E., MANEVITCH, A., KHATCHATOURIANTS, A., PAPPO, O., HYAM, E., DARASH-YAHANA, M., TAVOR, E., HONIGMAN, A., LEWIS, A. & GALUN, E. (2003) Femtosecond infrared laser-an efficient and safe in vivo gene delivery system for prolonged expression. *Mol Ther*, 8, 342-50.
- ZEIRA, E., MANEVITCH, A., MANEVITCH, Z., KEDAR, E., GROPP, M., DAUDI, N., BARSUK, R., HARATI, M., YOTVAT, H., TROILO, P. J., GRIFFITHS, T. G., 2ND, PACCHIONE, S. J., RODEN, D. F., NIU, Z., NUSSBAUM, O., ZAMIR, G., PAPO, O., HEMO, I., LEWIS, A. & GALUN, E. (2007) Femtosecond laser: a new intradermal DNA delivery method for efficient,

- long-term gene expression and genetic immunization. *Faseb J*, 21, 3522-33.
- ZHI, D., ZHANG, S., WANG, B., ZHAO, Y., YANG, B. & YU, S. (2010) Transfection efficiency of cationic lipids with different hydrophobic domains in gene delivery. *Bioconjugate chemistry*, 21, 563-577.
- ZILONY, N., TZUR-BALTER, A., SEGAL, E. & SHEFI, O. (2013) Bombarding Cancer: Biolistic Delivery of therapeutics using Porous Si Carriers. *Scientific reports*, 3.

Appendices

Appendix A: Derivation of equations

1. Derivation of beam radius polynomial

$$\omega(z) = \omega_0 \sqrt{1 + \left(\frac{M^2 \lambda (z - z_0)}{\pi \omega_0^2} \right)^2}$$

$$\omega^2(z) = \omega_0^2 \left(1 + \left(\frac{M^2 \lambda (z - z_0)}{\pi \omega_0^2} \right)^2 \right)$$

$$\omega^2(z) = \omega_0^2 + \omega_0^2 \left(\frac{M^2 \lambda (z - z_0)}{\pi \omega_0^2} \right)^2$$

$$\omega^2(z) = \omega_0^2 + \omega_0^2 \left(\frac{M^2 \lambda (z - z_0)}{\pi \omega_0^2} \right) \left(\frac{M^2 \lambda (z - z_0)}{\pi \omega_0^2} \right)$$

$$\omega^2(z) = \omega_0^2 + \omega_0^2 \left[\left(\frac{M^2 \lambda}{\pi \omega_0^2} \right)^2 (z - z_0)(z - z_0) \right]$$

$$\omega^2(z) = \omega_0^2 + \omega_0^2 \left[\left(\frac{M^2 \lambda}{\pi \omega_0^2} \right)^2 (z^2 - 2zz_0 + z_0^2) \right]$$

$$\omega^2(z) = \omega_0^2 + \left[\left(\frac{M^4 \lambda^2}{\pi^2 \omega_0^2} \right) (z^2 - 2zz_0 + z_0^2) \right]$$

$$\omega^2(z) = \omega_0^2 + \left(\frac{M^4 \lambda^2}{\pi^2 \omega_0^2} \right) z^2 - 2z_0 \left(\frac{M^4 \lambda^2}{\pi^2 \omega_0^2} \right) z + \left(\frac{M^4 \lambda^2}{\pi^2 \omega_0^2} \right) z_0^2$$

$$\omega^2(z) = \left(\frac{M^4 \lambda^2}{\pi^2 \omega_0^2} \right)^2 z^2 - 2z_0 \left(\frac{M^4 \lambda^2}{\pi^2 \omega_0^2} \right)^2 z + \left(\frac{M^4 \lambda^2}{\pi^2 \omega_0^2} \right)^2 z_0^2 + \omega_0^2$$

Appendix B: Formulae

1. Calculation of % viral inhibition

$$\% \text{ viral infectivity} = \frac{\text{Average Experimental RLU}}{\text{Average VC RLU}} \times 100\%$$

$$\% \text{ Inhibition} = (100 - \% \text{ infectivity})$$

2. Calculation of % viability

$$\% \text{ viability} = \left(\frac{(\text{Ave}_{Abs \text{ experiment}}) - (\text{Ave}_{Abs BC})}{(\text{Ave}_{Abs CC}) - (\text{Ave}_{Abs BC})} \right) \times 100$$

3. Calculation of TCID₅₀

$$TCID_{50} = \frac{\% \text{ infected at dilution above 50\%} - 50\%}{\% \text{ infected at dilution above 50\%} - \% \text{ infected at dilution below 50\%}}$$

Appendix C: Clearance Certificate



M130764M130764

R14/49 Ms Thulile Khanyile

HUMAN RESEARCH ETHICS COMMITTEE (MEDICAL)

CLEARANCE CERTIFICATE NO. M130764

NAME: Ms Thulile Khanyile
(Principal Investigator)

DEPARTMENT: Molecular Medicine & Haematology
Medical School


PROJECT TITLE: Photo-Translocation of Antiretroviral Drugs into
HIV-1 Permissive Cell Lines

DATE CONSIDERED: Ad hoc

DECISION: Approved unconditionally

CONDITIONS:

SUPERVISOR: Dr M Papathansopoulos

APPROVED BY: 

Professor PE Cleaton-Jones, Chairperson, HREC (Medical)

DATE OF APPROVAL: 05/08/2013

This clearance certificate is valid for 5 years from date of approval. Extension may be applied for.

DECLARATION OF INVESTIGATORS

To be completed in duplicate and **ONE COPY** returned to the Secretary in Room 10004, 10th floor, Senate House, University.

I/we fully understand the conditions under which I am/we are authorized to carry out the above-mentioned research and I/we undertake to ensure compliance with these conditions. Should any departure be contemplated, from the research protocol as approved, I/we undertake to resubmit the application to the Committee. **I agree to submit a yearly progress report.**

Principal Investigator Signature

M130764Date

PLEASE QUOTE THE PROTOCOL NUMBER IN ALL ENQUIRIES